Calibration, verification, and sensitivity analysis of the HEC-HMS hydrologic model

CFCAS project:
Assessment of Water Resources Risk and Vulnerability to Changing Climatic Conditions

Project Report IV.

August 2004

Prepared by

Juraj M. Cunderlik

and

Slobodan P. Simonovic

CFCAS Project Team:

University of Western Ontario
Slobodan P. Simonovic
Gordon McBean
Juraj M. Cunderlik

University of Waterloo
Donald H. Burn
Linda Mortsch
Mohammed Sharif

Upper Thames River Conservation Authority
Rick Goldt
Mark Helsten

Contents

List of Figures

List of Tables

Appendixes

I. INTRODUCTION

The main objective of this report is to describe the calibration, verification, and sensitivity analysis of the United States Army Corps of Engineers (USACE) Hydrologic Engineering Center's Hydrologic Modeling System (HEC-HMS) on the data from the Upper Thames River basin (UTRb) study area. The HEC-HMS model was chosen to be the most appropriate hydrologic modeling tool for achieving the goals set in the Canadian Foundation for Climatic and Atmospheric Sciences (CFCAS) funded project "Assessment of Water Resources Risk and Vulnerability to Changing Climatic Conditions" ("project" hereafter), (Cunderlik and Simonovic, 2003). The calibration, verification and sensitivity analysis of the HMS model are parts of the project Task 1: Development of a hydrologic model (ICLR, 2004).

This project report should be used in conjunction with the Project Report II (Cunderlik and Simonovic, 2004), which provides details on the hydrometric and climatic stations available in the UTRb, describes UTRb streamflow and precipitation regimes, and summarizes the hydro-climatic data selected for the calibration and verification of the event and continuous versions of the HMS model, including the data selection strategy. These topics are not repeated herein.

The following text is organized into two main sections, one dealing with the HEC-HMS event model, and the other one with the HEC-HMS continuous model. Both sections are then subdivided into 4 subsections describing model structure, calibration and verification procedures, sensitivity analysis, and the obtained results. The appendixes enclosed at the end of the report contain input data and calibrated values of all model parameters required to successfully run the event and continuous versions of the model in the UTRb. Included in this report are also technical details of all model components, and so the report can be used as a complete reference manual.

II. HEC-HMS EVENT MODEL

II.1 Event model structure

The physical representation of the UTRb was created in the HMS basin model environment (BME). In BME, individual hydrologic elements can be connected in a network imitating basin hydrologic structure. Each element represents specific physical process, and uses a mathematical model to describe the process. There are seven different hydrologic elements in the HMS 2.2.2 version of the program: subbasin, reach, junction, source, sink, reservoir and diversion. Detailed description of these elements is provided in USACE (2001).

Figure 1 shows a schematic of the UTRb created in the HMS BME. The event model uses all available hydrologic elements except for the diversion element. During the calibration, the source and sink elements are used to model actual reservoir operation (not shown in Figure 1), in the final version of the model these elements are replaced by the reservoir element. This is explained in Section II.1.6.

By means of the US Army Corps of Engineers HEC-GeoHMS software (USACE, 2000a), the UTRb was divided initially into 34 subbasins. During the revision of the HEC-GeoHMS output, the subbasins 6 and 7 were joined into one spatial unit since the subbasin 6 was an input into the subbasin 7. The remaining subbasin area of 19.636 km^2 below the station Avon River at Stratford (02GD018) was added to the area of the subbasin 5. The final 33 subbasins represent adequate spatial resolution for semi-distributed event hydrologic modeling of the UTRb (see Figure 1). Details of the hydro-climatic stations and subbasins depicted in Figure 1 are provided in the Project Report II (Cunderlik and Simonovic, 2004). The HEC-HMS event basin model is saved in the file "EVENT.basin" and included in the project "UTRCA_full.hms" (see Appendix I).

Figure 1. HEC-HMS event model representation of the UTRb.

Figure 2 depicts a diagram of the river basin rainfall-runoff processes included in the event model structure.

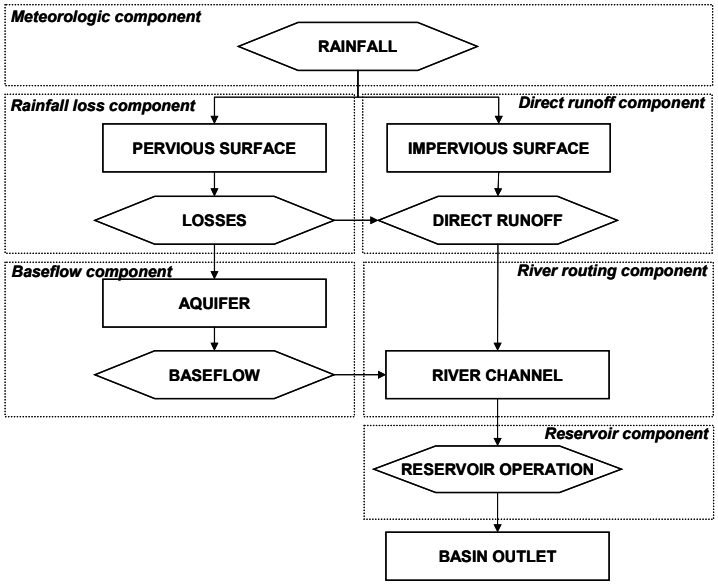

Figure 2. Rainfall-runoff processes included in the event model structure.

The river basin processes showed in Figure 2 are organized into six main components. The meteorologic component is the first computational component of the event model, by means of which rainfall input is spatially (interpolation, extrapolation) and temporally (missing observed values, hypothetical precipitation generation) distributed over the basin (the event model is limited to the analysis of rainfall precipitation). In the next step, spatially and temporally distributed rainfall falls on either pervious surface or on impervious surface. Rainfall from the pervious surface is subject to losses (interception, infiltration, evaporation and transpiration) modeled by the rainfall loss component. The effective rainfall from the loss component contributes to direct runoff and to groundwater flow in aquifers. Rainfall from the impervious surface is not subject to losses and instantly enters the direct runoff component, where is it transformed to overland flow. The movement of water in aquifers is modeled by the baseflow component. Both overland flow and baseflow enter river channels. The translation and attenuation of streamflow in river channels is simulated by the river routing component. Finally, the effect of hydraulic facilities (reservoirs, detention basins) and natural depressions (lakes, ponds, wetlands) is reproduced by the reservoir component of the model. The six component of the event model are characterized in detail in the following sections.

II.1.1 Meteorologic component

The present version (2.2.2) of the HEC-HMS meteorologic component can be used to model rainfall and evapotranspiration processes. In the event modeling, only the first process is usually considered since evapotranspiration can be often negligible in the simulation of short rainfall-runoff events. There are four methods that can be used in the HMS model to distribute observed rainfall over the basin: user hyetograph, user gage weighting, inverse-distance gage weighting, and gridded precipitation. All methods assume that the rainfall is distributed uniformly over the basin area for a given time duration. The last method can be used only in

connection with the gridded soil moisture accounting infiltration method of the HMS distributed basin model.

Among the three remaining methods, the inverse-distance method (IDM) is useful when the observed rainfall data contains missing values that should not be set to zero (USACE, 2001). Since the hourly rainfall records available for the study area contain significant portions of missing values, this method was adopted in the event model. In the IDM, subbasin hyetograph is computed for node locations that are selected to represent the subbasin. A quadrant system is drawn centered on the node (see Figure 3).

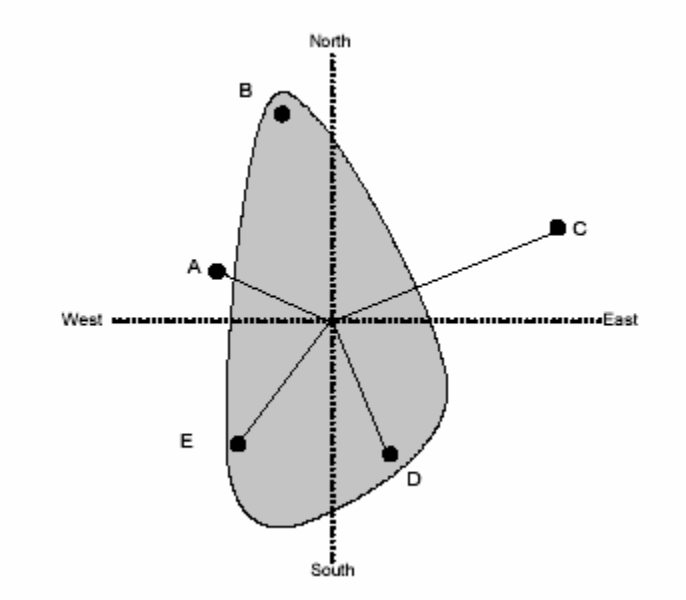

Figure 3. Illustration of the inverse-distance method (USACE, 2000b).

A weight for the closest rainfall gage, that does not have missing data, is computed in each quadrant as the inverse, squared distance between the gage and the node. For example, the weight for the gage C in Figure 3 in the northeastern quadrant of the grid is computed as (USACE, 2000b):

$$w_C = \frac{\frac{1}{d_C^2}}{\frac{1}{d_C^2} + \frac{1}{d_D^2} + \frac{1}{d_E^2} + \frac{1}{d_A^2}} \quad (1)$$

where w_C is the weight assigned to gage C, and d_X is the distance from node to gage X. The closest rainfall gage in each quadrant is determined separately for each time step. The next closest gage in a quadrant is automatically used when the closest gage has missing data (USACE, 2001). When the weights are computed, the node hyetograph ordinate at time t, $p(t)$, is for the example showed in Figure 3 determined as (USACE, 2000b):

$$p(t) = w_A p_A(t) + w_C p_C(t) + w_D p_D(t) + w_E p_E(t) \quad (2)$$

In the meteorologic component created for the event model, one node was defined for each subbasin. Thus, the inverse-distance method interpolates rainfall data into 33 different nodes in the UTRb. The nodes represent subbasins' centroids defined by latitude-longitude coordinates. The meteorologic component is saved in the HEC-HMS file "IDM-NEW.met". The hourly rainfall data, which are the input into the meteorologic component, are stored in the HEC-DSS database "UTRCA.dss" (see Appendix I). The evapotranspiration process is not considered in the meteorologic component of the event UTRb model.

II.1.2 Rainfall loss component

In the HEC-HMS model, all land and water in a river basin is categorized either as directly connected impervious surface or pervious surface (see Figure 2). From directly connected impervious surface all water runs off with no interception, evaporation, transpiration and infiltration. Rainfall on the pervious surface is subject to losses (USACE, 2001). The loss component of the event model is used to compute losses from rainfall (solid precipitation is not modeled by the event model). There are seven methods for estimating losses in the HEC-HMS

model: initial and constant, deficit and constant, Green and Ampt, SCS curve number, soil moisture accounting (SMA), gridded SCS curve number, and gridded soil moisture accounting.

For the modeling of short rainfall-runoff events a detailed accounting of the movement and storage of water through the system is not necessary (e.g. SMA method). The SCS curve number method (Soil Conservation Service, 1972) was initially considered for the event modeling, but the loss rate in this method continuously decreases towards zero, and the method is not sensitive to rainfall intensity (USACE, 2002). Therefore, the event model created for this project uses the initial and constant-rate loss method. According to USACE (2000b), this method has been used successfully in hundreds of studies throughout the USA, is easy to set up and use, and is parsimonious.

In the initial and constant-rate method, the maximum potential rate of rainfall loss, *Lr*, is constant throughout an event. An initial loss, *Li*, represents interception and depression storage. The rainfall excess, Re_t, at time *t*, is then given by (USACE, 2000b):

$$Re_t = \begin{cases} 0 & \text{if } \sum R_i < Li \\ R_t - Lr & \text{if } \sum R_i > Li \text{ and } R_t > Lr \\ 0 & \text{if } \sum R_i > Li \text{ and } R_t < Lr \end{cases} \qquad (3)$$

where R_t is the rainfall depth during the time interval Δt. The initial and constant-rate method includes three parameters, which represent a) basin initial condition, b) physical properties of the basin soils, and c) physical properties of basin land use:

- Initial loss *Li*, [mm],
- Constant loss rate *Lr*, [mm/hr],
- Impervious area of the subbasin *Ai*, [%].

The initial loss parameter defines basin initial condition. If the basin is in a saturated condition, *Li* will approach zero. If the basin is dry, then *Li* will represent the maximum rainfall depth that can fall on the basin with no runoff. The constant loss rate is the ultimate infiltration capacity of the soils (USACE, 2000b).

II.1.3 Direct runoff component

In the direct runoff component, excess rainfall is transformed into direct runoff. The HEC-HMS model allows modeling direct runoff with six different methods: Clark unit hydrograph, Snyder unit hydrograph, SCS unit hydrograph, user-defined unit hydrograph, the ModClark quasi-distributed linear transform, and conceptual kinematic wave model.

USACE (2000b) provides general recommendations for choosing a direct runoff method. These include: availability of information for calibration and parameter estimation, appropriateness of the model assumptions, and user preference and experience. The kinematic wave method is a data intensive conceptual direct runoff model based on a finite difference approximation of the shallow water equations. The modClark method can only be used in a spatially distributed HMS model. Among the remaining four unit hydrograph-based direct runoff methods available in the HEC-HMS, the Clark unit hydrograph (Clark, 1945) is a frequently used technique for modeling direct runoff resulting from individual storm events (Sabol, 1988, Nelson et al., 1999, Straub et al., 2000, Fleming and Neary, 2004). The technique is particularly valuable for unusually shaped watersheds, and for application to watersheds containing several different physiographic areas (Sabol, 1988).

The Clark unit hydrograph method represents two key processes in the transformation of excess rainfall to runoff: translation and attenuation. Translation is based on a synthetic time–area histogram and the time of concentration, *Tc*. The time-area histogram specifies the basin

area contributing to flow at the outlet as a function of time. Attenuation is modeled with a linear reservoir (USACE, 2001). The reservoir represents the aggregated impacts of all basin storage, *St*. The average outflow from the reservoir during a period *t* is (USACE, 2000b):

$$O_t = C_A I_t + C_B O_{t-1} \tag{4}$$

where I_t is the average inflow to storage at time *t*, and C_A and C_B are routing coefficients given by:

$$C_A = \frac{\Delta t}{St + 0.5\Delta t} \quad \text{and} \quad C_B = 1 - C_A \tag{5}$$

where Δt is the computational time step. The required parameters of the Clark method are:

- Time of concentration, *Tc*, [hr],
- Storage coefficient, *St*, [hr].

Both parameters can be estimated via calibration if observed rainfall and streamflow data are available.

II.1.4 River routing component

River routing is a process of computing the travel time and attenuation of water flowing in open channels. There are six methods included in the HEC-HMS model to compute river routing: lag, kinematic wave, modified Puls, Muskingum, Muskingum-Cunge standard section, and Muskingum-Cunge 8-point section.

USACE (2000b) provides a list of issues to be considered when selecting a river routing method. These include: backwater effects, floodplain storage, channel slope and hydrograph characteristics, flow network configuration, subcritical and supercritical flow occurrence, and data availability. After reviewing the technical aspects of the available methods, the modified

Puls method was selected for the event model. This method is the only method that can simulate backwater effects (e.g. caused by dams), can take into account floodplain storage, and can be applied to a broad range of channel slopes. The modified Puls method is also recommended for hydrologic river routing in many North American regions (see e.g. Hydrology Standards, 1996)

The modified Puls method models river reach as a series of cascading level pools with a user-specified storage-outflow relationship. The method is based on a finite difference approximation of the continuity equation, coupled with an empirical representation of the momentum equation. The continuity equation has the form (USACE, 2000b):

$$\left(\frac{S_t}{\Delta t}+\frac{O_t}{2}\right)=\left(\frac{I_{t-1}+I_t}{2}\right)+\left(\frac{S_{t-1}}{\Delta t}-\frac{O_{t-1}}{2}\right) \qquad (6)$$

where I_t is the inflow at time t, O_t is the outflow at time t, Δt is the computational time step, and S_t is the storage in channel at time t. Equation (6) has two unknown parameters at each time t: S_t and O_t. Therefore, a functional relationship between storage and outflow is necessary to solve Equation (6). The required parameters of the method are:

- Storage-outflow curve, *SO*, [storage, *S*, [1000×m^3], outflow, *O*, [m^3s^{-1}]],
- Number of subreaches, *Si*, [#],
- Initial condition, *Ri*, [outflow or outflow=inflow].

The storage-outflow curve is divided by the number of subreaches and used with the initial condition for all subreaches.

There are 21 river reaches included in the event model structure. For each reach, calibrated storage-outflow curves were provided by the Upper Thames River Conservation Authority (UTRCA hereafter). These curves were not subsequently modified in this model, and

hence, the river routing component was not subject to calibration. The storage-outflow curves for all 21 reaches used in the model are provided in Appendix IIIa. In all reach components, the number of subreaches is set to one, and the initial condition is modeled as outflow=inflow. The river reaches have 3(4)-digit unique identification numbers assigned by the HEC-GeoHMS software, which are preceded by the letter "R" (e.g. R333 or R3333).

II.1.5 Baseflow component

Baseflow is a flow of water that returns to the stream or land surface from groundwater aquifers. In the modeling of short rainfall-runoff events baseflow does not usually play significant role in the formation of flood hydrographs. Nevertheless, the baseflow component is important for modeling recession limbs of flood hydrographs as well as for more accurate estimation of flood volumes. The HEC-HMS model includes three methods for modeling baseflow: constant monthly, linear reservoir, and recession. The constant monthly method is a simple approach that uses a constant baseflow at all simulation time steps falling within a particular month. The linear reservoir method can only be used in conjunction with the SMA loss method. The recession method uses an exponentially declining baseflow developed from standard baseflow separation techniques.

In this project the recession method was adopted for modeling baseflow. The method is suitable for basins where the volume and timing of baseflow is strongly influenced by precipitation events (USACE, 2000b). The recession method is also often used as a technique for baseflow separation and groundwater recharge estimation (Arnold et al., 2000).

In the exponential recession model the baseflow at time t, B_t, is defined as:

$$B_t = Bi \cdot Rc^t \tag{7}$$

where *Bi* is the initial baseflow at time t_0, and *Rc* is the exponential decay constant. The parameters of the recession method are:

- Initial baseflow, *Bi*, [m^3s^{-1} or $m^3s^{-1}km^{-2}$],
- Recession constant, *Rc*, [-]; $Rc \in \langle 0, 1 \rangle$,
- Threshold, *Td*, [m^3s^{-1} or ratio-to-peak].

The initial flow is equal to the baseflow at the beginning of the simulation. The recession constant describes the rate of baseflow decay. It is the ratio of baseflow at time *t* to the baseflow at time *t*-1. The threshold is the point on the hydrograph where baseflow replaces overland flow as the source of flow from the basin (USACE, 2001).

II.1.6 Reservoir component

The HEC-HMS reservoir component represents uncontrolled water body modeled by monotonically increasing storage-outflow function. The storage-outflow relationship can be specified from three available methods:

- Storage-outflow,
- Elevation-storage-outflow,
- Elevation-area-outflow.

Outflow from the reservoir is computed with the level-pool routing model. The model solves recursively the following one-dimensional approximation of the continuity equation (USACE, 2000b):

$$I - O = \frac{\Delta S}{\Delta t} \tag{8}$$

where I (O) is the average inflow (outflow) during the time interval Δt, and ΔS is the storage change during this interval.

In the elevation-storage-outflow method, outflow is computed from the storage-outflow data, and then, elevation is computed from the elevation-storage data. Required parameters for this method are:

- Initial condition, *Di*, [inflow=outflow, elevation [m], storage [$1000 \times m^3$] or outflow [$m^3 s^{-1}$]],
- Elevation-storage-outflow relationship, *ESO*, [elevation, *E*, [m], storage, *S*, [$1000 \times m^3$], outflow, *O*, [$m^3 s^{-1}$].

The present version of the HEC-HMS reservoir component assumes that the outflow is a function of the upstream water-surface elevation. This implies that the reservoir component cannot model gated structures in which the gate operation is not uniquely a function of storage (USACE, 2000b). In some cases, the outflow from an uncontrolled reservoir component may significantly differ from actual water release reflecting specific water management practices or operation rules. Situation-specific reservoir operations cannot be captured in a simple elevation-storage-outflow relationship. Therefore, to properly calibrate the contribution of ungaged subbasins located below reservoirs, the reservoir components were replaced during the calibration by a set of source and sink components. The reservoir inflow produced in the subbasins upstream of the reservoir flows into the sink component. The source component then produces outflow that is identical with the actual controlled dam release for the specific time period. Once the ungaged subbasins located below the reservoir are calibrated, the pair of source-sink components is replaced by the reservoir component. Thus, the final version of the model includes only reservoir components.

There are three reservoirs included in the event model: Wildwood, Fanshawe and Pittock. The Wildwood reservoir is constructed on the Trout Creek, upstream of the Town of St. Marys. The dam was completed in 1965, and is designed for both flood control and flow augmentation purposes. The dam can reduce flood flows on Trout Creek by up to 95%, and on the North Thames below St. Marys by 10%. The Fanshawe reservoir was constructed on the Upper Thames River in 1950-1952. The primary purpose of the reservoir is to assist in flood control efforts to reduce flood damage in the City of London. The dam can reduce flood peaks downstream by up to 40%. The construction of the Pittock dam on the South Thames River started on in 1964 and was completed in 1967. The main functions of the dam are flood protection of downstream communities and improvement of the base flows during the drier summer months (UTRCA, 2003).

The reservoir outflow data used in the source components are stored in the project file "EC dam qs.dss". The parameters of the elevation-storage-outflow method for each reservoir provided by the UTRCA were not subject to calibration, and are given in Appendix IIIb.

II.2 Event model calibration

II.2.1 Calibration procedure

Model calibration is a systematic process of adjusting model parameter values until model results match acceptably the observed data. The quantitative measure of the match is described by the objective function. In the precipitation-runoff models, this function measures the degree of variation between computed and observed hydrographs. The calibration process finds the optimal parameter values that minimize the objective function. Further, the calibration estimates some model parameters that cannot be estimated by observation or measurement, or have no direct physical meaning. Calibration can either be manual or automated (optimization). Manual calibration relies on user's knowledge of basin physical properties and expertise in hydrologic

modeling. In the automated calibration model parameters are iteratively adjusted until the value of the selected objective function is minimized.

Madsen et al. (2002) provides a comparison of different strategies for calibration of rainfall-runoff models. Novel approaches to rainfall-runoff model calibration can be found e.g. in Yu and Yang (2000), Madsen (2000), or Eckhardt and Arnold (2001).

The latest version of the HEC-HMS model includes optimization manager that allows automated model calibration. There are five objective functions available in the optimization manager (USACE, 2000b):

- Peak-weighted root mean square error (*PWRMSE*). Using a weighting factor, the PWRMSE measure gives greater overall weight to error near the peak discharge:

$$PWRMSE = \sqrt{\frac{\sum_{t=1}^{N}\left(Q_O(t)-Q_M(t)\right)^2 \frac{Q_O(t)+Q_A}{2Q_A}}{N}} \quad ; \quad Q_A = \frac{1}{N}\sum_{t=1}^{N} Q_O(t) \tag{9}$$

  where Q_O (Q_M) is the observed (modeled) flow at time t, and Q_A is the average observed flow.

- Sum of squared residuals (*SSR*). The *SSR* measure gives greater weight to large errors and lesser weight to small errors (USACE, 2001):

$$SSR = \sum_{t=1}^{N}\left(Q_O(t)-Q_M(t)\right)^2 \tag{10}$$

- Sum of absolute residuals (*SAR*). The *SAR* function gives equal weight to both small and large errors:

$$SAR = \sum_{t=1}^{N}\left|Q_O(t)-Q_M(t)\right| \tag{11}$$

- Percent error in peak flow (*PEPF*). The *PEPF* measure only considers the magnitude of computed peak flow and does not account for total volume or timing of the peak:

$$PEPF = 100\left|\frac{Q_O(peak) - Q_M(peak)}{Q_O(peak)}\right| \tag{12}$$

- Percent error in volume (*PEV*). The *PEV* function only considers the computed volume and does not account for the magnitude or timing of the peak flow:

$$PEV = 100\left|\frac{V_O - V_M}{V_O}\right| \tag{13}$$

where V_O (V_M) is the volume of the observed (modeled) hydrograph.

Two search methods are available in the HEC-HMS model for minimizing the objective functions defined above (USACE, 2001):

- The univariate gradient method (UG). The UG method evaluates and adjusts one parameter at a time while holding other parameters constant.
- The Nelder and Mead method (NM). The NM method uses a downhill Simplex to evaluate all parameters simultaneously and determine which parameter to adjust.

Complete technical description of these search methods is provided in (USACE, 2000b).

Initial values of parameters that are subject to automated calibration are required to start an optimization process. The HEC-HMS model has default hard constraints that limit the range of optimized values within reasonable physical intervals. Values within hard constraints do not cause numeric instabilities or errors in computations. Soft constraints can be defined by the user and allow limiting the range of values within the wider range of hard constraints.

The calibration procedure adopted in the event hydrologic modeling involved a combination of both manual and automated calibrations. The manual calibration preceded the

optimization to ensure that a physically-meaningful set of initial parameters is used in the model. The parameter values were based on available physical data from the study area. The manual calibration was used to determine the soft limits for the automated optimization. The optimization then tuned-up the model parameters within the soft limits obtained by manual calibration. The univariate gradient search method was applied to optimize the set of model parameters by minimizing the peak-weighted root mean square error objective function. The optimization output was assessed by means of the following five tools:

1. Flow comparison graph. The HEC-HMS flow comparison graph shows the modeled and observed hydrographs at the optimization location. An example of this type of graph is given in Figure 4.

2. Scatter graph. The HEC-HMS scatter graph is a plot of the modeled flow value for each time step against the observed flow for the same step. The straight line on the plot represents equality of calculated and observed flow and assists in identifying model bias. Points plotted above the line represent streamflow that is over-predicted by the model, and points below the line represent under-predicted stremflow. The spread of points around the line provides an indication of the fit of the model. If the spread is large, then the random errors in the prediction are large relative to the magnitude of the flows. Large random errors imply poor model performance (USACE, 2001). Figure 5 shows an example of scatter graph.

3. Residual graph. The HEC-HMS residual graph indicates how prediction errors are distributed throughout the duration of the simulation. By inspecting this graph parameters that need further effort for estimation can be identified (e.g. if the greatest residuals are grouped at the start, the initial loss parameter may have been poorly chosen (USACE, 2001). Residuals of a well calibrated model should be grouped closely

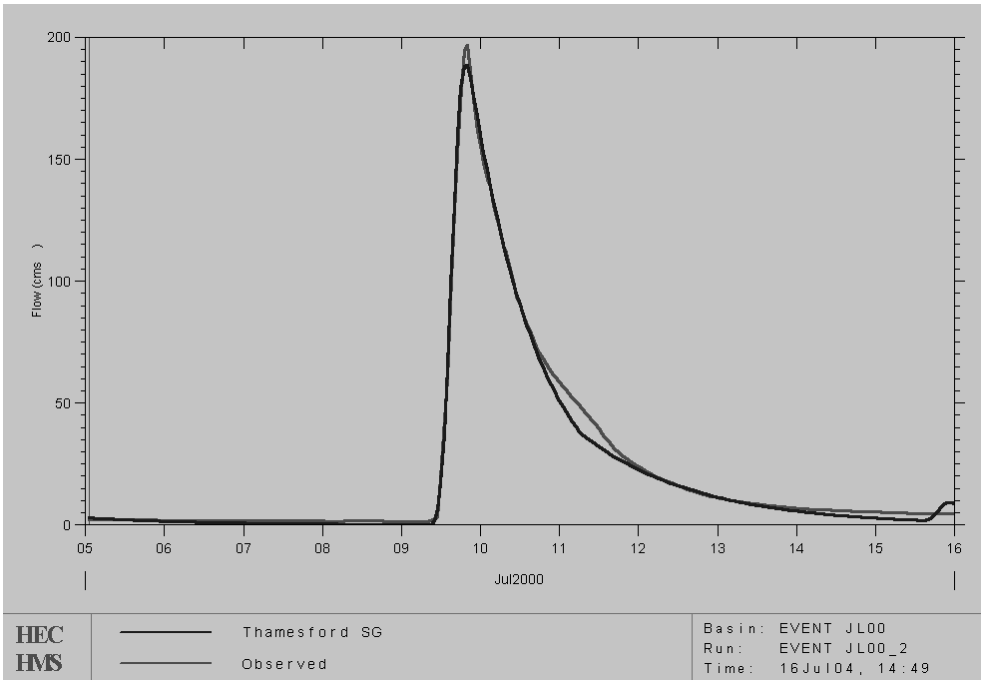

Figure 4. An example of the HEC-HMS flow comparison graph (The July 2000 event at Thamesford).

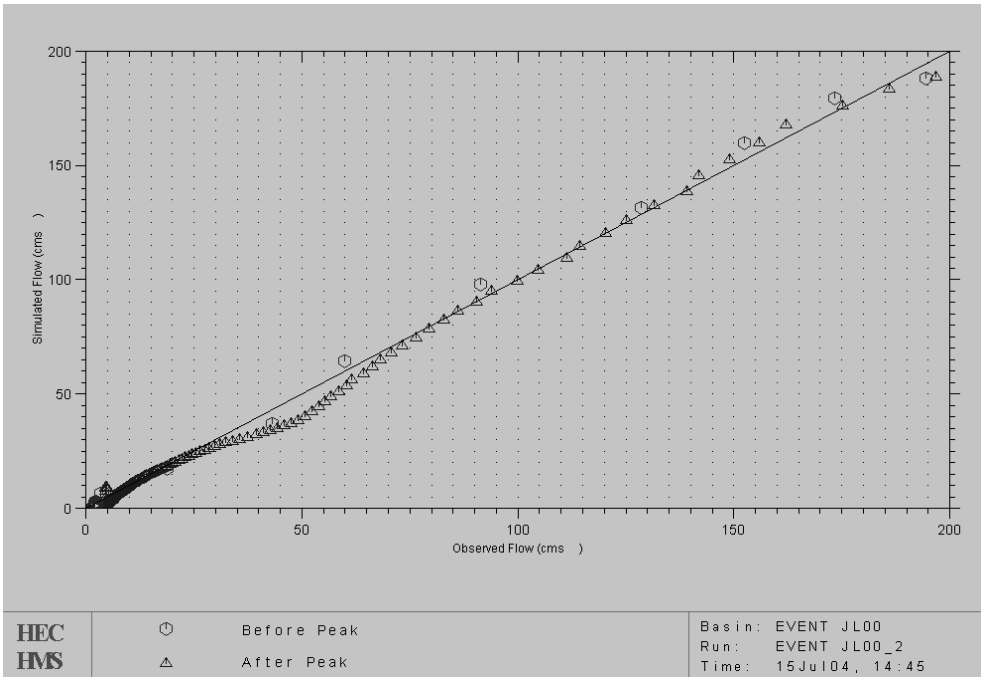

Figure 5. An example of the HEC-HMS scatter graph (The July 2000 event at Thamesford).

to the x-axis with no systematic variation. An example of residual graph is shown in Figure 6.

4. Objective function graph. The HEC-HMS objective function graph shows the value of the objective function at the end of each iteration. The graph can be used to evaluate the convergence of the solution. A monotonically decreasing coordinates suggest that a global minimum of the objective function was found during the optimization. An example of objective function graph is given in Figure 7.

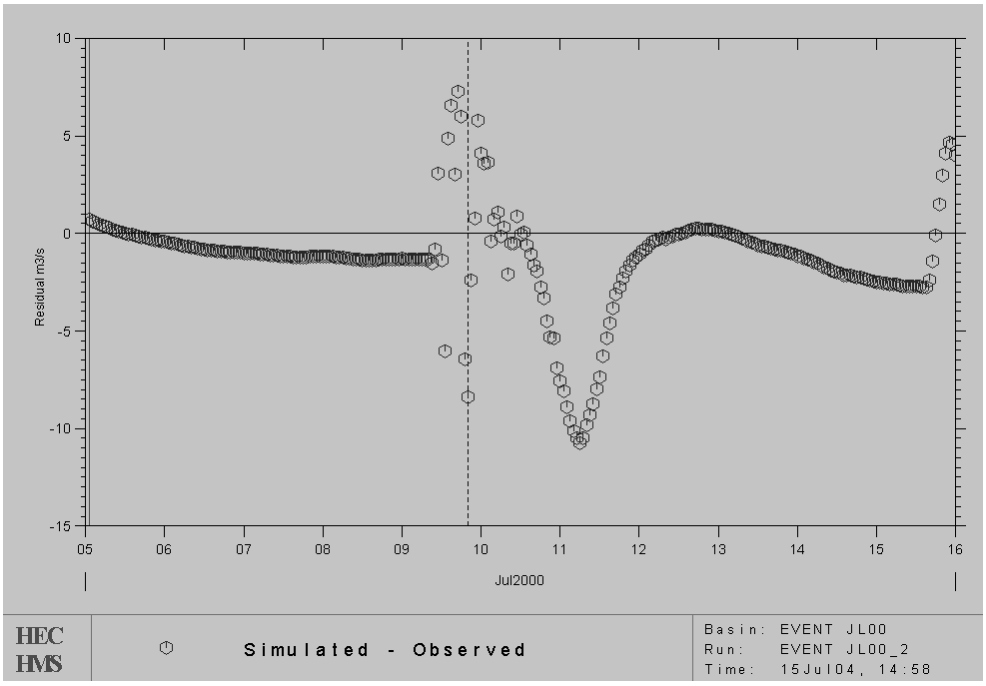

Figure 6. An example of the HEC-HMS residual graph (The July 2000 event at Thamesford).

5. Statistical goodness-of-fit measures. A comprehensive summary of statistical performance measures used for the evaluation of the performance of hydrologic models is given by Sorooshian et al. (1983). Here, six different statistical measures were evaluated at each gaged location to assess the performance of the model. The first measure was the percent error in peak as defined in Equation (12), the second measure the percent error in volume (Equation (13)), the third measure the linear lag-0 cross-correlation coefficient, the fourth measure the relative bias, the fifth measure relative root mean squared error, and the last measure was the relative peak weighted

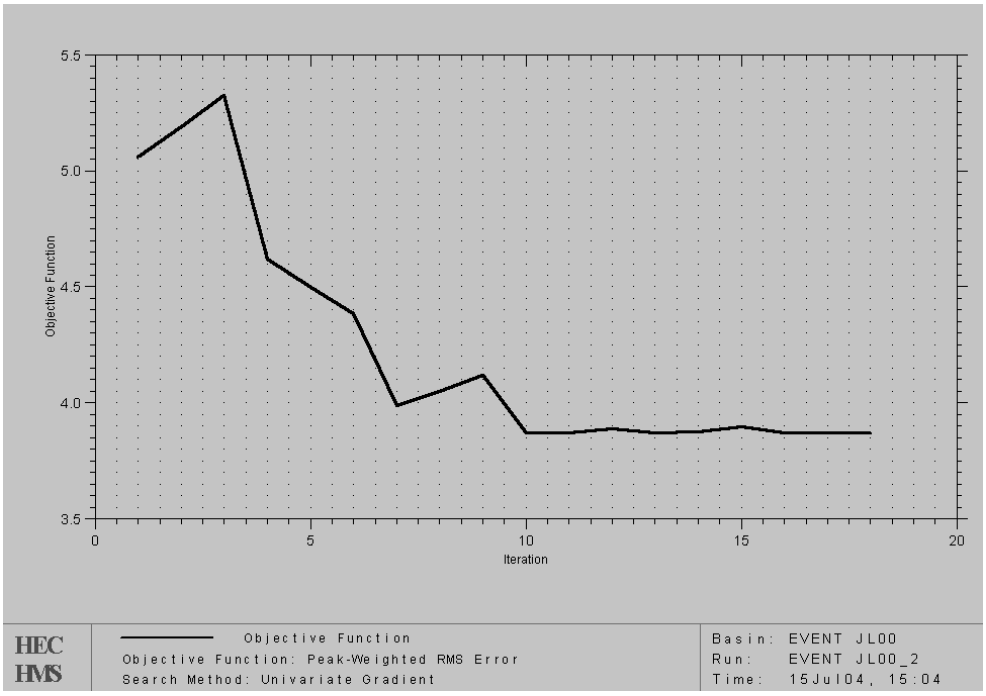

Figure 7. An example of the HEC-HMS objective function graph (The July 2000 event at Thamesford).

root mean squared error (Equation (9) modified to non-dimensionality). The lag-0 cross correlation coefficient, *CORR*, was calculated as:

$$CORR = \frac{\sum_{t=1}^{N}\left(O_t - \overline{O}\right)\times\left(M_t - \overline{M}\right)}{\sqrt{\left[\sum_{t=1}^{N}\left(O_t - \overline{O}\right)^2 \times \sum_{t=1}^{N}\left(M_t - \overline{M}\right)^2\right]}} \tag{14}$$

where O_t (M_t) is the observed (modeled) flow at time t, and $\overline{O}$ ($\overline{M}$) is the average observed (modeled) flow during the calibration period. The relative bias, *RBIAS,* and the relative root mean squared error, *RRMSE,* were calculated as:

$$RBIAS = 100 \times \frac{1}{N}\sum_{t=1}^{N}\frac{M_t - O_t}{O_t} \quad ; \quad RRMSE = 100 \times \sqrt{\frac{1}{N}\sum_{t=1}^{N}\left(\frac{M_t - O_t}{O_t}\right)^2} \tag{15}$$

where N is the number of streamflow ordinates and the meaning of the remaining symbols is the same as in Equation (14).

Each optimization output was assessed according to the above described criteria. If the output was acceptable, the calibration process was completed, otherwise the initial optimization parameters were altered and the process repeated. The calibration process started with hydrometric stations that represented outlets of single subbasins. Once these stations were calibrated, hydrometric stations with more than one contributing subbasins followed. At this stage the parameters of ungaged contributing subbasins were also estimated. In the final stage, individually calibrated subbasins were linked into one model and the calibration finalized.

II.2.2 Calibration results

Two rainfall-runoff events (July 2000 and November 2003) were chosen for the calibration of the UTRb event hydrologic model (Cunderlik and Simonovic, 2004). The July 2000 event represents convective rainfall-driven flood, whereas the November 2003 event represents frontal rainfall induced flood. During the manual calibration it was found that one set of model parameters cannot be used for simulating both types of events with acceptable accuracy. The autumn type of rainfall event is characterized by longer duration and lower intensity than the summer type of rainfall event. Results from the manual calibration showed that in autumn, more detailed accounting of the movement and storage of water through the system is necessary, which cannot be achieved by the structure of the event model (the initial and constant loss method is not suitable for modeling longer rainfall events and no-rainfall periods). Therefore a decision was made to model autumn rainfall events with the continuous version of the model (see Section III).

The July 2000 event is exceptionally suitable for rainfall-runoff calibration both in terms of its magnitude and spatial extent. The July 2000 storm produced in most subbasins well defined, uni-modal flood hydrographs. In those subbasins where observed streamflow data were missing during this period or the subbasins were hit by the July 2000 event only partially, other rainfall

events had to be used for the calibration. The August 2000 and September 2000 verification events were used to crosscheck the values of model parameters at several steps of the calibration. Table 1 lists the subbasins, for which rainfall events other than the July 2000 event were used for model calibration.

Table 1. Rainfall-runoff events used for the calibration of the HEC-HMS event model.

Subbasin	**Calibration event**
17	July 1992
20	July 1987, July 1990
25	May 2003, July 2003
27	August 1992
32	July 2003
34	September 2002
All other	July 2000

The performance of the event model is evaluated at five locations in the UTRb. The locations were selected to represent different physiographic subregions of the UTRb, as well as to reflect different subbasin areas and streamflow regimes. The evaluation of the model performance at all gaged locations in the UTRb would involve exceptionally intensive data processing, which is beyond the scope of the project. Table 2 lists the selected five hydrometric stations and Figure 8 shows the location of the stations on the map of the UTRb.

Table 2. Hydrometric stations selected for demonstrating the performance of the event model.

ID	**Name**	**Area [km^2]**
02GD014	North Thames River near Mitchell	319
02GD015	North Thames River near Thorndale	1,340
02GD004	Middle Thames River at Thamesford	306
02GD021	Thames River at Innerkip	149
02GE002	Thames River at Byron	3,110

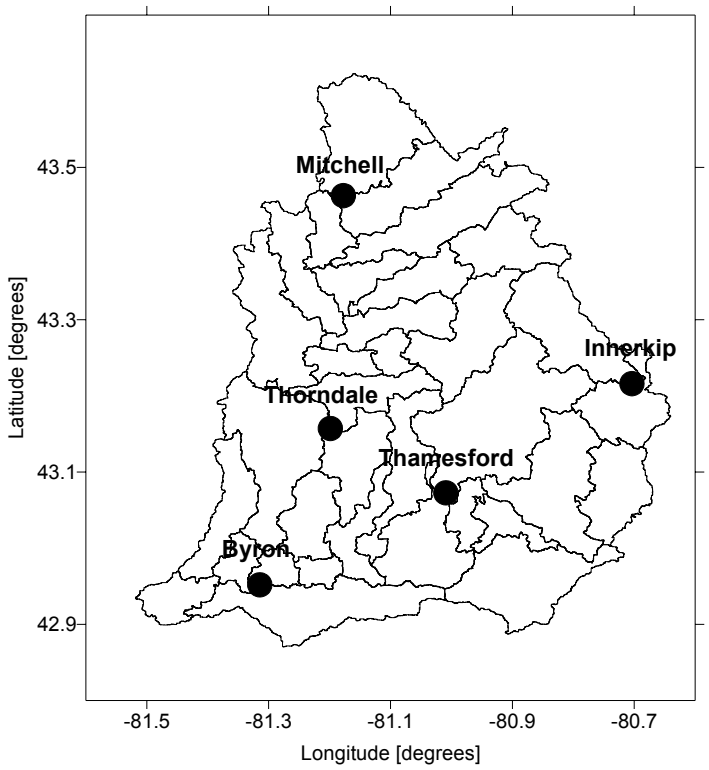

Figure 8. Location of hydrometric stations selected for demonstrating the performance of the event model.

Figure 8 and Table 2 show that the selected hydrometric stations are located at all three branches of the Thames River. The station 02GE002 (Thames River at Byron) is the last gaged station at the Thames River in the UTRb, and is considered as the UTRb outlet station for the purposes of the overall evaluation of the model performance.

Figures 9-13 compare the modeled and observed streamflow hydrographs at the selected locations listed in Table 2. In all five cases the event model fits the observed hydrographs very well. All peak flows are captured with high accuracy except for the peak at Byron, where the modeled peak occurred earlier and was higher than the observed. The observed peak at Innerkip, has for not known, reason a bi-modal structure (perhaps observation or data processing error; also the rapid recession does not resemble a typical, natural behavior), but the model captured the first peak well. The rising parts of the hydrographs are generally better

modeled than the recession limbs; this can be attributed to the limited ability of the event model to simulate longer dry-weather periods.

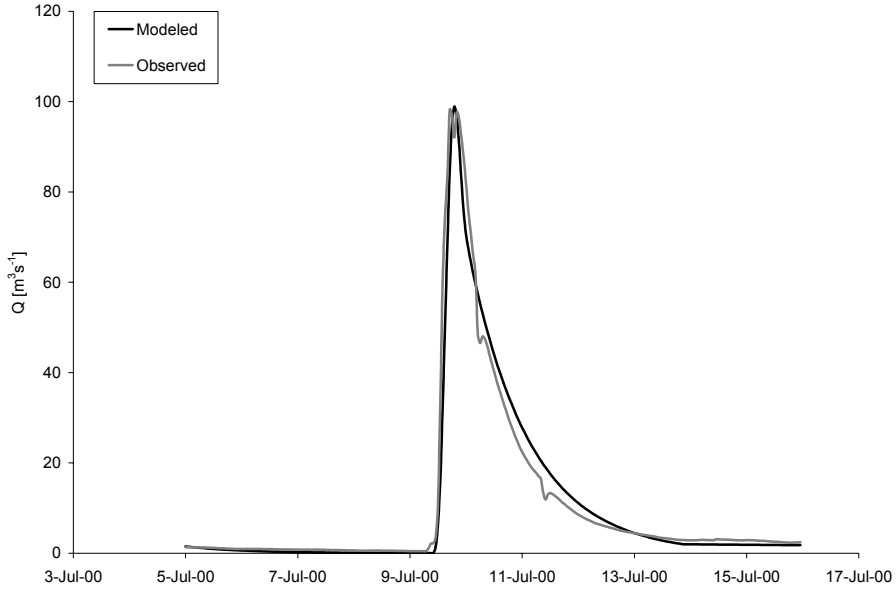

Figure 9. Observed and modeled hydrographs for the July 2000 event at Mitchell.

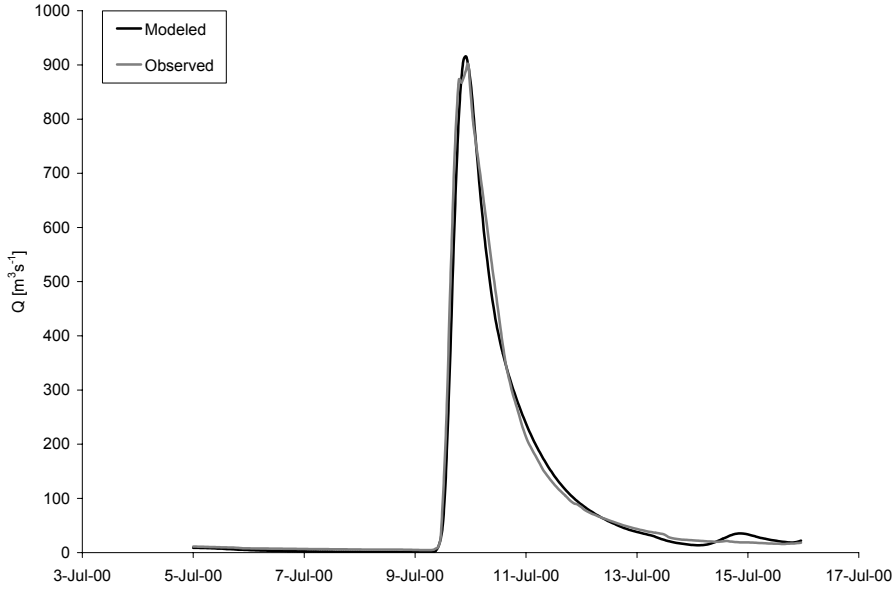

Figure 10. Observed and modeled hydrographs for the July 2000 event at Thorndale.

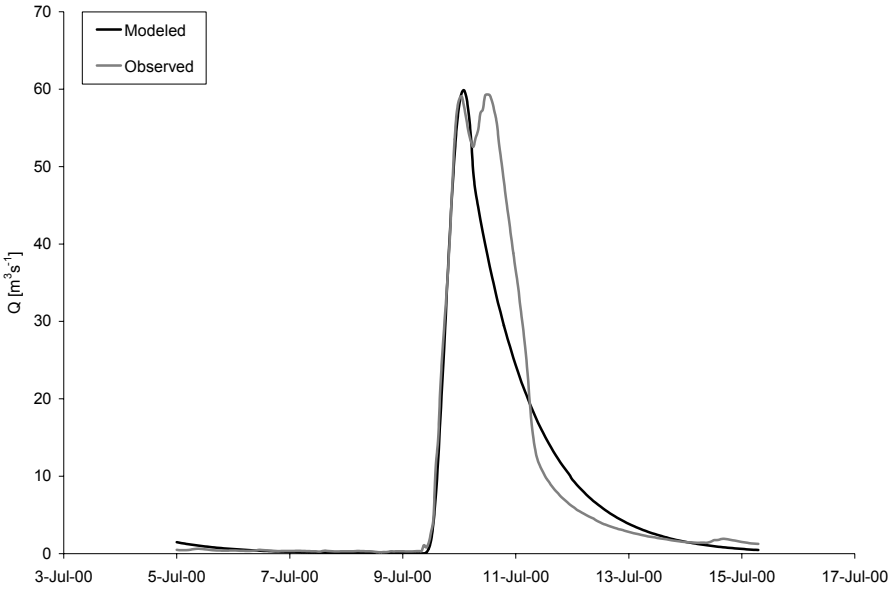

Figure 11. Observed and modeled hydrographs for the July 2000 event at Innerkip.

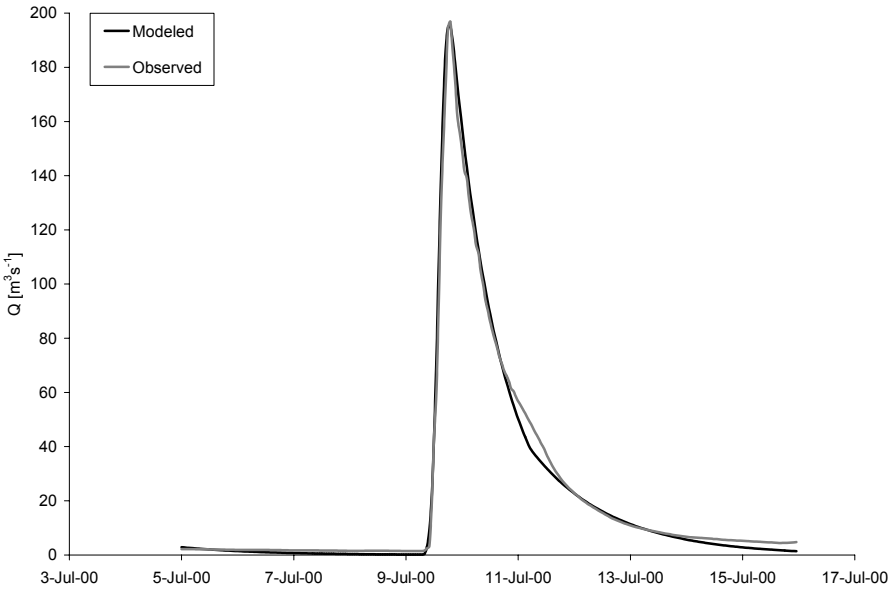

Figure 12. Observed and modeled hydrographs for the July 2000 event at Thamesford.

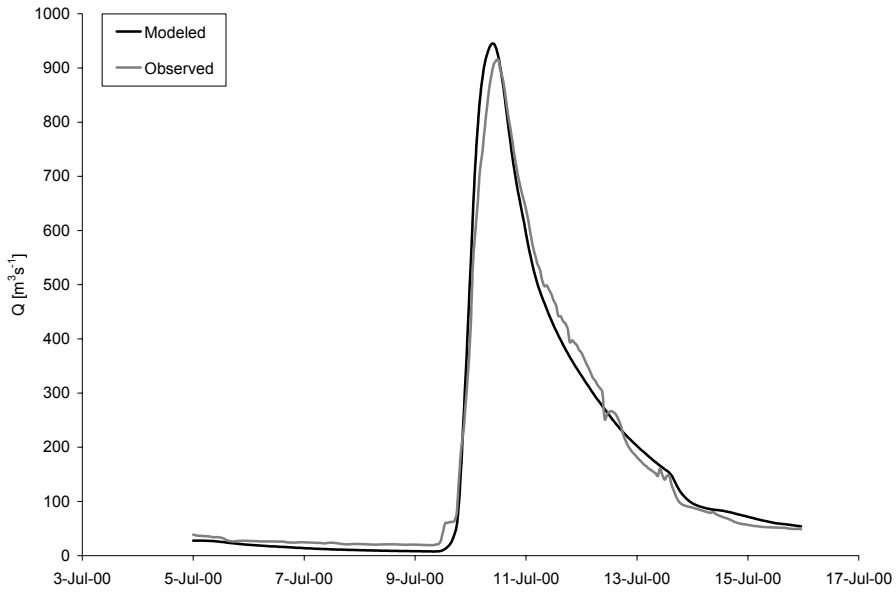

Figure 13. Observed and modeled hydrographs for the July 2000 event at Byron.

Table 3 compares the statistical performance measures obtained for each location. The percentage error in peak flow, *PEPF*, is in all locations very low, in three cases even below 1%. The value of this measure at Byron (3.2%) confirms that the peak flow at this location was not very well captured by the model, however the value is still acceptably low. The second measure, the percentage peak in volume, *PEV*, is high at Innerkip (12.8%), due to the questionable, bi-modal observed peak. In the remaining locations *PEV* is below 4%. The lag-0 cross-correlation coefficient, *CORR*, given in the fourth column in Table 3 suggests a very good correspondence between the modeled and observed hydrograph ordinates at all evaluated locations.

Table 3. Statistical performace measures for the selected locations in the UTRb for the July 2000 event.

Location	***PEPF* [%]**	***PEV* [%]**	***CORR* [-]**	***RBIAS* [%]**	***RRMSE* [%]**	***RPWRMSE* [%]**
Mitchell	0.739	1.518	0.983	-28.530	48.731	38.204
Thorndale	1.618	3.885	0.995	-21.740	46.220	34.877
Innerkip	0.963	12.772	0.963	-8.378	59.328	48.155
Thamesford	0.950	2.781	0.998	-28.316	45.294	34.061
Byron	3.211	1.405	0.992	-15.047	32.076	25.314

The last three performance measures given in Table 3 require a cautious evaluation. The relative bias, *RBIAS*, is negative in all cases, ranging from -8% (Innerkip) up to -28% (Mitchell, Thamesford). The relative *RMSE* values are even higher, up to 60% at Innerkip. The relative *RMSE* results are improved if the measure is weighted by the peak, *PWRMSE* (48% at Innerkip). The rather high values of all three measures are caused by the limited ability of the event model to simulate low flows preceding and succeeding flood events. This is demonstrated in Figure 14, which shows the *RBIAS* measure for the July 2000 event at Thamesford as a function of time. The *RBIAS* during the peak hydrograph (July 10-13) is actually within the range of ± 20%. It is the period of low flows (before and after the peak), where the model systematically underestimates the observed streamflow. High relative errors in low flows consequently lead to high values of all relative performance measures.

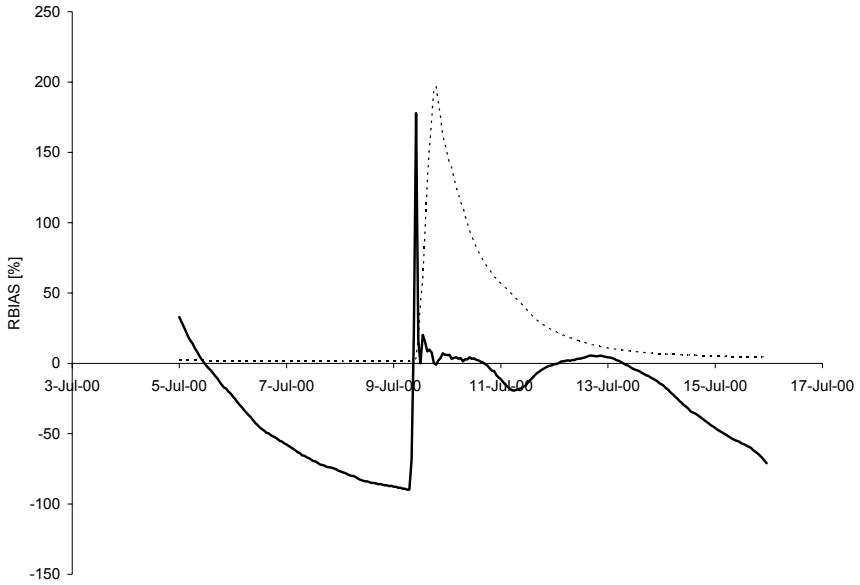

Figure 14. *RBIAS* of the model results for the July 2000 event at Thamesford. The thin dashed line outlines the observed hydrograph.

Figure 15 depicts the errors from Figure 14 in absolute terms. The absolute *BIAS* in the period of low flows is negligible, within the range of ± 2.5 m^3s^{-1}. The maximum *BIAS* occurred during the peak hydrograph (up to ± 15 m^3s^{-1}).

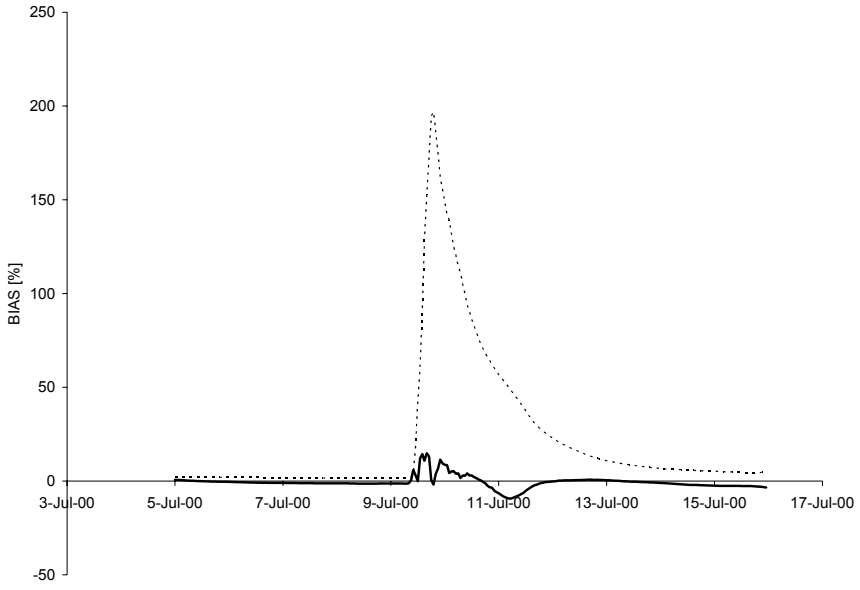

Figure 15. *BIAS* of the model results for the July 2000 event at Thamesford. The thin dashed line outlines the observed hydrograph.

The sensitivity of relative performance measures on the parts of hydrograph which are less important in the event modeling is a feature that has to be accounted for in the overall evaluation of the event model. On the other hand, the use of relative measures is the only approach for comparing model performance at stations with different streamflow magnitudes.

II.3 Event model verification

II.3.1 Verification procedure

Model verification is a process of testing model ability to simulate observed data other than those used for the calibration, with acceptable accuracy. During this process, calibrated model parameters are not subject to change, their values are kept constant. The quantitative

measure of the match is again the degree of variation between computed and observed hydrographs.

In the verification procedure adopted in this project, most parameters of the event model were kept constant; except for the parameters describing basin initial conditions (initial loss, *Li*, and initial baseflow, *Bi*). The Clark's time of concentration, *Tc*, was also deemed to be event dependent, since large, intensive storms can quickly saturate the basin, which then acts as if it is impervious (the larger, more intensive is the event, the shorter is the time of concentration). However, the time of concentration depends not only on the magnitude of the event, but also on the basin initial conditions. The verification output was assessed by flow comparison graphs, scatter graphs, residual graphs, and the statistical goodness-of-fit measures described in Section II.2.1.

II.3.2 Verification results

The September 2000 and the November 2001 rainfall-runoff events were chosen for the verification of the single-event hydrologic model (Cunderlik and Simonovic, 2004). Both events had fairly large spatial coverage in the UTRb although not as large as the exceptional July 2000 event. Since one set of parameters of the event HMS model cannot be used for simulating both summer convective and autumn frontal rainfall types of events, the November 2001 autumn event was replaced by the August 2000 event. The verification of the event model involved running the model calibrated on the July 2000 event on the August and September 2000 events. Figures 16-21 show flow comparison graphs for both events at the selected gaged locations.

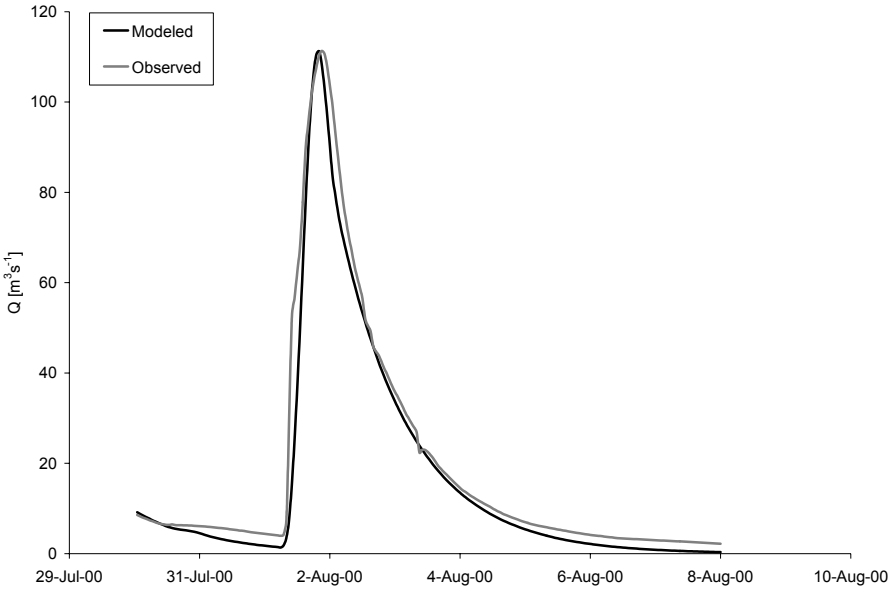

Figure 16. Observed and modeled hydrographs for the August 2000 event at Mitchell.

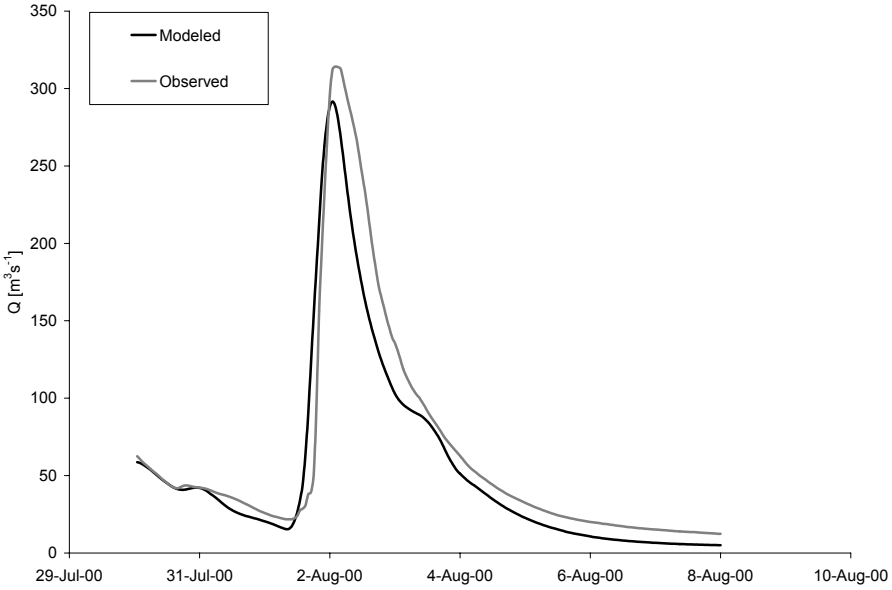

Figure 17. Observed and modeled hydrographs for the August 2000 event at Thorndale.

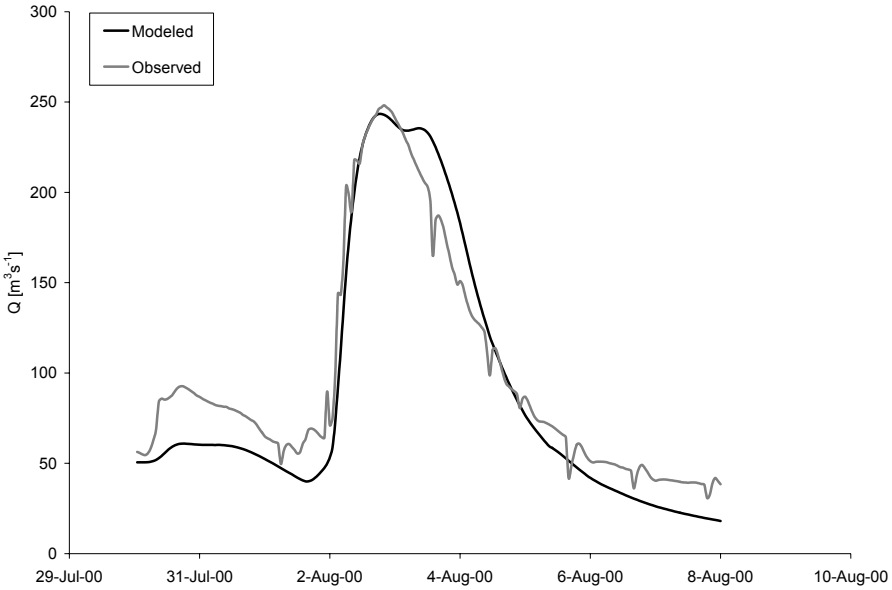

Figure 18. Observed and modeled hydrographs for the August 2000 event at Byron.

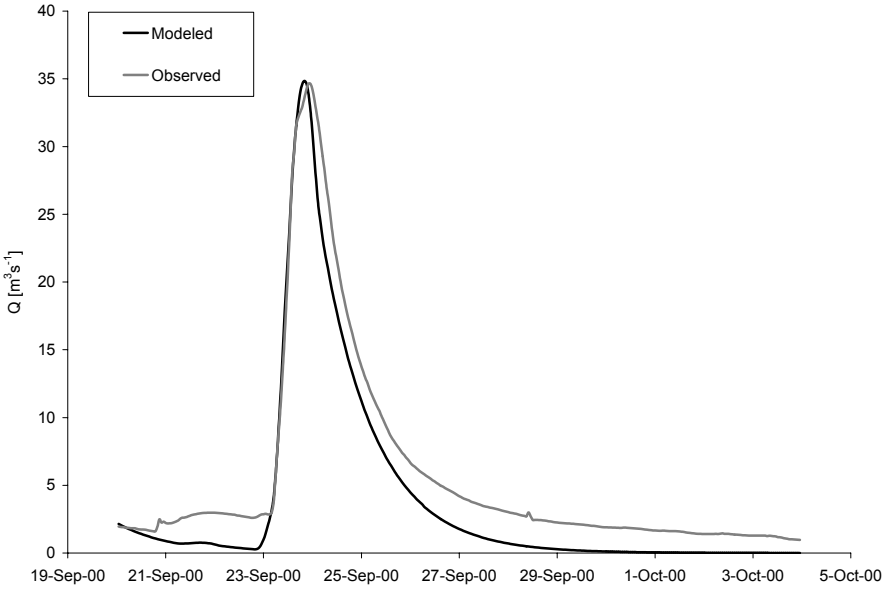

Figure 19. Observed and modeled hydrographs for the September 2000 event at Mitchell.

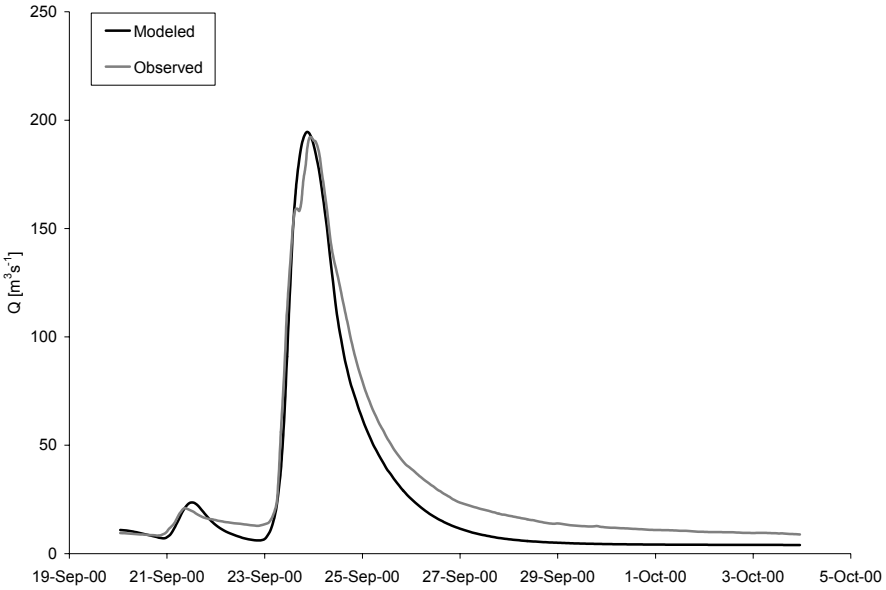

Figure 20. Observed and modeled hydrographs for the September 2000 event at Thorndale.

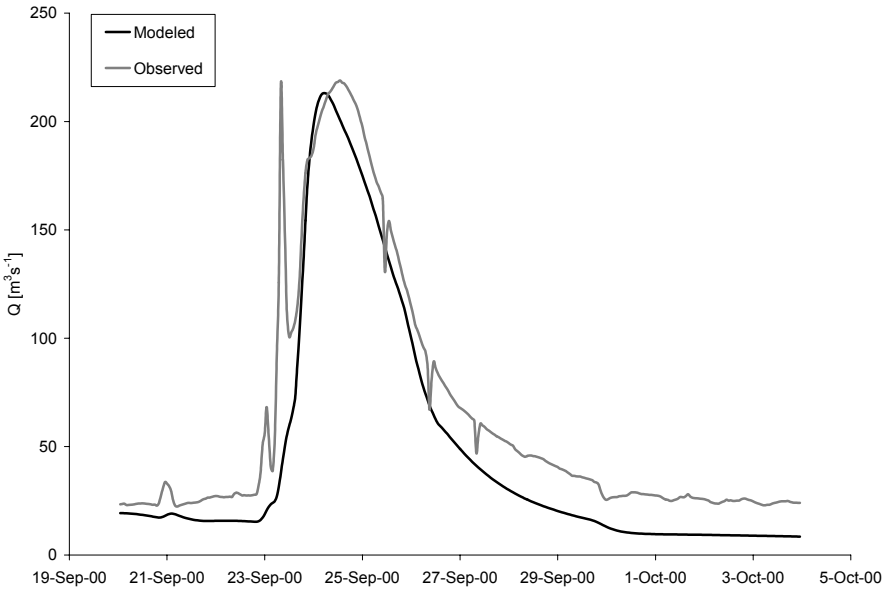

Figure 21. Observed and modeled hydrographs for the September 2000 event at Byron.

Figure 16 depicts the modeled and observed hydrographs generated by the August 2000 event at Mitchell. The overall fit of the model is very well; only in the recession parts of the hydrograph before and after the peak, the modeled hydrograph tends to recede more quickly.

Figure 17 compares the modeled and observed hydrographs generated by same rainfall event at Thorndale. The model fit well the timing and shape of the peak hydrograph, but the peak magnitude was underestimated by 6%. Figure 18 compares the observed and modeled hydrographs for the August 2000 event at Byron. The observed hydrograph is rather irregular; the fluctuations are caused by water releases at the Fanshawe dam. The fit of the model is good, except for the recession limb after August 5 2000 that tends to fall more quickly. The higher observed flow at the beginning of the event between July 30 and August 1 2000 was again caused by dam operation. Figure 19 shows the model performance in the simulation of the September 2000 event at Mitchell. The peak is well fitted, the recession parts of the modeled hydrograph preceding and succeeding the peak are underestimated compared to the observed data. Figure 20 compares the observed and modeled hydrographs for the September 2000 event at Thorndale. Again, the peak hydrograph is very well captured, except for the recession part that tends to recede more quickly. Figure 21 depicts the September 2000 event at Byron. The modeled peak occurred 5 hours earlier than the observed peak. The falling limb of the hydrograph is again underestimated. Table 4 compares the statistical performance measures at each selected location for the August and September 2000 events.

Table 4. Statistical performance measures for the selected locations in the UTRb for the August and September 2000 events.

Aug-00	***PEPF* [%]**	***PEV* [%]**	***CORR* [-]**	***RBIAS* [%]**	***RRMSE* [%]**	***RPWRMSE* [%]**
Mitchell	0.063	14.466	0.987	-32.413	42.245	34.176
Thorndale	7.204	14.799	0.959	-22.046	40.975	36.522
Innerkip	26.921	15.833	0.978	-31.326	46.470	38.973
Thamesford	9.844	45.757	0.553	-51.846	69.056	66.007
Byron	1.937	8.743	0.977	-17.101	26.166	23.994
Sep-00	***PEPF* [%]**	***PEV* [%]**	***CORR* [-]**	***RBIAS* [%]**	***RRMSE* [%]**	***RPWRMSE* [%]**
Mitchell	0.659	32.377	0.990	-64.586	73.185	61.228
Thorndale	1.333	22.686	0.989	-39.674	47.112	40.716
Innerkip	4.902	9.831	0.944	-49.295	68.057	55.821
Thamesford	7.417	56.604	0.858	-70.859	77.730	71.851
Byron	2.686	26.919	0.967	-40.230	45.421	40.740

The percentage error in peak flow (*PEPF*) is for both events below 10% except at Innerkip for the August 2000 event, where the *PEPF* was 27%. The performance of the model in terms of the percentage error in volume (*PEV*) was better for the August 2000 event than for the September 2000 event. Very high values of the *PEV* measure were found at Innerkip (46% for the August event) and at Thamesford (57% for the September event). The lag-0 cross-correlation coefficient (*CORR*) was in most cases around 0.95 and higher, at Thamesford the *CORR* value was 0.55 (August event) and 0.86 (September event). The values of the last three measures, *RBIAS*, *RRMSE* and *RPWRMSE* were again influenced by the recession periods and low-flow periods preceding the peak, especially at Thamesford for both events. The absolute values of these measures were low. The rather poor model results at Thamesford were caused by the fact that both August and September events partially missed the Thamesford subbasin, and the HEC-HMS IDM algorithm interpolated rainfall intensities and amounts that were different from the true values.

Except for the August 2000 event results at Innerkip, the *PEPF* values obtained from the verification data are comparable with the *PEPF* values from the calibration period. The average *PEPF* value from the calibration data is 1.5% and from the verification data 9.2% (August 2000 event) and 3.4% (September 2000 event) respectively. The results from the calibration and verification periods differ considerably in terms of the *PEV* measure, especially for the September 2000 event, and at Thamesford for both verification events. The average calibration value of the *PEV* measure is 4.5% in contrast to 19.9% for the August event and 29.7% for the September event. The verification performance results are similar to the calibration results according to the *CORR* measure (0.99 for calibration and 0.89 and 0.95 for verification events). The average values of the relative measures *RBIAS*, *RRMSE*, and *RPWRMSE* obtained from the calibration data (-20.4%, 46.3% and 36.1%) are comparable with the values for the August

2000 verification event (-30.9%, 45.0% and 39.9%). The relative measures for the September 2000 event are significantly higher (-52.9%, 62.3% and 54.1%).

The final model verification involved replacing the source-sink components with the uncontrolled-output reservoir components. Figures 22-24 compare the reservoir model outputs with the outputs from the source-sink model and with the observed hydrograph at the location Byron for the calibration and verification events. In all three cases the dam components caused an increase in the peak hydrograph of about 5-10%.

In the next step, the initial and constant loss parameters of the loss component and the storage parameter of the direct runoff component were adjusted to eliminate the discrepancy between the modeled and observed peak hydrographs. Adjusting the calibrated event model parameters is an inevitable compromise between the performance of the model at some locations of the UTRb and the necessity to use the reservoir component in practical applications of the model defined by the project objectives. The results are given in Figures 25-27.

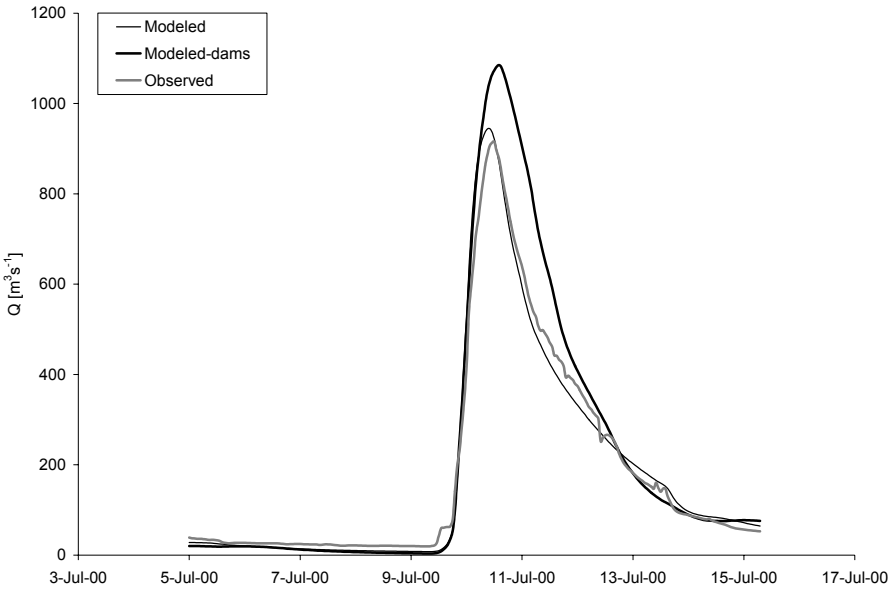

Figure 22. Observed, modeled, and modeled-with-dams hydrographs for the July 2000 event at Byron.

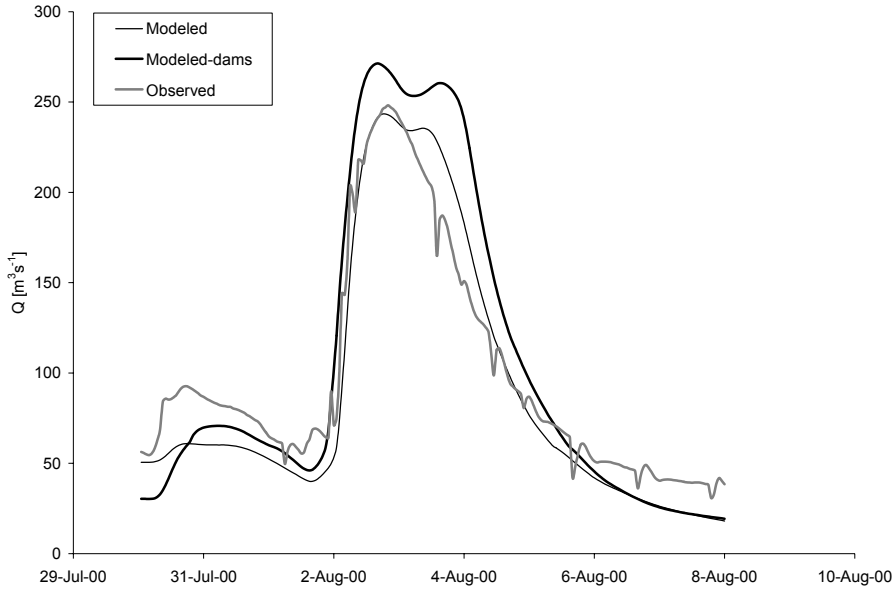

Figure 23. Observed, modeled, and modeled-with-dams hydrographs for the August 2000 event at Byron.

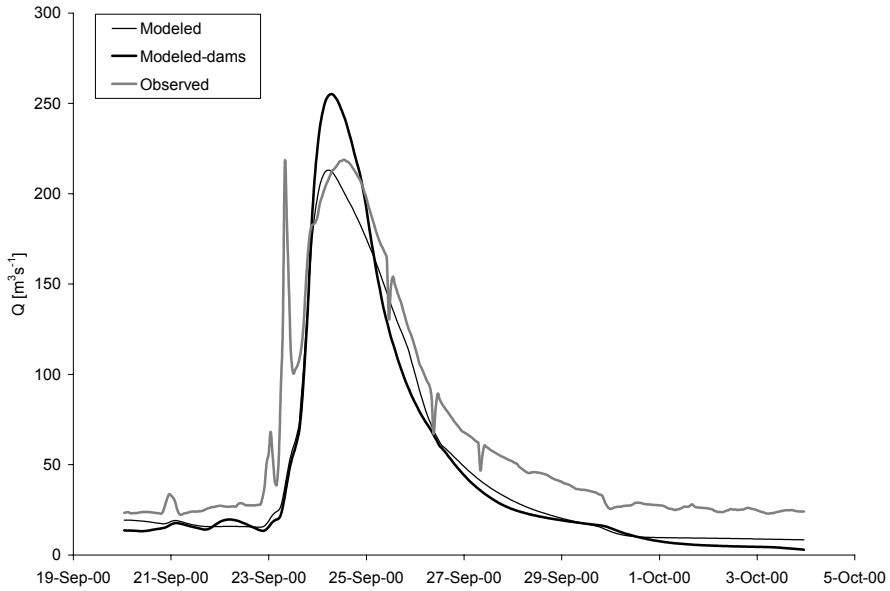

Figure 24. Observed, modeled, and modeled-with-dams hydrographs for the September 2000 event at Byron.

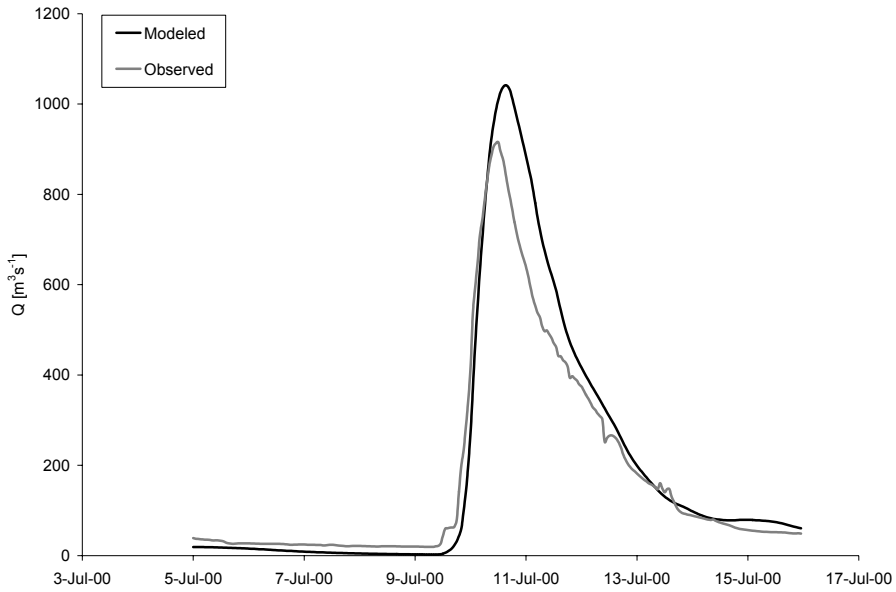

Figure 25. Observed and recalibrated modeled-with-dams hydrographs for the July 2000 event at Byron.

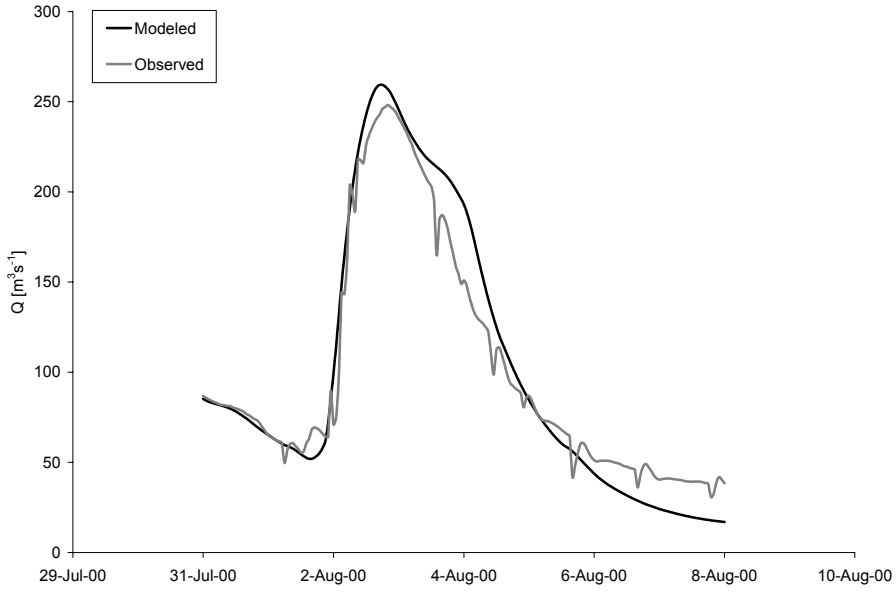

Figure 26. Observed and recalibrated modeled-with-dams hydrographs for the August 2000 event at Byron.

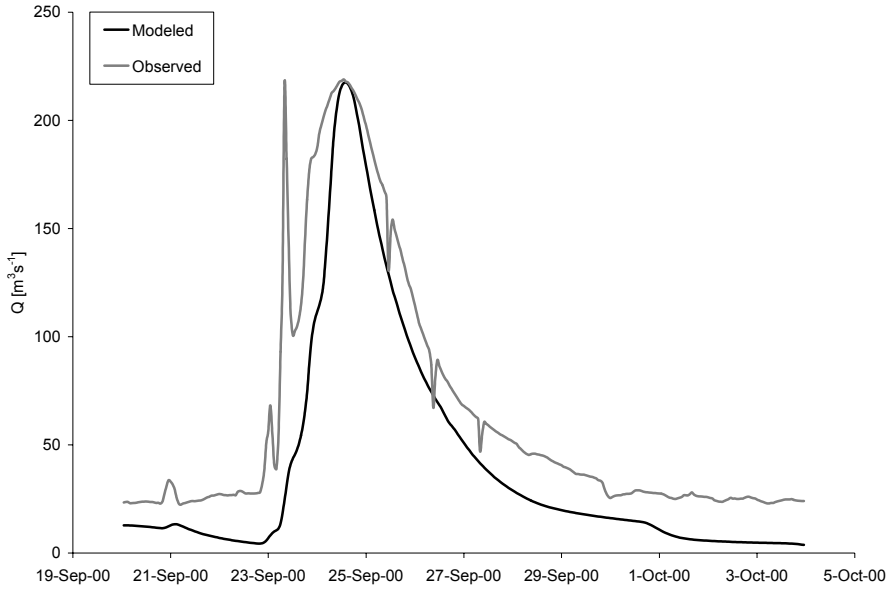

Figure 27. Observed and recalibrated modeled-with-dams hydrographs for the September 2000 event at Byron.

Except for the July 2000 event (Figure 25), the re-calibrated model led to visibly improved fits to the observed hydrographs at Byron. The new model hydrograph generated by the September 2000 event (Figure 27) does not have a bi-modal structure and fits the observed peak better than the bi-modal hydrograph obtained by the previous version of the model (Figure 24). The final set of the event model parameters is given in Appendix IVa.

In some subbasins of the UTRb very large values of the initial loss parameter had to be used in order to achieve a good fit between the modeled and observed hydrographs (see Appendix IVa). These cases represent situations, when the rainfall amount interpolated by the inverse-distance method exceeded the true rainfall amount that fell on the subbasin (e.g. a storm did not hit a given subbasin, but the IDM interpolation allocated substantial rainfall amount to that subbasin, and thus a large initial loss had to be applied in order to eliminate the erroneous rainfall amount). Therefore, some values of the initial loss parameter given in Appendix IVa do not always have to have a physical meaning.

II.4 Event model sensitivity

II.4.1 Sensitivity procedure

Sensitivity analysis is a method to determine which parameters of the model have the greatest impact on the model results. It ranks model parameters based on their contribution to overall error in model predictions. Sensitivity analysis can be local and global (Haan, 2002). In the local sensitivity analysis, the effect of each input parameter is determined separately by keeping other model parameters constant. The result is a set of sensitivity functions, one for each model parameter. In the global sensitivity analysis all model inputs are allowed to vary over their ranges at the same time. Global sensitivity is based on the use of probabilistic characteristics of the input random variables.

Three types of coefficients can be used in local and global sensitivity analyses. The absolute sensitivity coefficient, *SA*, is defined as (Haan, 2002):

$$SA = \frac{\partial O}{\partial P} \tag{16}$$

where O is the model output and P represents a particular input parameter. The absolute sensitivity coefficients are affected by units of output and input and therefore cannot be used for the comparison of parametric sensitivities. The relative sensitivity, *SR*, is defined as (Haan, 2002):

$$SR = \frac{\partial O / O}{\partial P / P} = \frac{\partial O}{\partial P}\frac{P}{O} \tag{17}$$

The relative sensitivity coefficients are dimensionless and thus can be compared across parameters. Finally, the deviation sensitivity, *SD*, is quantified as the change in the output ΔO (McCuen, 2003):

$$SD = \Delta O = \frac{\partial O}{\partial P}\Delta P \cong \frac{\Delta O}{\Delta P}\Delta P \tag{18}$$

The deviation sensitivity has the same units as the variable *O*.

Analytical differentiation is not used extensively for evaluating the sensitivity of hydrologic models because the complexity of most hydrologic models precludes analytical differentiation. The method of factor perturbation is more commonly used method in hydrologic analysis (McCuen, 2002). The partial derivates of equations (16-19) can be approximated by numerical derivates as (Haan, 2002):

$$\frac{\partial O}{\partial P} \cong \frac{O_{P+\Delta P} - O_{P-\Delta P}}{2\Delta P} \tag{19}$$

where ΔP is the change in parameter value from its base value (usually 10% or 15% of *P*).

In this study, a local sensitivity analysis was adopted for evaluating the event model. The final set of the parameters of the calibrated model was deemed as baseline/nominal parameter set. Then, the model was run repeatedly with the starting baseline value for each parameter multiplied, in turn, by 0.7, 0.8, 0.9, 1.1, 1.2 and 1.3, while keeping all other parameters constant at their nominal starting values. The hydrographs resulting from the scenarios of adjusted model parameters were then compared with the baseline model hydrograph. The performance measures defined in Section II.2.1 were used as sensitivity functions. Since these measures are dimensionless, the absolute sensitivity coefficient (Equation (16)) was used to compare the results from different sensitivity scenarios.

II.4.2 Sensitivity results

The sensitivity procedure described in the previous section was applied to the subbasin nr. 23 (Middle Thames River at Thamesford, ID 02GD004), using the rainfall data from the July

2000 event. The subbasin 23 is centrally located in the UTRb, relatively pristine, and representative in terms of the UTRb hydro-climatic regime.

There are seven parameters of the event model that were subject to the sensitivity analysis (see Appendix IIa for a summary of event model parameters). The initial loss parameter, *Li*, accounts for the interception and depression storage and represents basin initial condition (Equation (3)). Figure 28 compares the baseline hydrograph with the hydrographs generated by the six sensitivity scenarios according to which the initial loss was increased/decreased by ±10%, ±20% and ±30%. According to expectations, the highest relative differences between the generated hydrographs and the baseline hydrograph are observed at the beginning of the flood event, where the relative differences reach up to ±120% (absolute differences are negligible compared to the peak magnitude). Generally, when the *Li* parameter decreased (increased), the flood started earlier (later) and the peak discharge increased (decreased) (one hour earlier (later) and 6% increase (decrease) for the -30% decrease (increase) in the *Li* scenario). After flood peak the generated hydrographs differ from the baseline hydrograph by almost constant rate (not exceeding ±6% for the most extreme scenario). The hydrographs are identical with the baseline hydrograph up to the start of the flood event. In terms of absolute differences, maximum differences between the hydrographs occur in the peak ordinates (up to ± 15 m^3s^{-1} for the ±30% scenarios).

The second parameter of the event model is the constant loss rate, *Lr*, (Equation (3)), which can be viewed as the ultimate infiltration capacity of the soils (USACE, 2000b). Figure 29 depicts the streamflow hydrographs generated from scenarios where the constant loss rate was adjusted by ±10%, ±20% and ±30%. The hydrographs differ from the baseline hydrograph from the start of the flood event onwards by up to ±12% for the most extreme scenarios (±30% change in *Lr*). The hydrograph coordinates preceding the beginning of the flood event were

identical with the baseline hydrograph. The absolute differences reached up to ± 25 m^3s^{-1} at the time of the peak flow.

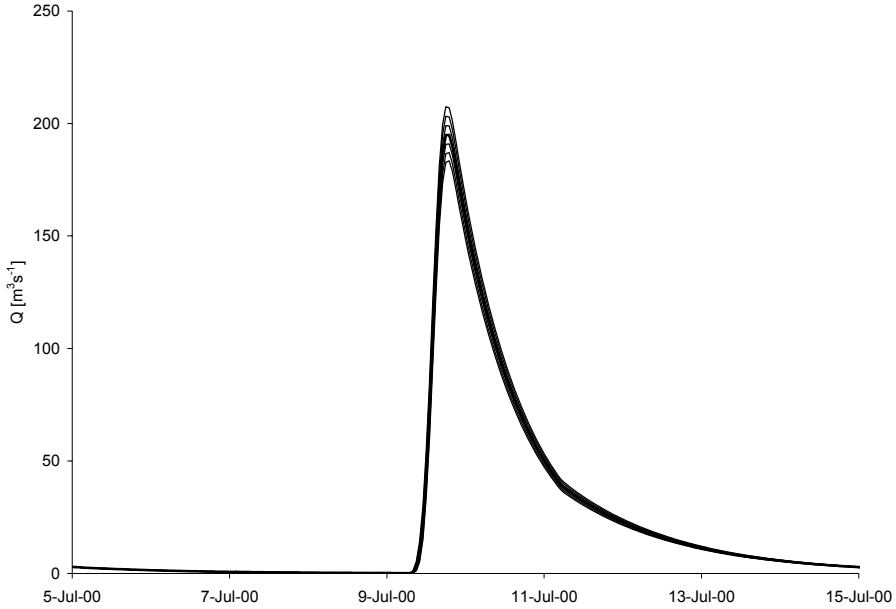

Figure 28. Event model sensitivity on the initial loss, *Li*.

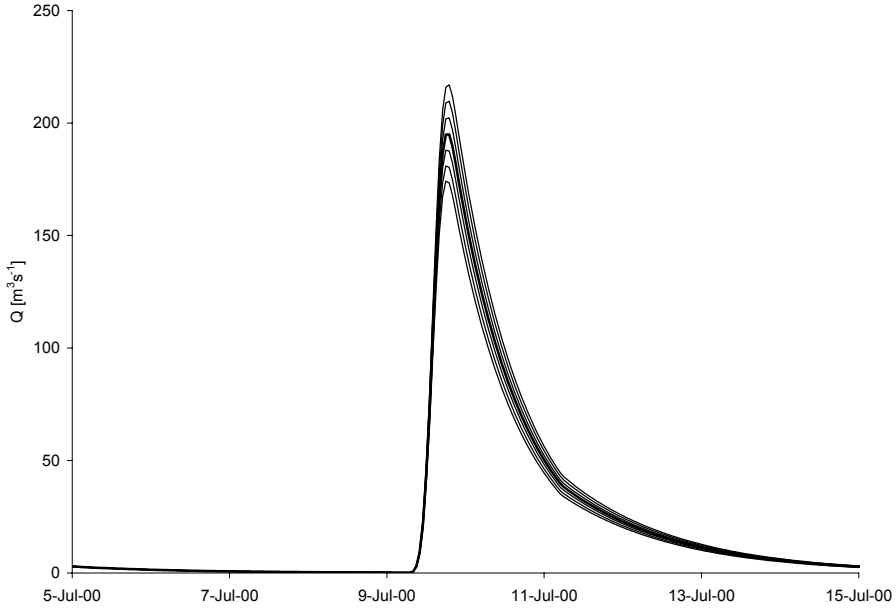

Figure 29. Event model sensitivity on the constant loss rate, *Lr*.

The Clark's time of concentration parameter, *Tc*, represents the travel time from the hydraulically furthermost point in the basin to the outlet. Figure 30 shows how the streamflow hydrograph changed when the time of concentration was altered. When *Tc* was shortened, the peak increased and occurred earlier (2 hours earlier and 2.5% increase for the -30% change in the *Tc* scenario). Similarly, when the time of concentration was lengthened, the peak decreased and occurred later (2 hours later and 2.5% decrease for the +30% change in the *Tc* scenario). The highest relative differences between the generated hydrographs and the baseline hydrograph did not occurred in the peak but in the rising part of the hydrograph (up to ±60%). The portion of the hydrograph before the rising limb was not affected by the change in this parameter. Also after the inflection point the hydrographs differed from the baseline hydrograph only by up to ±2%. The maximum absolute differences between the hydrographs occurred in the rising limb of the hydrograph - over ± 40 m^3s^{-1} for the most extreme scenarios.

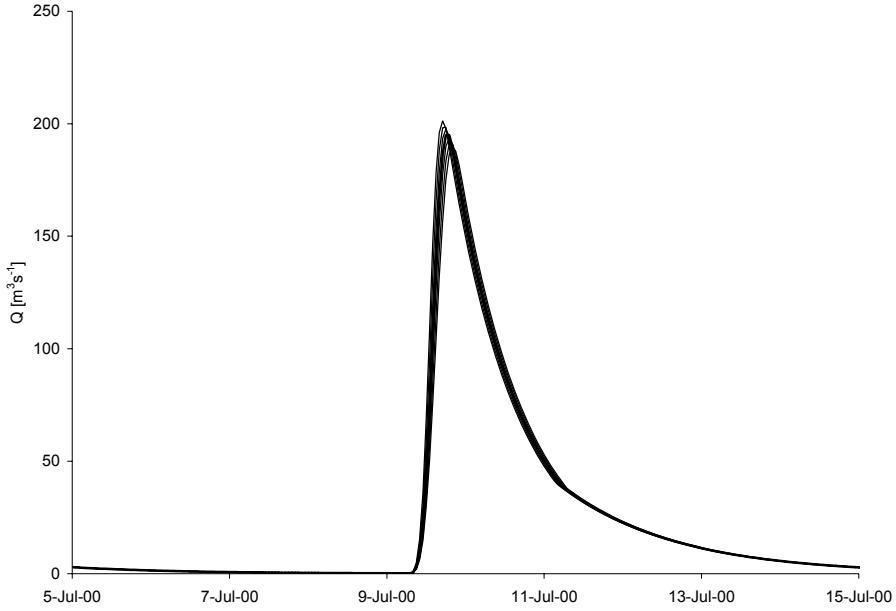

Figure 30. Event model sensitivity on the time of concentration, *Tc*.

The highest differences between the generated peak hydrographs and the baseline peak hydrograph were caused by altering the Clark's storage coefficient, *St*, (Figure 31). The storage coefficient (Equation (5)) is an index of the temporary storage of precipitation excess in the basin as it drains to the outlet point (USACE, 2000b). When the *St* parameter decreases, the peak discharge increases and flood hydrograph becomes sharper (the recession limb of the hydrograph falls faster), whereas when the *St* parameter increases, the peak discharge decreases and the flood hydrograph becomes flatter. The maximum relative differences between the hydrographs occurred in the rising part of the hydrograph (up to ±40%). The differences in the peak ordinates were up to ±30%, and near the inflection point ±20%. The hydrographs are identical before the time to rise, and similar after the inflection point of the recession hydrograph (differences up to ±2.5%). The absolute difference for the -30% scenario was around 60 m^3s^{-1} and for the +30% scenario around 40 m^3s^{-1}.

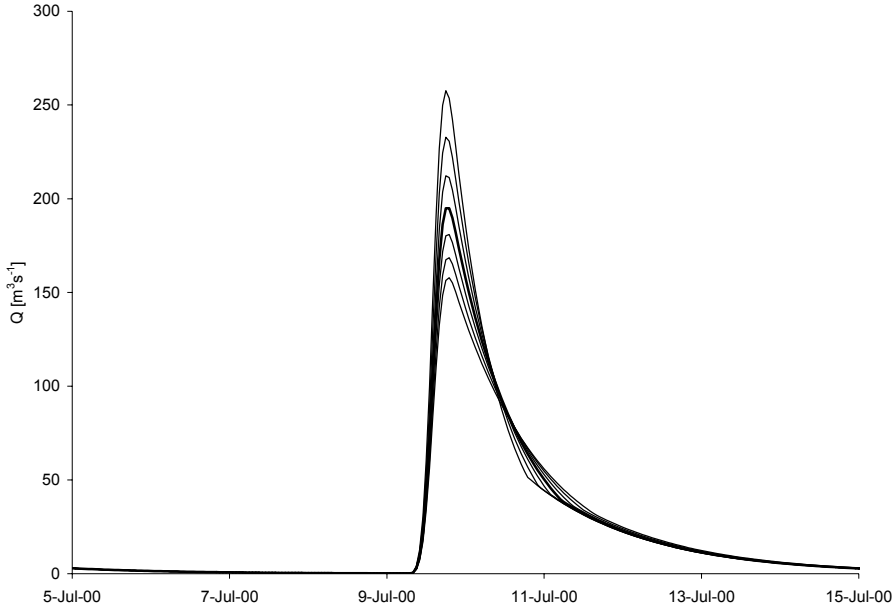

Figure 31. Event model sensitivity on the Clark's storage coefficient, *St*.

The initial baseflow, *Bi* (Equation (7)), is a parameter describing initial conditions of the recession baseflow component. Figure 32 shows that the changes in *Bi* had a greatest impact on the generated hydrographs before the time to rise. When the *Bi* value decreased (increased), the modeled hydrograph ordinates decreased (increased) of up to -30% (+30%) for the -30% (+30%) scenario. The changes in hydrograph ordinates after the peak occurrence were negligible ($< |0.05\%|$). In absolute values the maximum differences were smaller than 1 m^3s^{-1}.

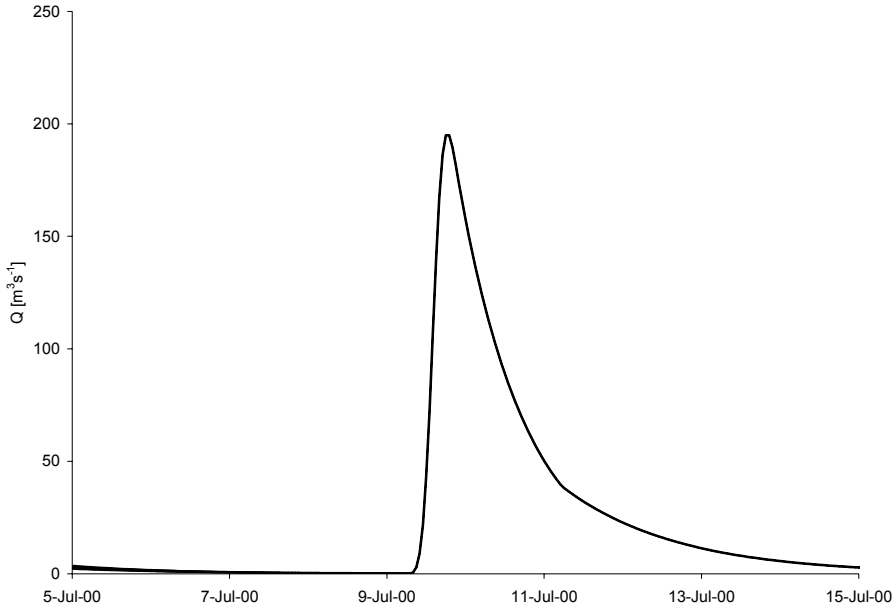

Figure 32. Event model sensitivity on the initial baseflow, *Bi*.

The baseflow recession constant, *Rc* (Equation (7)), is the ratio of baseflow at time *t* to the baseflow at time *t*-1, and defines the rate of baseflow decay. Figure 33 depicts the streamflow hydrographs generated according to the scenarios of the change in the *Rc* parameter. When the value of *Rc* decreased, the recession part of the hydrograph (before and after the peak) after the inflection point decreased (up to -80% for the -30% scenario). An increase in *Rc* has even more pronounced effect on the recession hydrographs; particularly the increase of +30% caused an increase of more than +200%. The effect on the peak hydrograph

was negligible. The absolute differences between the generated and baseline hydrographs were small, within the range of ± 7 m^3s^{-1}.

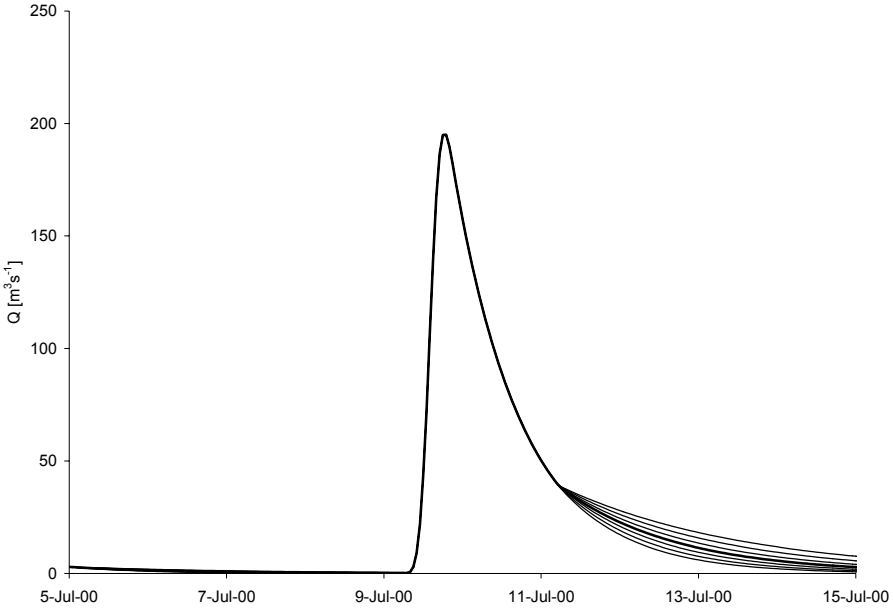

Figure 33. Event model sensitivity on the recession constant, *Rc*.

The last parameter of the recession baseflow component, the threshold, *Td*, is the point on the hydrograph where the baseflow replaces overland flow as the source of flow from the basin. A decrease in *Td* generated decreased streamflow in the recession hydrographs after the inflection point. The generated hydrographs prior the inflection point were identical with the baseline hydrograph (Figure 34). A decrease of -30% in *Td* caused a decrease of up to -15%. An increase of +30% raised the recession limb by +11%. The absolute differences between the hydrographs were again low, within the range of ± 5 m^3s^{-1}.

Figure 35 and Figure 36 summarize the absolute differences obtained from the $\pm 30\%$ scenarios for each parameter of the event model. The highest differences were generated by the change in the Clark's storage parameter, *St*. High absolute differences were also generated by the change in the parameters of the loss method (initial, *Li*, and constant, *Lr*, losses) and by

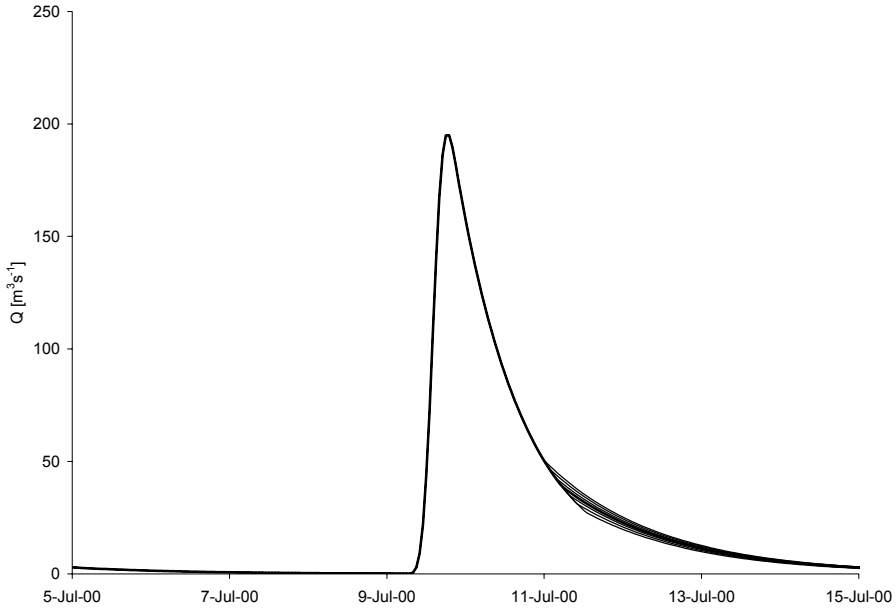

Figure 34. Event model sensitivity on the baseflow threshold, *Td*.

the change in the Clark's time of concentration, *Tc*. The baseflow threshold and recession constant parameters generated considerably lower absolute differences between the hydrographs and only in the falling limb of the hydrographs. The initial baseflow parameter led to very low differences at the beginning of the hydrographs.

The hydrographs generated according to the scenarios of the change in the model parameters were also compared with the reference – baseline hydrograph by means of the performance measures introduced in Section II.2.1. The results are summarized in Figures 37-42 and tabulated in Appendix Va.

Figure 37 compares the percentage error in the peak flow, *PEPF*, of the model results generated from the sensitivity scenarios of the change in the event model parameters. The error is highest for the scenarios of the change in the Clark's storage coefficient, *St*, up to 25% for the ±30% change scenarios. Moderate values of the *PEPF* measure were obtained by changing

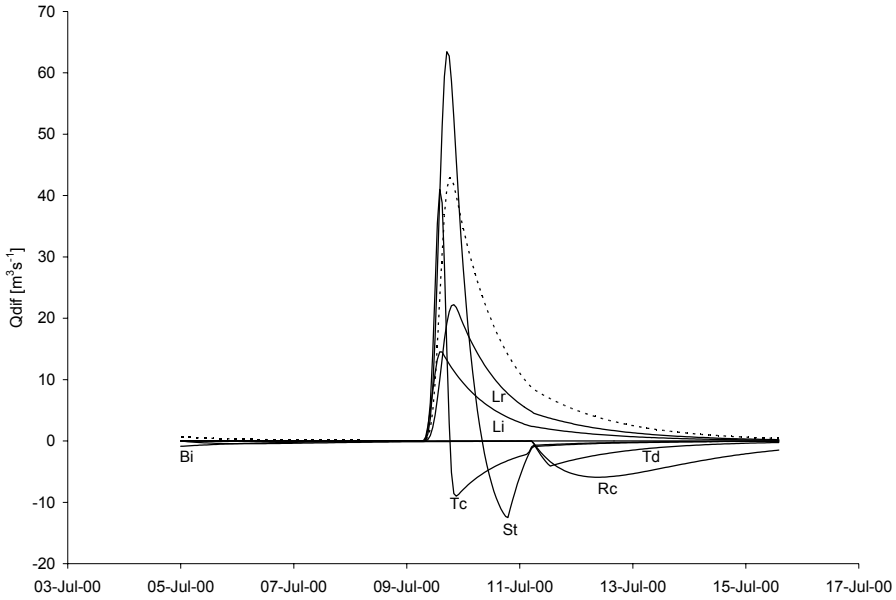

Figure 35. Comparison of the absolute streamflow discharge differences between the hydrograph generated according to the scenario of a -30% change in the event model parameters and the baseline hydrograph. The thin dashed line outlines the observed hydrograph (scaled).

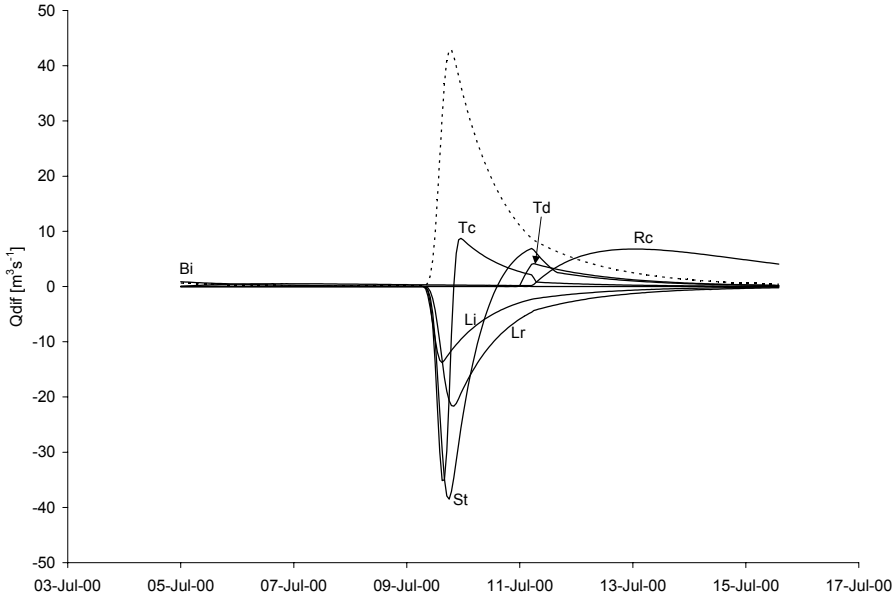

Figure 36. Comparison of the absolute streamflow discharge differences between the hydrograph generated according to the scenario of a +30% change in the event model parameters and the baseline hydrograph. The thin dashed line outlines the observed hydrograph (scaled).

the initial and constant loss parameters, and the time of concentration. The *PEPF* values of the baseflow parameters are less than 0.05% (see Appendix Va).

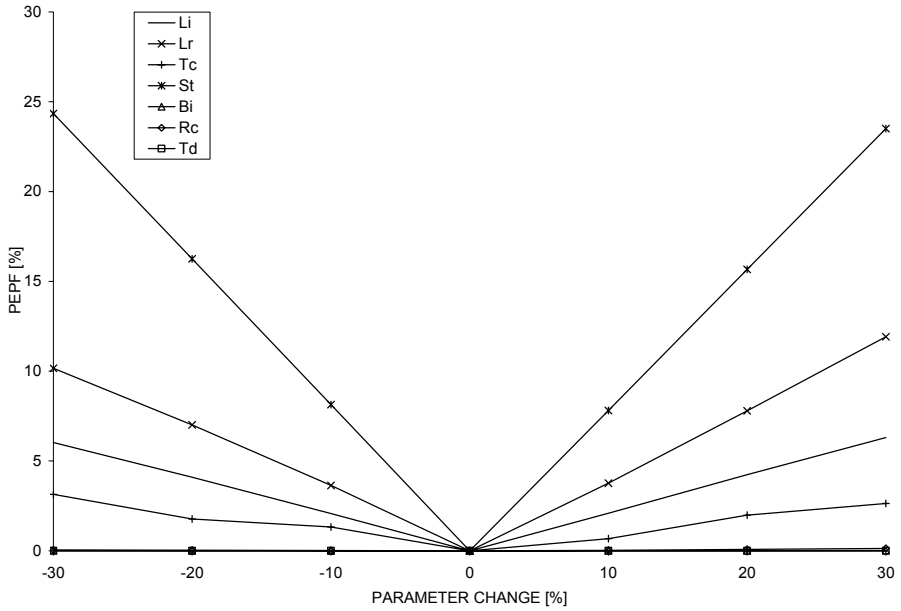

Figure 37. *PEPF* of the model results generated from the sensitivity scenarios of the change in the event model parameters.

Figure 38 compares the percent error in the volume, *PEV* performance measure for the different parameter change scenarios. The constant loss rate, *Lr*, generated the highest values of the *PEV* measure, over 10% for the ±30% scenarios. High *PEV* values were obtained also from scenarios of the change in the baseflow recession constant, Clark's storage, and initial loss parameters. The *PEV* values for the baseflow threshold scenarios are within the range of 0-3%. The *PEV* values for the initial baseflow and the time of concentration are very low, and both lower than 0.5%.

Figure 39 depicts the values of the lag-0 linear cross-correlation coefficient between the sensitivity outputs and the reference, baseline data. Almost functional forms, with the *CORR* values approaching 1.0 were found for the constant loss, initial baseflow and baseflow threshold

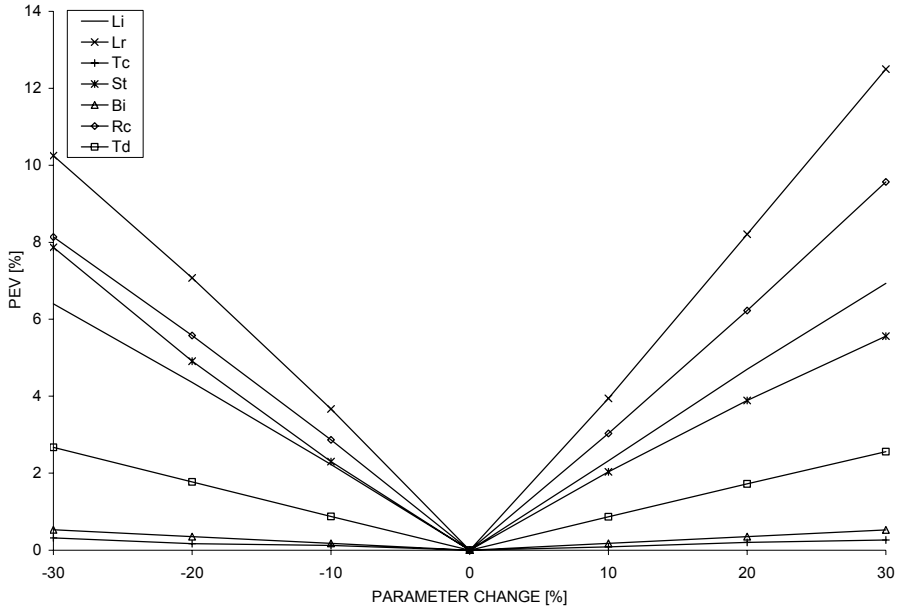

Figure 38. *PEV* of the model results generated from the sensitivity scenarios of the change in the event model parameters.

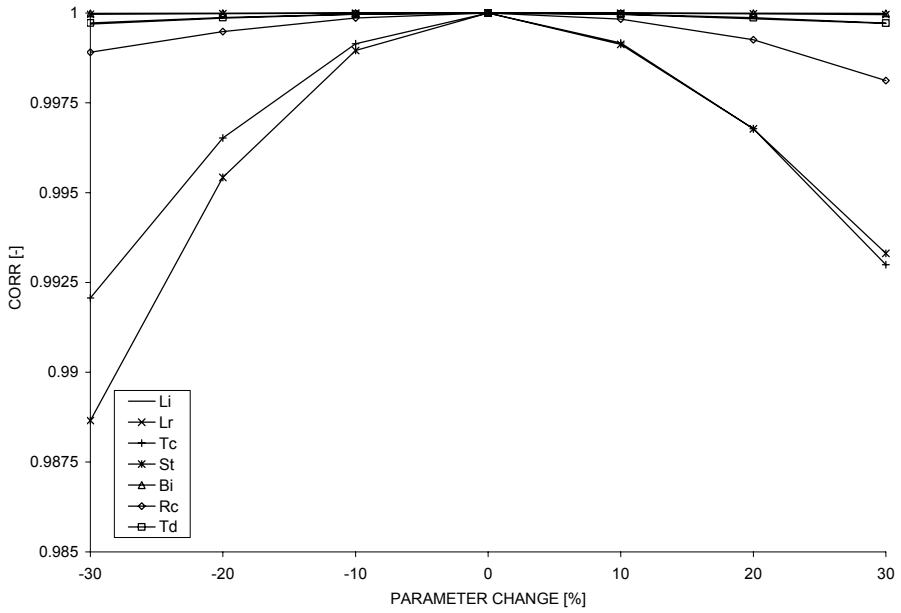

Figure 39. *CORR* of the model results generated from the sensitivity scenarios of the change in the event model parameters.

scenarios. Very high values exceeding *CORR* = 0.9975 were also found for the initial loss and recession constant parameters. The lowest values of *CORR* were obtained for the scenarios

corresponding to the change in the time of concentration and surface storage parameters, because the change in these parameters generate the highest differences between the hydrographs.

Figure 40 compares the relative *BIAS* obtained from the individual sensitivity scenarios. The change in the recession constant led to the highest values of this measure, exceeding 100% for the -30% scenario. The effect of the error in low flow ordinates on the relative performance measure was explained in Section II.2.2. The results for the remaining parameters were within the range of ±20%. The lowest values of the *RBIAS* were obtained for the time of concentration (< 0.5%), because this parameter modifies only the peak ordinates of the hydrograph.

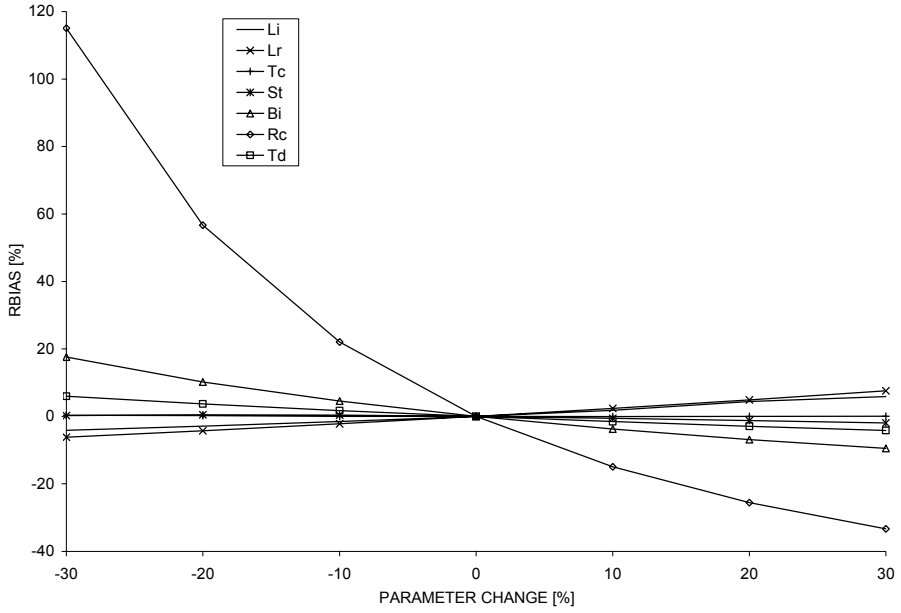

Figure 40. Relative *BIAS* of the model results generated from the sensitivity scenarios of the change in the event model parameters.

Figure 41 depicts the relative *RMSE* values for the individual sensitivity scenarios. Again, the change in the recession constant led to the highest values of this measure, exceeding 160% for the -30% scenario and 40% for the +30% scenario. The high difference between the

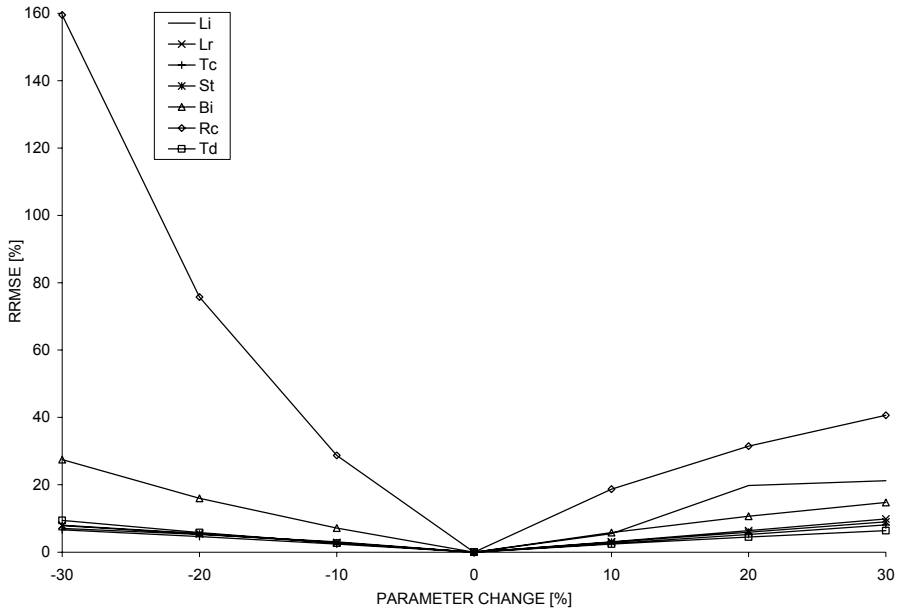

Figure 41. Relative *RMSE* of the model results generated from the sensitivity scenarios of the change in the event model parameters.

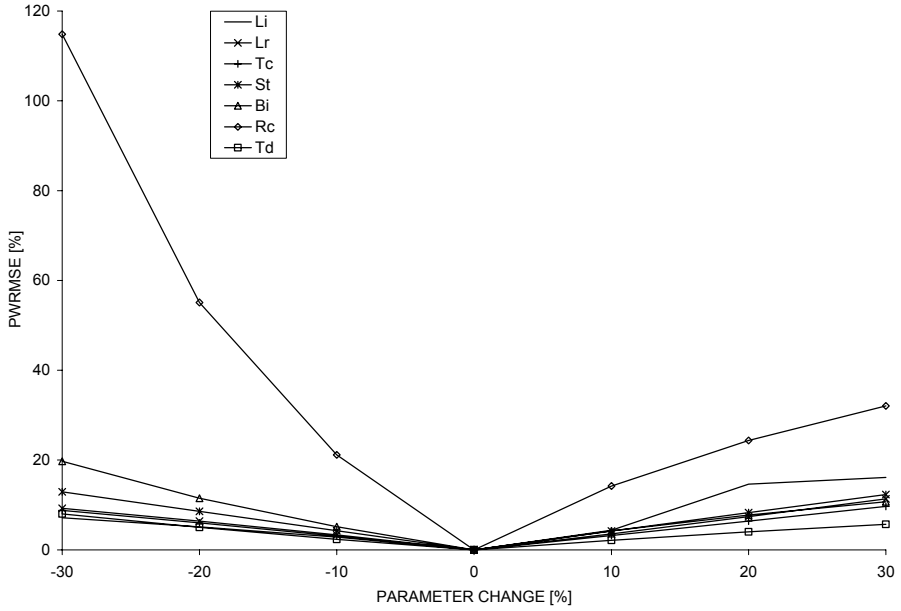

Figure 42. Relative *PWRMSE* of the model results generated from the sensitivity scenarios of the change in the event model parameters.

outputs of the ±30% scenarios was likely caused by the baseline set of parameter values at Thamesford. The *RRMSE* value corresponding to +30% scenario is much lower, only 40%.

Relatively high values of *RRMSE* were also observed for the scenarios of a decrease in the initial baseflow and with an increase in the initial loss parameters. The results for the remaining parameters are below 20%.

Figure 42 compares the relative peak-weighted *RMSE* values for the different sensitivity scenarios. The results are very similar to the results obtained for the *PWRMSE* measure. The change in the recession constant led to the highest values of this measure, reaching almost 120% for the -30% scenario, and 32% for the +30% scenario. Again, the high difference between the ±30% scenarios can be attributed to the baseline set of parameter values at Thamesford. The results of the remaining model parameters are below 20%.

An event hydrologic model is aimed primarily at reproducing flood magnitudes and volumes. With respect to flood magnitudes, the event HEC-HMS model calibrated on the data from the UTRb is most sensitive to the Clark's storage coefficient. Only a small change in this parameter can generate significant variation in peak hydrographs. Also the time of concentration and the loss component parameters play crucial role in the modeling of peak hydrographs. In terms of peak volume, the event model was found to be most sensitive to the loss parameters and the Clark's storage coefficient. When a subbasin is gaged, then these parameters can be reliably estimated via the process of calibration. In the case a subbasin is ungaged, the values of these parameters need be carefully chosen based on the information available in the study area.

Finally, it must be remembered that the presented results were obtained by a local sensitivity analysis. Thus, the results reflect the given combination of model parameters (Appendix IVa). Different parameter combination may generate different values of the performance measures used in the sensitivity analysis, although a significant change in the pattern of the sensitivity results is unlikely.

III. HEC-HMS CONTINUOUS MODEL

III.1 Continuous model structure

Similarly to the event model, the physical representation of the UTRb in the continuous model was created using the HMS basin model environment. Figure 43 shows the UTRb schematic created in the HMS BME. The event model uses again all available hydrologic elements except for diversion. During the calibration of the continuous model, the source and sink elements were used to model actual reservoir operation, in the final version of the model these elements were replaced by the reservoir element, as it was previously explained in Section II.1.6.

Figure 43. HEC-HMS continuous model representation of the UTRb.

In addition to joining subbasins 6 and 7 into one spatial unit (see Section II.1), in the continuous model the subbasins 1 and 2 were also grouped into one subbasin (see Figure 43),

since they were contributing to the same gaged junction component (North Thames River near Mitchell, ID 02GD014). The HEC-HMS continuous basin model is saved in the file "CONTINUOUS+DAMS.basin" and included in the project "UTRCA_full.hms" (see Appendix I).

Figure 44 represents a diagram of the basin precipitation-runoff processes included in the continuous model.

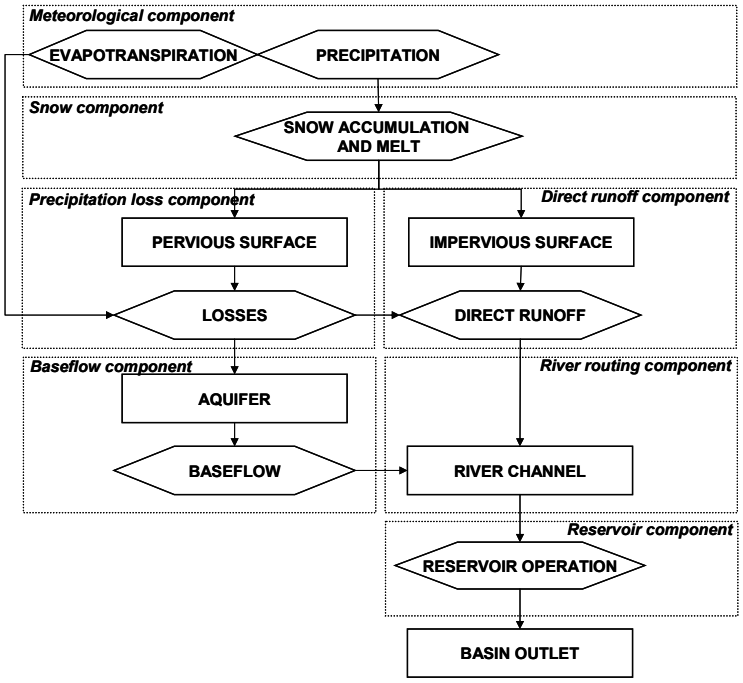

Figure 44. Precipitation-runoff processes included in the continuous model structure.

In the continuous version of the UTRb model, river basin processes considered in the model structure are organized into seven main components. The meteorologic component is used to spatially and temporally model precipitation and evapotranspiration processes in the basin. The spatially and temporally distributed precipitation is then an input into the snow component, which separates the precipitation input into liquid and solid forms, and simulates solid precipitation accumulation and melt. Precipitation adjusted by the snow component falls on previous and impervious surfaces of the basin. Precipitation from the pervious surface is subject

to losses (interception, infiltration, evaporation and transpiration) modeled by a detailed precipitation loss component. The remaining continuous model structure is identical with the structure of the event model. The effective precipitation from the precipitation loss component contributes to direct runoff and to groundwater flow in aquifers. Precipitation from the impervious surface enters the direct runoff component, where it is transformed to overland flow. The baseflow component models the movement of water in aquifers. Both, overland flow and baseflow, enter river channels. Streamflow in river channels is simulated by the river routing component. Finally, the effect of hydraulic facilities and significant natural depressions is reproduced by the reservoir component of the model. The seven components of the continuous model are characterized in detail in the proceeding sections.

III.1.1 Meteorologic component

An overview of the HEC-HMS meteorologic component was given in Section II.1.1. In the continuous hydrologic modeling, a detailed accounting of the movement and storage of water through all components of the system is usually required. Evapotranspiration as an important loss component was therefore included in the meteorologic component of the continuous model.

The present HEC-HMS 2.2.2. evapotranspiration method allows splitting river basin into different evapotranspiration zones. For each zone monthly average evapotranspiration values are defined. An evapotranspiration coefficient can be used to correct pan evapotranspiration data. The UTRb area was divided previously into three evapotranspiration zones by the UTRCA. The zones are depicted in Figure 45. The monthly average evapotranspiration value for each zone, as well as the identification number of a subbasin belonging to the particular zone is provided in Appendix IIIc. The monthly evapotranspiration values were obtained from UTRCA and were corrected by the pan coefficient of 0.7 (see e.g. Doorenbos and Pruitt (1975) for details on pan coefficients).

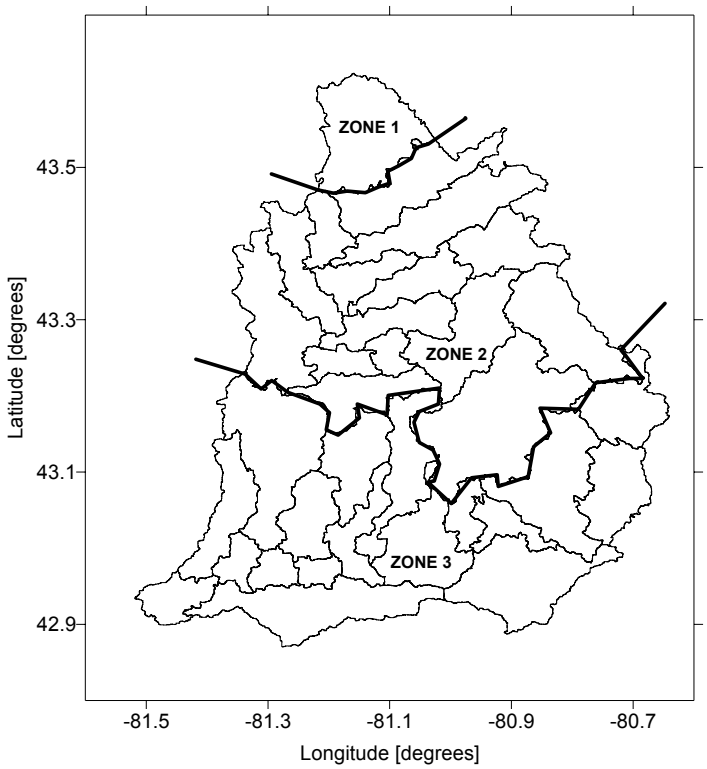

Figure 45. Division of the UTRb into three evapotranspiration zones.

The inverse-distance precipitation interpolation method (IDM) was adopted in the continuous model for spatial and temporal distribution of precipitation input over the UTRb. Details of the IDM method were given in Section II.1.1 and are not repeated here. The daily precipitation data are interpolated at 32 locations in the UTRb defined by subbasin's centroids. The meteorologic component is saved in the HEC-HMS file "CONT_SNOW_PET.met". The daily precipitation data corrected by Environment Canada (EC), which are the input into the meterologic component, are stored in the HEC-DSS database "EC.dss" (see also Appendix I).

III.1.2 Snow component

The structure of the present version (2.2.2) of the HEC-HMS software does not account for snow accumulation and melt processes. The UTRb is located in a climatic zone where snow accumulation and melt processes are important for streamflow regime, and they cannot be

neglected in the model structure. An external snow model was therefore developed and linked with the HEC-HMS.

Figure 46 describes the algorithm of the snow model. In the first step, daily precipitation and temperature data are interpolated (extrapolated) at the 32 subbasin centroid nodes by the HEC-HMS inverse distance method. In the next step, the precipitation amount for the time interval Δt is separated into solid (snowfall) or liquid (rainfall) based on the average temperature for the time interval Δt. The solid precipitation is then subject to the snow accumulation and melt algorithm. This algorithm is based on a degree-day method. At each time interval Δt, the melted portion of snow, if any, is added to the liquid precipitation amount. The adjusted precipitation is then an input to the HEC-HMS model.

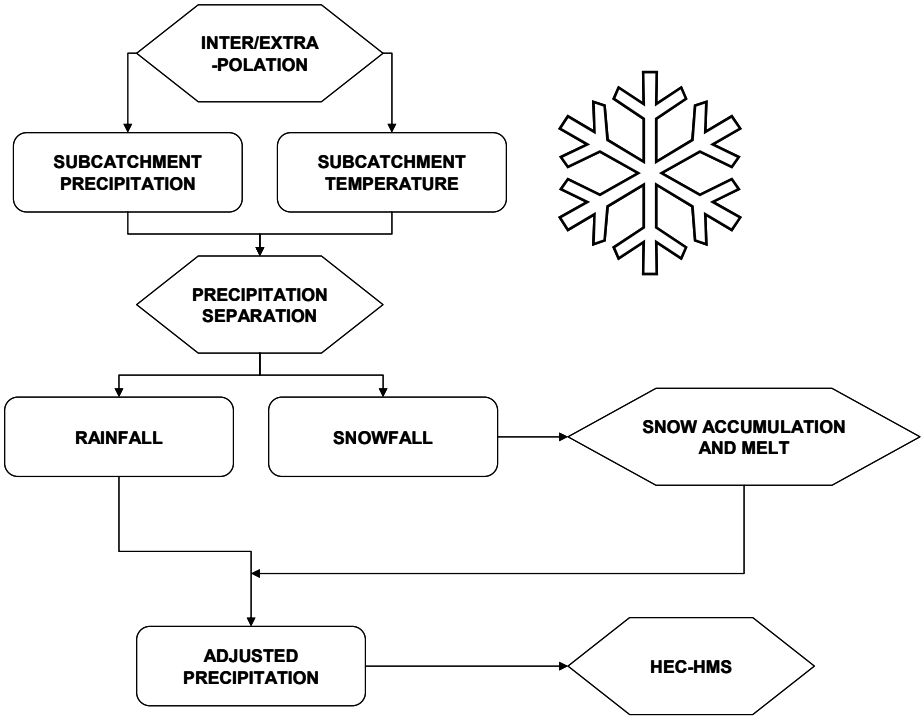

Figure 46. Flow chart of the snow model.

Temperature index models are usually the most common approach for melt modeling due to four reasons (Hock, 2003): 1) wide availability of air temperature data, 2) relatively easy

interpolation and forecasting of air temperature, 3) good model performance in spite of their simplicity, and 4) computational simplicity. Most operational runoff models (HBV, SRM, UBC, HYMET, SHE) rely on temperature-index methods for melt modeling (Hock, 2003).

There are four parameters in the snow model:

- Upper temperature threshold, *Tmax*, [°C], defines the temperature above which all precipitation is treated as rainfall.
- Lower temperature threshold, *Tmin*, [°C], defines the temperature below which all precipitation is treated as snowfall.
- Critical temperature for snowmelt, *Tcrt*, [°C], defines the temperature above which snowmelt process can occur.
- Snowmelt rate, *Mr*, [mm/°C/day], defines the rate at which snow melts.

Since the code of the HEC-HMS model is not in public domain, it was impossible to incorporate the snow subroutine directly into the main HEC-HMS code. Therefore, the snow subroutine runs as a stand-alone program, which produces outputs that represent adjusted precipitation inputs to the HEC-HMS. The main disadvantage of this procedure is that the parameters of the snow model cannot be optimized, and must be calibrated manually.

The snow model was written in Visual Basic (VB) programming language. The code consists of one subroutine saved in a VB class module "Snow.cls" and exported into a dynamic-linked-library (dll). The dll file (snow.dll) can be called from other Windows-operating programs. The code of the subroutine is provided in Appendix VI. The adjusted precipitation output from the snow model is converted into the HEC Data Storage System Visual Utility Engine (DSSVue) database (USACE, 2003a) using the HEC DSS MS Excel Add-In (USACE, 2003b). The database is stored in the project file "NEW PRECIP.dss".

III.1.3 Precipitation loss component

Among the different methods available in HEC-HMS to simulate precipitation losses, only the deficit and constant method and the soil-moisture accounting method can be used for continuous hydrologic modeling. The one-layer deficit and constant model is suitable for simple continuous modeling, whereas the 5-layer soil-moisture accounting (SMA) model can be used for continuous modeling of complex infiltration and evapotranspiration environments. The SMA model simulates both wet and dry weather behavior, and is based on the Precipitation-Runoff Modeling System of Leavesley et al. (1983). In this model, the river basin is represented by a series of interconnected storage layers (see Figure 47).

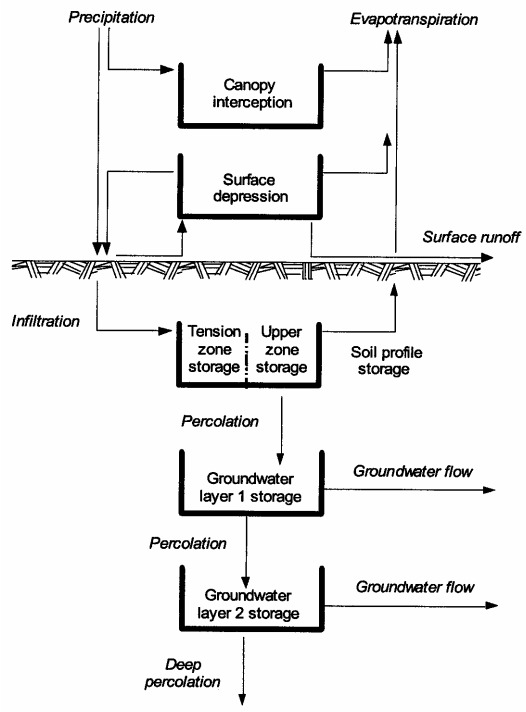

Figure 47. Structure of the soil moisture accounting model (USACE, 2000b).

There are four different storages in the SMA model:

- Canopy-interception storage (precipitation captured on trees, grasses, etc…).
- Surface-depression storage (water held in shallow surface depressions).

- Soil-profile storage (water stored in the top layer of the soil; the upper zone represents water held in soil pores and the tension zone water attached to soil particles).
- Groundwater storage (the model can include either one or two groundwater layers).

The movement of water into, out of, and between the storages is administered by the following processes (USACE, 2000b):

- Precipitation. This process represents an input into the SMA system.
- Evapotranspiration. In the HEC-HMS, evapotranspiration is modeled as vaporization of water directly from the soil and vegetative surface, and transpiration through plant leaves. The potential evapotranspiration demand is computed from monthly pan evapotranspiration depths, multiplied by monthly-varying pan correction coefficients, and scaled to the time interval. When evapotranspiration is from interception storage, surface storage or from the upper soil zone, actual evapotranspiration is equivalent to *PET*. When *PET* is drawn from the tension zone, the actual evapotranspiration (*AET*) is a percentage of the *PET* (USACE, 2000):

$$AET = PET \cdot f\left(CTs, Ts\right) \tag{20}$$

  where *CTs* is the current tension zone storage and *Ts* is the maximum tension zone storage. Evapotranspiration is modeled in HEC-HMS only if no precipitation occurs.

- Infiltration. The potential infiltration volume, *PIV*, is calculated in the SMA method as:

$$PIV = If - \frac{CSs}{Ss} If \tag{21}$$

  where *If* is the maximum soil infiltration rate, *CSs* is the current soil storage, and *Ss* is the maximum volume of the soil storage.

- Percolation. The percolation rate from the soil profile into groundwater layer 1, *CSp*, is computed as:

$$CSp = Sp\left(\frac{CSs}{Ss}\right)\left(1 - \frac{CGs}{Gs}\right) \tag{22}$$

where *Sp* is the maximum soil percolation rate, *CSs* is the current soil storage, *Ss* is the maximum soil storage, *CGs* is the current storage in groundwater layer 1, and *Gs* is the maximum storage in groundwater layer 1. Similarly, the percolation rate from groundwater layer 1 to layer 2, *CGp*, is given by:

$$CGp = Gp\left(\frac{CGs}{Gs}\right)\left(1 - \frac{CGs}{Gs}\right) \tag{23}$$

where *Gp* is the maximum groundwater percolation rate.

- Surface runoff. Surface runoff is the water that exceeds the infiltration rate and overflows the surface storage.

- Groundwater flow. The SMA method models groundwater flow as:

$$Gw_{t+1} = \frac{CSp + Gs_t - PGp_i - 0.5Gw_t \cdot T}{RGs_i + 0.5TS} \tag{24}$$

where Gw_t is the groundwater flow rate at the beginning of the time interval *t*, *CSp* is the actual soil percolation, PGp_i is the potential percolation from groundwater layer *i*, RGs_i is the groundwater flow routing coefficient from groundwater storage *i*, and *T* is the simulation time step. The volume of groundwater flow from the river basin is computed as:

$$Gw = 0.5\left(Gw_{t+1} + Gw_t\right)T \tag{25}$$

This volume is then an input into the HEC-HMS baseflow component.

Required parameters of the SMA method are the SMA unit (SMU) and the initial storage for each layer. The SMUs contain storage and infiltration parameters for each layer of the SMA model, and are stored in the project file "UTRCA_full.smu".

III.1.4 Direct runoff component

Similarly to the event model, the Clark unit hydrograph method is used also in the continuous model to transform excess rainfall into direct runoff. The water that exceeds the infiltration rate and overflows the surface storage in the SMA model is the input to the direct runoff component. The parameters of this method, the time of concentration and the surface storage coefficient can be estimated via calibration if observed precipitation and streamflow data are available. Details of this method were given in Section II.1.3 and are not repeated here.

III.1.5 River routing component

The modified Puls method based on a finite difference approximation of the continuity equation, coupled with an empirical representation of the momentum equation is used in the continuous model to compute the travel time and attenuation of water flowing in open channels. The continuous model uses the same 21 river reaches that are included in the event model structure. Appendix IIIa provides the storage-outflow curves for all 21 river reaches. Further details of this method are given in Section II.1.4.

III.1.6 Baseflow component

The soil moisture accounting method is designed to be used in conjunction with the linear reservoir baseflow model. In this model, outflows from SMA groundwater layers are inflows to baseflow linear reservoirs. Required parameters of the linear reservoir baseflow model are:

- Storage coefficient, *Bs*, [hr],

- Number of reservoirs, *Br*, [#].

These parameters can be specified for each SMA groundwater layer separately.

III.1.7 Reservoir component

The elevation-storage-outflow method of level-pool routing model is used in the continuous model to compute outflow from the reservoir. Due to the previously mentioned difficulties with the calibration of ungaged subbasins downstream of dams, the reservoir component is used only in the final stage of the calibration. Details of this method are given in Section II.1.6. Appendix IIIb provides the elevation-storage-outflow curves for each of the three reservoirs located in the UTRb.

III.2 Continuous model calibration

III.2.1 Calibration procedure

The initial attempt in the calibration of the continuous model was to follow the procedure adopted in the event hydrologic modeling, which involved a combination of both manual and automated calibrations. However, due to the complexity of the continuous model (all five layers of the SMA model used in the model) or the HEC-HMS program limitations, the automated optimization based on the univariate gradient search method constantly led to a local minimum, regardless of the objective function and initial set of parameters being used. The local minimum represented according to the statistical performance measures as well as the visual tools available for calibration in the HEC-HMS significantly worse set of results than the results obtained by the manual calibration. Further, the Nelder and Mead method kept crashing the HEC-HMS program making it impossible to optimize any set of initial model parameters. Therefore, a systematic approach to the manual calibration was chosen as the only viable approach to the calibration of the continuous model.

The systematic manual calibration relied on the measured and estimated values of the model parameters available from the UTRCA. This ensured that a physically meaningful set of initial parameter values was used for the calibration. In the next step, a calibration scheme was defined, which systematically changed the value of a given parameter while keeping the remaining parameters constant. A 10% increase/decrease step was used to linearly change parameter values until the soft limits were reached. The soft limits were defined as the 25% - 175% of the initial parameter value (initial value $\pm$75%), which encompassed all reasonably expected values. The definition of the soft limits was also confronted with the information on the HEC-HMS parameter values available in literature (USACE, 1994, GeoSyntec Consultants, 2003, Henneman, 2003, Fleming and Neary, 2004, and others).

The parameters of the snow model were also calibrated manually, using the systematic approach described above. The continuous model was first calibrated on rainfall-induced streamflow, and only after that the snow component was added to the model and the calibration finalized on the solid precipitation data. The parameters of the snow model were varied linearly over the defined soft-limit range until acceptable model performance was achieved.

The input data for the continuous model are available in a daily time step. Since some small subbasins in the study area have concentration time shorter than 24 hours, the model computation step was changed to 6 hours. As a result, values of the daily input data were divided into 4 6-hour long intervals.

III.2.2 Calibration results

Cunderlik and Simonovic (2004) selected the 9-year long observation period from November 1979 to October 1988 for the calibration of the continuous model. This period has the

highest spatio-temporal data density in the UTRb, as well as hydrologic variability representative of the whole analyzed 1940-2002 common observation record. Also, an 8-year long calibration period or longer should according to Yapo et al. (1996) assure that the results will be insensitive to the period selected.

Preliminary results obtained from the model systematically underestimated winter and spring hydrographs and overestimated summer and autumn hydrographs. This error is associated with the discrepancy between the nonlinear rainfall-runoff response in the UTRb and the linear structure of the SMA model. A semiannual parametrization approach was therefore applied, in which separate parameter sets were established for summer and winter seasons. The summer season was defined from May 01 to October 31, and the winter season from November 01 (the beginning of a hydrologic year) to April 30. A semiannual model is recommended also by Fleming and Neary (2004). The authors showed that the performance of a semiannual HEC-HMS model is better than the annual, single-parameter set model.

The semiannual approach applied in this project separates parameters that can take different values in summer and winter seasons, from the parameters that are assumed seasonally invariant. Apart from the parameters describing basin initial conditions, the SMA surface storage capacity and the maximum soil infiltration rate were considered as seasonally dependent parameters. The rationale behind the seasonal alteration of these parameters is that in winter, precipitation is mostly accumulated on the surface, which alters the attenuation of water represented by the Clark's surface storage parameter. Further, the dominant solid precipitation and changed physical properties of soils (such as hydraulic conductivity due to frozen water in soil pores) reduce winter soil infiltration rates. The remaining model parameters are constant in both summer and winter models.

The winter and summer seasons are modeled using the HEC-HMS "start/save states" feature. The start-state option uses states to initialize a run instead of the initial conditions in the basin model. State variables describe the conditions that change during a simulation, for example reservoir storage and initial subbasin baseflow. States contain basin model state variable values at a particular time during a previous run. They represent a complete snap-shot of a basin model responding to a particular meteorologic input at a particular moment in time (USACE, 2001). When the start/save option is used, model initial conditions are estimated only once – for the first season. The model state variables are then saved at the end of the first season, and used as starting states (initial conditions) for the subsequent season (USACE, 2001).

The output from the manual calibration was assessed by flow comparison graphs, scatter graphs, residual graphs, and the statistical goodness-of-fit measures defined in Section II.2.1. The performance of the continuous model is demonstrated again at the same five locations of the UTRb showed in Figure 8 and characterized in Table 2.

Figures 48-52 compare the modeled and observed daily streamflow hydrographs at the selected locations listed in Table 2. Only a time window of four subsequent seasons (November 1, 1983 to October 31, 1985) is showed in these figures, because the streamflow hydrographs could not be well discerned for the whole calibration period 1979-1988 (20 seasons). Three main conclusions regarding the continuous model performance can be drawn from Figures 48-52. Firstly, the external snow model adequately reproduces the snow accumulation and melt processes. Particularly the temporal occurrence of spring snowmelt-generated peaks is well captured by the model. Secondly, some flood peaks are underestimated by the model, other are overestimated, but there is no systematic bias in the winter season peaks or summer season peaks present in the seasonal version of the model. Also, the performance of the model in the

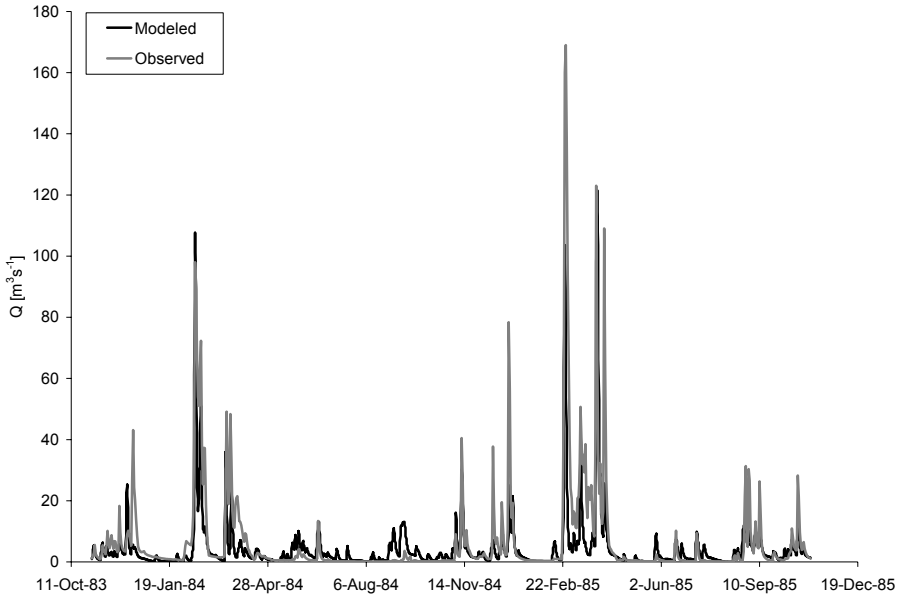

Figure 48. Observed and modeled hydrographs for the calibration period November 1, 1983 to October 31, 1985 at Mitchell.

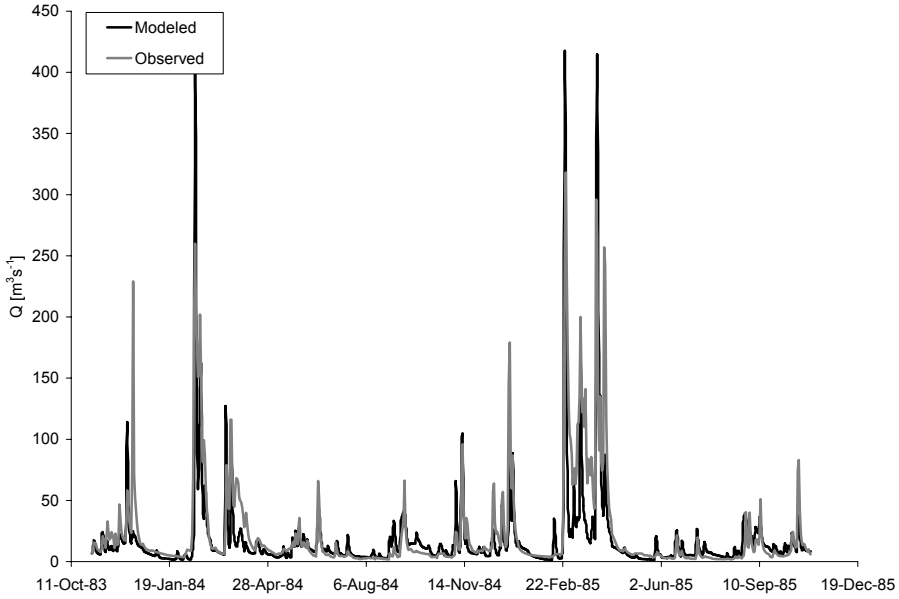

Figure 49. Observed and modeled hydrographs for the calibration period November 1, 1983 to October 31, 1985 at Thorndale.

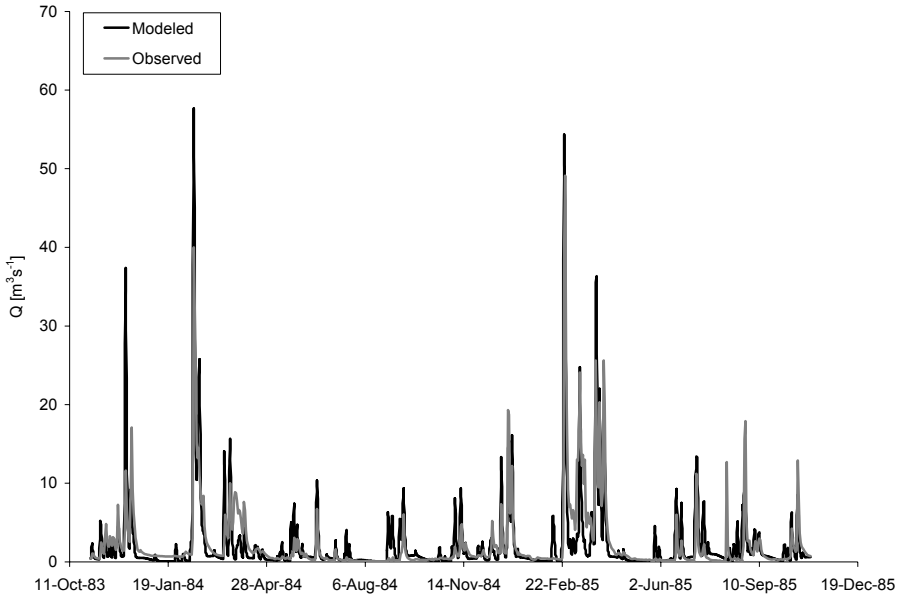

Figure 50. Observed and modeled hydrographs for the calibration period November 1, 1983 to October 31, 1985 at Innerkip.

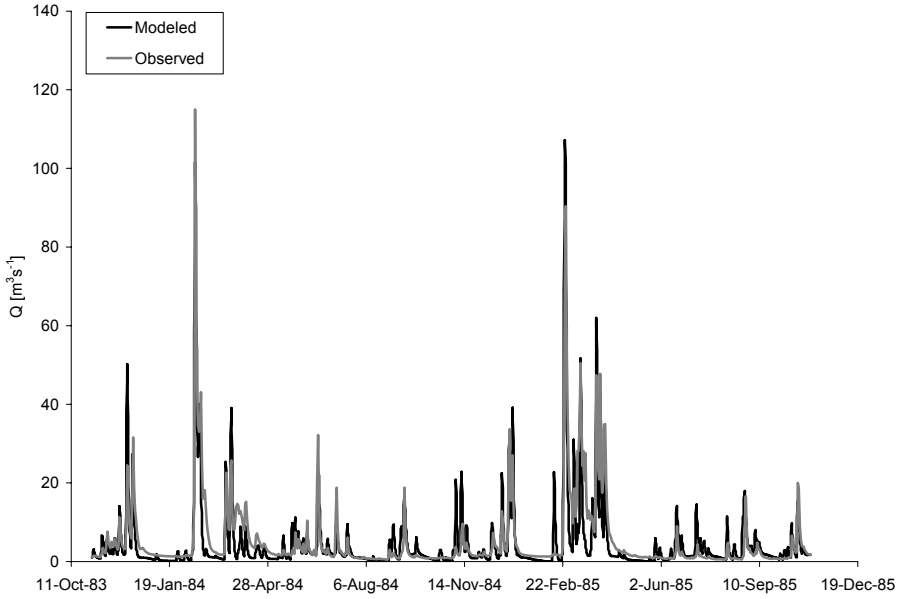

Figure 51. Observed and modeled hydrographs for the calibration period November 1, 1983 to October 31, 1985 at Thamesford.

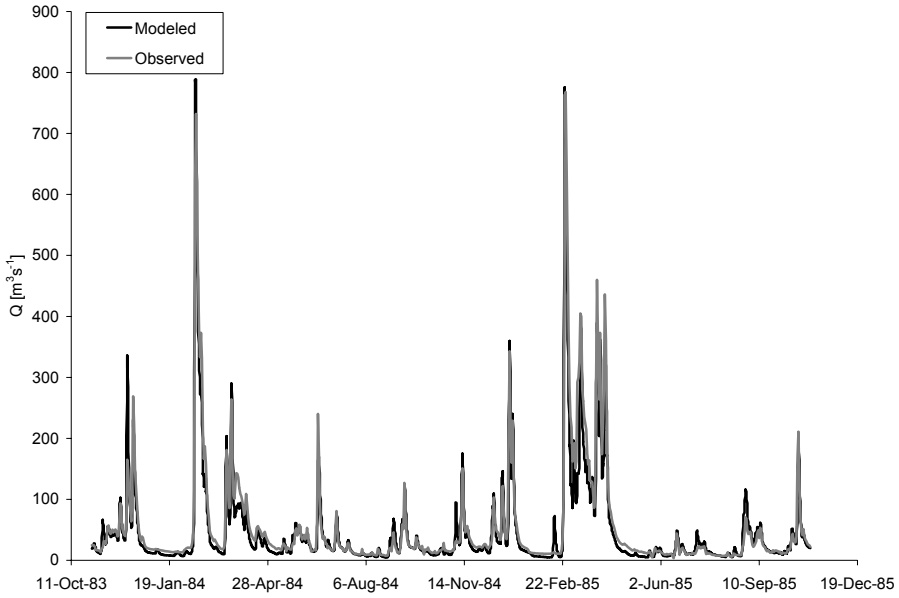

Figure 52. Observed and modeled hydrographs for the calibration period November 1, 1983 to October 31, 1985 at Byron.

simulation of dry periods of low flows is good. Finally, as the contributing area increases, the model performance improves. Due to its semi-distributed structure, the continuous model may lack the ability to capture subbasin-specific features, but as more subbasins become included in the contributing area, the ability of the model to reproduce observed hydrographs improves.

Table 5 compares the statistical performance measures for each station selected for the model evaluation. The percentage error in peak flow (*PEPF*) varies considerably, from 8.8% at Thorndale to almost 44% at Mitchell. The *PEPF* measure is lowest at locations, where more than one subbasin is contributing to the total runoff (Thorndale and Byron). Similar conclusions also apply to the second measure – the percentage error in volume (*PEV*). The *PEV* values at Innerkip and Byron are comparable with the *PEV* values obtained by the event model. The lag-0 cross-correlation coefficients are in the range of 0.74-0.79, only at Byron the *CORR* measure was almost 0.95. The values of the relative *BIAS* differ greatly at the selected locations, from as low as 6.5% at Byron to almost 100% at Innerkip. Very high values were also observed for the

relative *RMSE* measure, especially at Mitchell, with *RRMSE* = 193%. The relative peak-weighted *RMSE* values were lower than the *RRMSE* values, but still high at some locations, such as Mitchell.

Table 5. Statistical performance measures for the selected locations in the UTRb for the November 1979-October 1988 calibration period.

Location	***PEPF* [%]**	***PEV* [%]**	***CORR* [-]**	***RBIAS* [%]**	***RRMSE* [%]**	***RPWRMSE* [%]**
Mitchell	43.759	24.683	0.759	87.885	193.366	131.979
Thorndale	8.852	12.075	0.781	42.271	99.732	82.128
Innerkip	16.438	7.402	0.741	98.200	89.438	77.356
Thamesford	16.536	15.139	0.786	17.627	105.342	94.140
Byron	10.667	8.827	0.946	-6.443	44.826	40.707

The model performance at Mitchell is considerably lower, and at Byron considerably higher than at the remaining stations. The rather poor model performance at Mitchell could be possibly attributed to the location of subbasins 1 and 2 in the upper part of the UTRb, where the meteorological data interpolated by the model may not be well representative. The station at Byron is basically the outlet of the UTRb with a contributing area of 3.110 km^2, consisting of 30 subbasins, which apparently provide a good spatial detail for the model.

III.3 Continuous model verification

III.3.1 Verification procedure

In the verification procedure of the continuous model adopted in this project, only the parameters describing basin initial conditions (initial storage of the canopy, surface, soil and groundwater layer) were changed over time. All the other parameters of the continuous model were kept constant during the model verification. The verification output was assessed by flow comparison graphs, scatter graphs, residual graphs, and the statistical goodness-of-fit measures described in Section II.2.1.

The 9-year long observation period from November 1988 to October 1997 was selected for the calibration of the continuous model (Cunderlik and Simonovic, 2004). Similarly to the calibration period, this period has high spatio-temporal data density in the UTRb, as well as hydrologic variability representative of the whole analyzed 1940-2002 record.

III.3.2 Verification results

Figures 53-57 show flow comparison graphs for the time window from November 1995 to October 1997 for the selected locations at which the model was evaluated.

The modeled hydrograph does not provide a good fit to the observed data at Mitchell. Some peaks are not captured by the model, others are noticeably biased (Figure 53). The model performance improves further downstream at Thorndale (Figure 54), as the contribution area increases from 319 km^2 to 1340 km^2. The model fit at Innerkip is good, except for the peaks

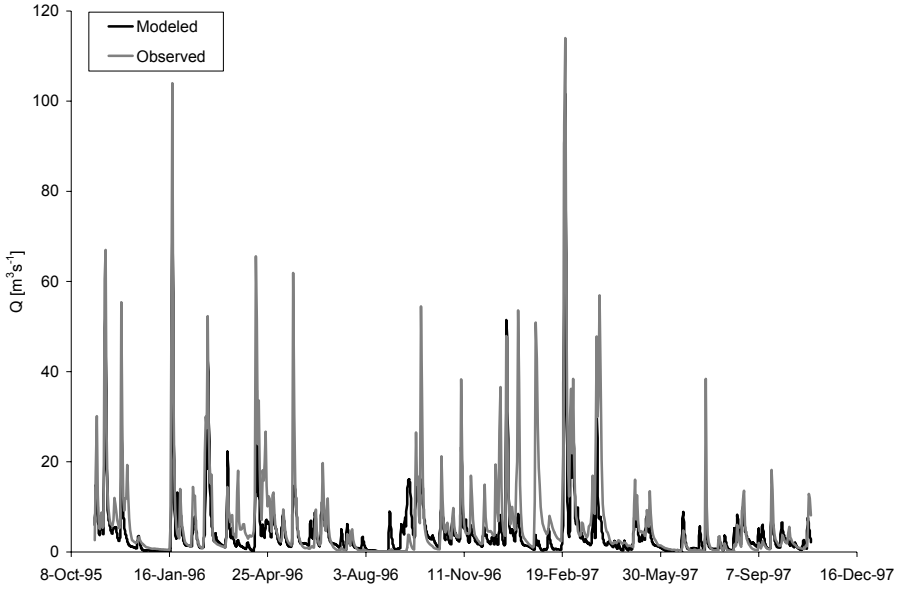

Figure 53. Observed and modeled hydrographs for the verification period November 1, 1995 to October 31, 1997 at Mitchell.

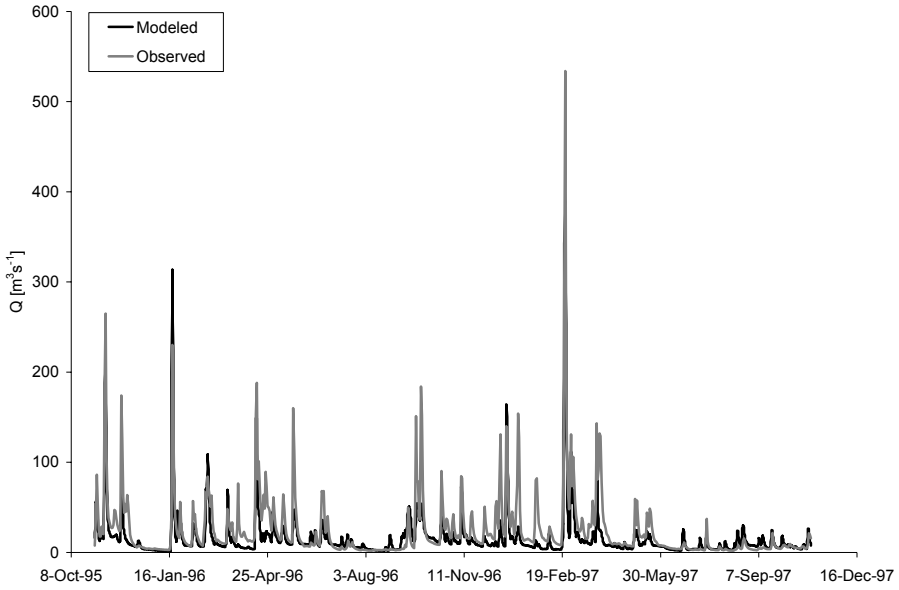

Figure 54. Observed and modeled hydrographs for the verification period November 1, 1995 to October 31, 1997 at Thorndale.

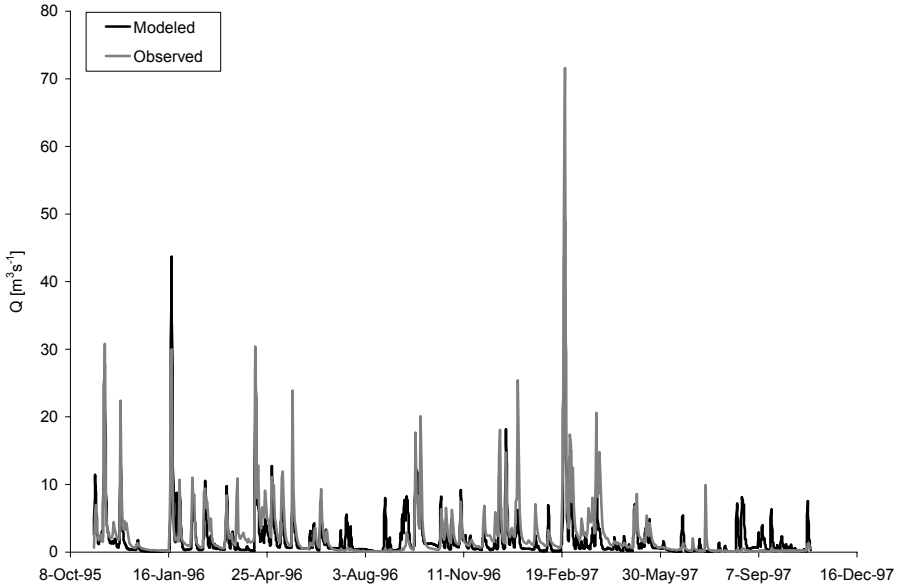

Figure 55. Observed and modeled hydrographs for the verification period November 1, 1995 to October 31, 1997 at Innerkip.

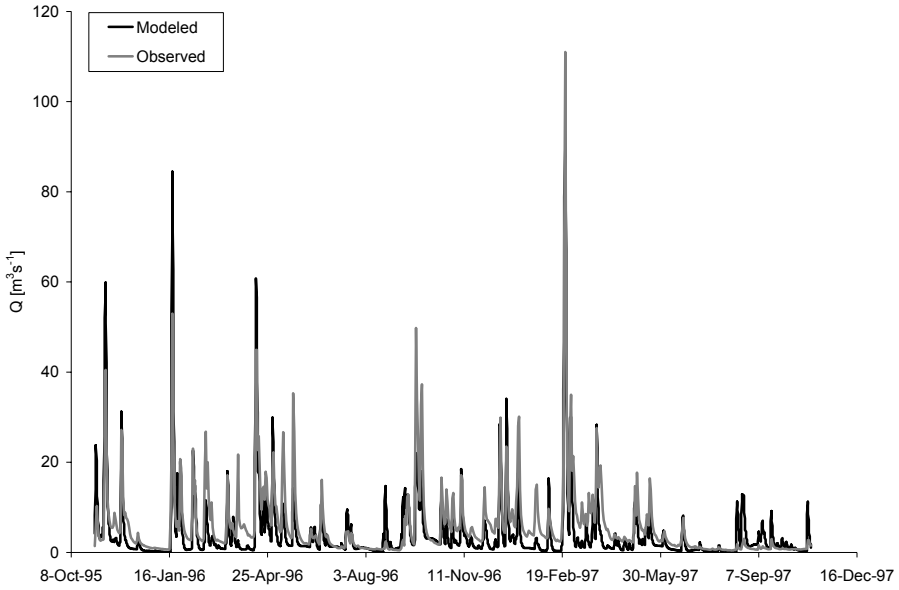

Figure 56. Observed and modeled hydrographs for the verification period November 1, 1995 to October 31, 1997 at Thamesford.

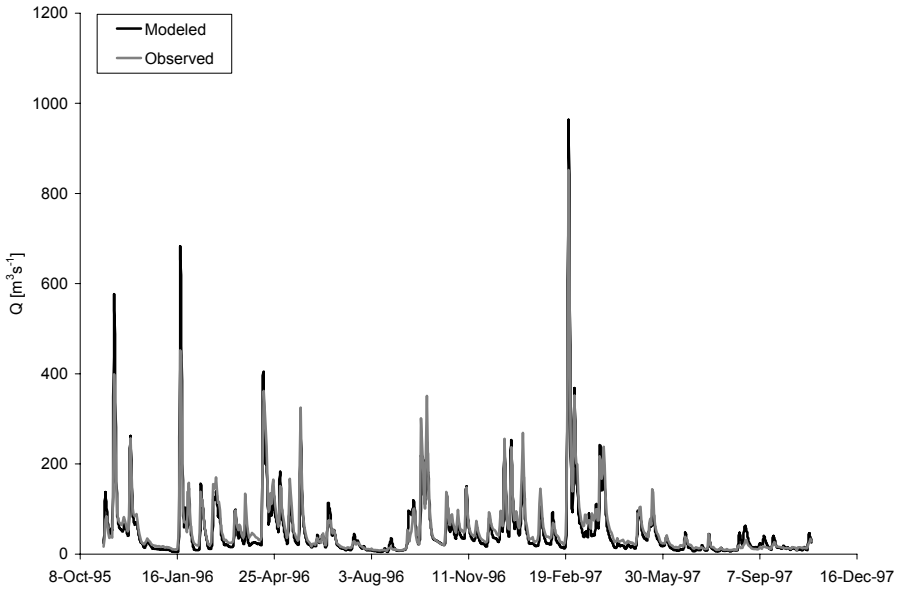

Figure 57. Observed and modeled hydrographs for the verification period November 1, 1995 to October 31, 1997 at Byron.

generated during the summer seasons that were not present in the observed data (Figure 55). At Thamesford, the model systematically underestimated the lows between the peaks of the winter seasons (Figure 56). Finally, the performance of the model at the outlet station Byron is very good (Figure 57).

Table 6 compares the statistical performance measures calculated for each station selected for the model evaluation. The percentage error in peak flow (*PEPF*) is very low for the verification period at Thamesford, only 2.6%. The maximum value of the *PEPF* measure is observed again at Mitchell (30.4%). The results for the percentage error in volume (*PEV*) follow the pattern of the calibration results. The lowest values of *PEV* were again observed at Innerkip and Byron, both less than 10%. The lag-0 cross-correlation coefficient values, *CORR*, were very similar to the values obtained from the calibration period, within the range of 0.74-0.79, and at Byron 0.95. The values of the relative *BIAS* differ greatly at the selected locations, from -7.6% at Byron to over 100% at Innerkip. Very high values were also observed for the relative RMSE measure, at Mitchell the *RRMSE* was 239%. The relative peak-weighted *RMSE* values were lower than the *RRMSE* values.

Table 6. Statistical performance measures for the selected locations in the UTRb for the November 1988-October 1997 verification period.

Aug-00	***PEPF* [%]**	***PEV* [%]**	***CORR* [-]**	***RBIAS* [%]**	***RRMSE* [%]**	***RPWRMSE* [%]**
Mitchell	30.425	23.966	0.765	97.274	238.654	122.518
Thorndale	27.067	27.911	0.795	33.635	88.553	90.714
Innerkip	25.922	3.424	0.789	104.514	78.654	95.261
Thamesford	2.649	10.464	0.794	19.546	108.358	104.278
Byron	13.096	7.607	0.939	-7.615	46.488	42.245

In general, the verification performance results given in Table 6 are very similar to the calibration results summarized in Table 5. The average *PEPF* value from the calibration data is 19.2% and from the verification data 19.8%. The performance results are also similar according to the *PEV* and *CORR* measures. The average calibration *PEV* is 13.6% and the verification *PEV*

14.7. The average *CORR* from the calibration data is 0.80 and from the verification data 0.82. According to the relative measures *RBIAS*, *RRMSE* and *PWRMSE*, the continuous model performed better on the data from the calibration period (average *RBIAS* 47.9%, average *RRMSE* 106.5% and average *PWRMSE* 85.3%) than on the data from the verification period (49.5%, 112.1% and 91.0%).

The final model verification involved replacing the source-sink components with the uncontrolled-output dam components. Figures 58-59 show the corresponding model outputs compared with the observed hydrograph at the location Byron for the selected time windows of the calibration and verification periods. In both cases the dam components increased spring peak hydrographs and decreased low flows in the winter periods. The performance of the model in the summer periods was affected minimally.

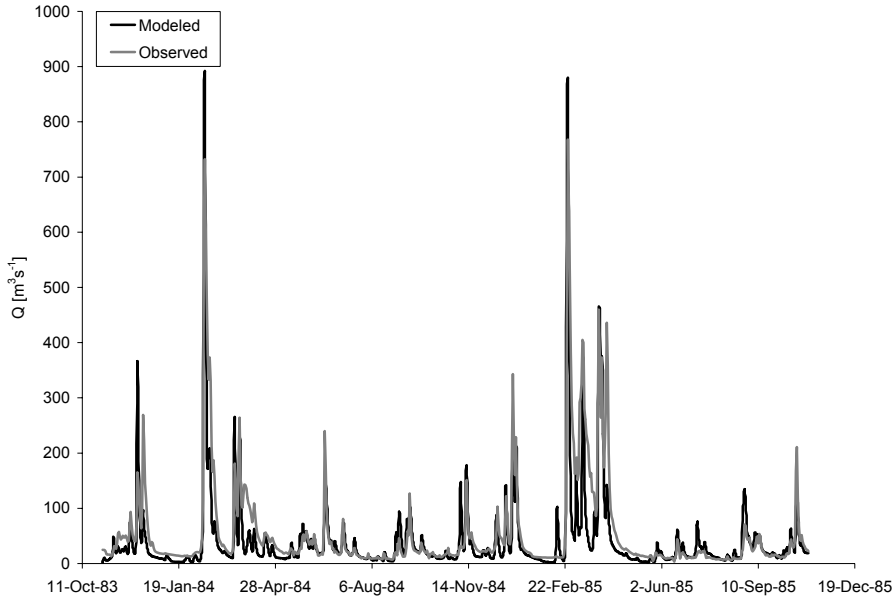

Figure 58. Observed and modeled-with-dams hydrographs for the calibration period November 1, 1983 to October 31, 1985 at Byron.

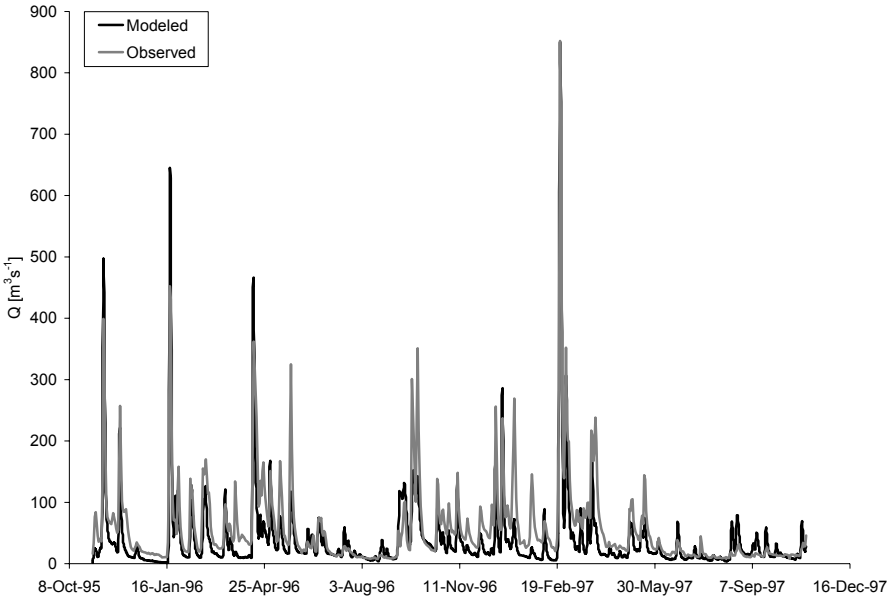

Figure 59. Observed and modeled-with-dams hydrographs for the verification period November 1, 1995 to October 31, 1997 at Byron.

In the next step, the parameters of the SMA model were adjusted to eliminate the discrepancy between the modeled and observed peak hydrographs. Again, adjusting the calibrated continuous model parameters is a compromise between the performance of the model and the necessity to use the reservoir component in practical applications of the model defined by the project objectives. The final set of model parameters is given in Appendix IVb. Figures 60-61 show the results obtained by the re-calibrated version of the model.

The performance of the recalibrated model visibly improved during the winter seasons. Particularly the magnitudes of snowmelt-induced peaks, which were overestimated by the previous model, are now in better agreement with the observed peak discharges.

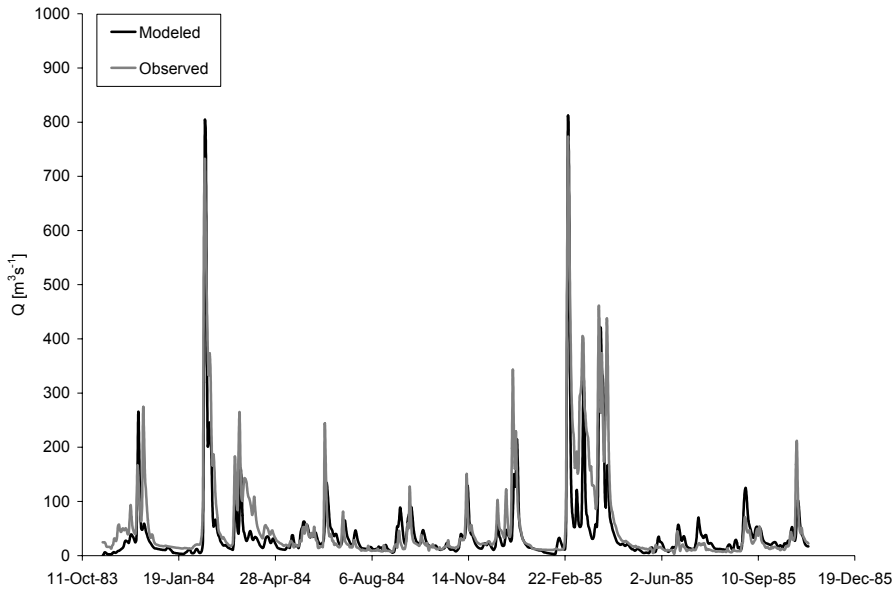

Figure 60. Observed and recalibrated modeled-with-dams hydrographs for the calibration period November 1, 1983 to October 31, 1985 at Byron.

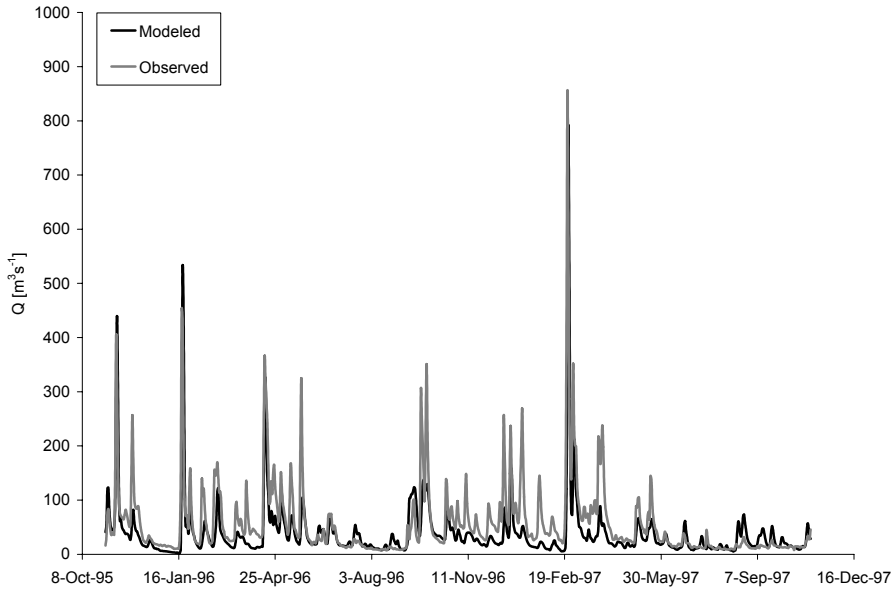

Figure 61. Observed and recalibrated modeled-with-dams hydrographs for the verification period November 1, 1995 to October 31, 1997 at Byron.

III.4 Continuous model sensitivity

III.4.1 Sensitivity procedure

A local sensitivity analysis was adopted for evaluating the parameters of the continuous model. The final set of the parameters of the calibrated model was considered as a baseline/nominal parameter set. The model was run repeatedly with the baseline value for each parameter multiplied, in turn, by 0.8 and 1.2, while keeping all other parameters constant at their nominal starting values. The hydrographs resulting from the scenarios of adjusted model parameters were then compared with the baseline model hydrograph. The performance measures defined in Section II.2.1 were used as sensitivity functions. Since these measures are dimensionless, the absolute sensitivity coefficient (Equation (16)) was used to compare the results from different sensitivity scenarios.

There are 23 parameters used in the continuous model, when all five layers are included in the SMA component (12 SMA loss parameters with another 5 parameters defining initial conditions in the SMA layers, 2 transform parameters, and 4 baseflow parameters). The SMA initial parameters were not included in the sensitivity analysis, because they influence only the beginning of the first season; the subsequent seasons have initial conditions automatically set to the conditions at the end of the previous seasons. Furthermore, the parameters of the two SMA groundwater layers and the two sets of baseflow parameters were not analyzed separately, which reduced the number of parameters to 13 (see Appendix IIb for a summary of continuous model parameters).

III.4.2 Sensitivity results

The sensitivity procedure described in the previous section was applied to the subbasin nr. 23 (Middle Thames River at Thamesford, ID 02GD004), using the precipitation data from the time period November 1, 1983 to October 31, 1985. The number of scenarios (-20% and +20%

change in the parameter value), as well as the length of the modeling period (2 winter and 2 summer seasons) was reduced, considering the number of parameters of the continuous model, and the lengthy process of modeling separate winter and summer seasons.

Figure 62 compares the percentage error in the peak flow, *PEPF*, for the two scenarios of increased and decreased parameter values of the continuous model. The highest value of *PEPF*, almost 10%, was generated by changing the value of the Clark's storage coefficient, *St*. Moderate values of *PEPF* were obtained for scenarios of changed upper soil, *Us*, and tension soil, *Ts*, level storages and the infiltration rate, *If*. The *PEPF* for the remaining scenarios were around 1% and less.

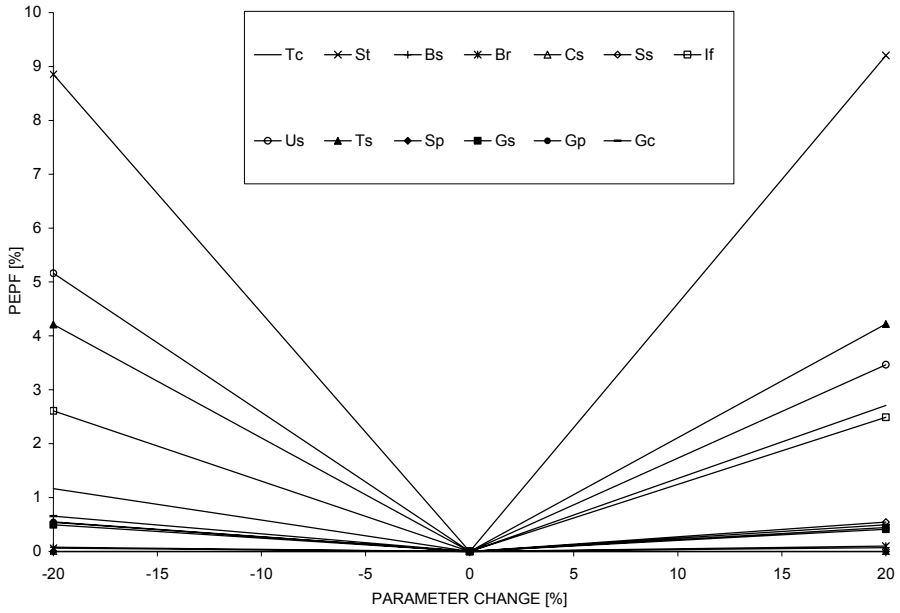

Figure 62. *PEPF* of the model results generated from the sensitivity scenarios of the change in the continuous model parameters.

Figure 63 shows the results evaluated according to the percentage error in volume, *PEV*. Changed values of all three groundwater layer parameters and the upper soil storage parameter generated the highest errors in the hydrograph volume. All four parameters led to similar results with *PEV* values ranging approximately between 6-9%. Relatively high *PEV* values were

generated also by the tension soil storage and the infiltration rate. The remaining scenarios generated *PEV* values around 1.5% and less.

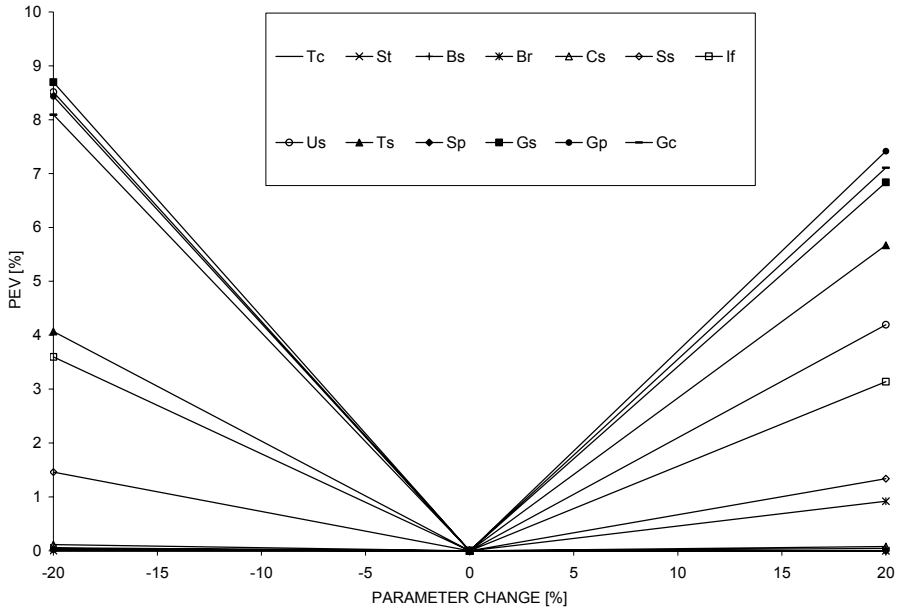

Figure 63. *PEV* of the model results generated from the sensitivity scenarios of the change in the continuous model parameters.

Figure 64 depicts the sensitivity scenarios compared according to the lag-0 cross-correlation coefficient, *CORR*. The results are similar for most scenarios except for the ground water storage, *Gs*, and the deep percolation, *Gp*, parameters, which generated hydrographs less correlated with the baseline data than the remaining scenarios (*CORR* values lower than 0.985).

Figure 65 compares the relative *BIAS* for the evaluated sensitivity scenarios. The *RBIAS* values above 10% were obtained by changing the three groundwater layer parameters, the groundwater storage, *Gs*, percolation rate, *Gp*, and the storage coefficient, *Gc*. The *RBIAS* values for the baseflow parameters were between 5-10%. The *RBIAS* values for the remaining parameters were low, within ±2.5%.

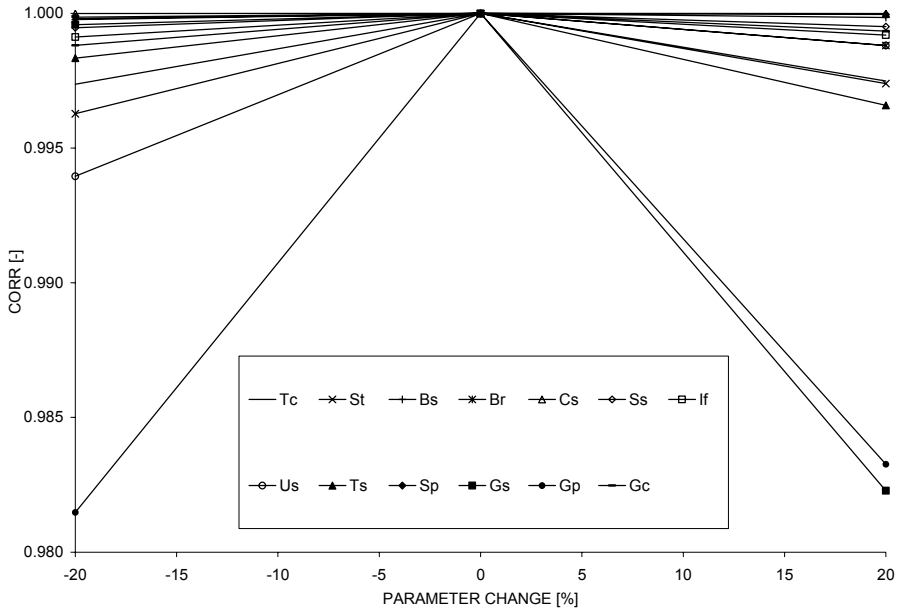

Figure 64. *CORR* of the model results generated from the sensitivity scenarios of the change in the continuous model parameters.

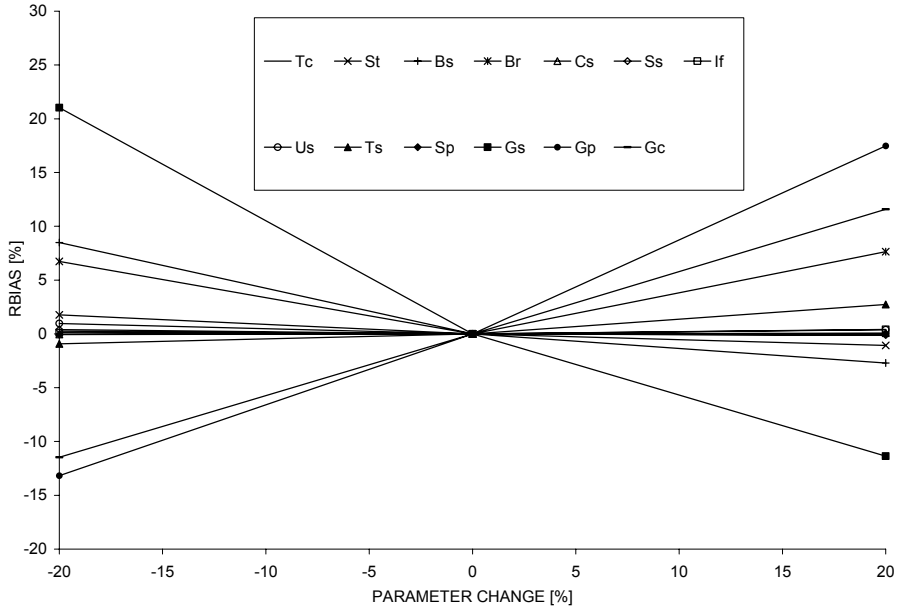

Figure 65. Relative *BIAS* of the model results generated from the sensitivity scenarios of the change in the continuous model parameters.

Figure 66 compares the relative *RMSE* for the different scenarios of the ±20% change in the continuous model parameters. The highest value, 64% was obtained by changing the

number of reservoirs, *Br*, in the baseflow model. *RRMSE* values above 20% were generated by changing the baseflow storage, *Bs*, groundwater storage, *Gs*, and deep percolation, *Gp*, parameters. Relatively high values, within the range of 10-20% were obtained by changing the soil storage parameters (*Us* and *Ts*) and the groundwater storage coefficient, *Gc*.

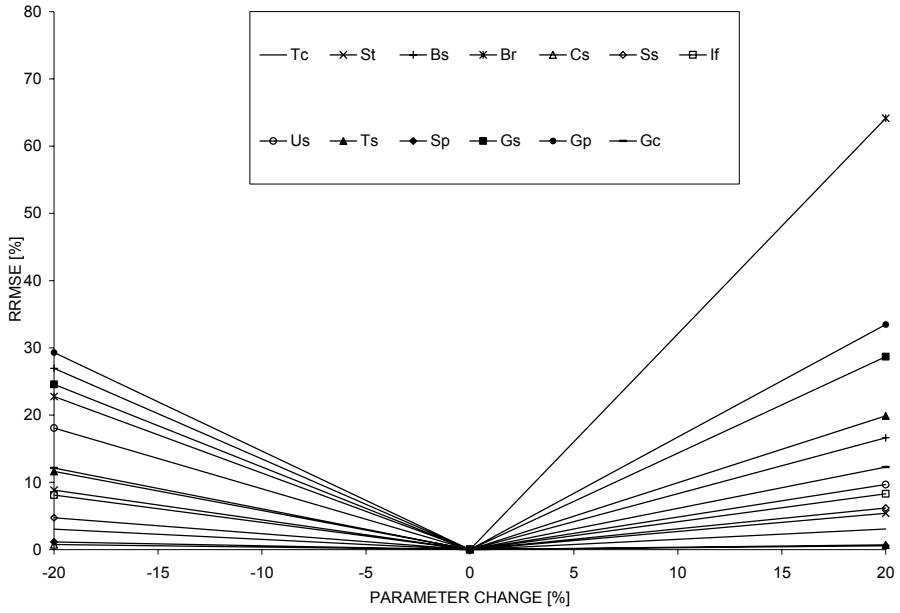

Figure 66. Relative *RMSE* of the model results generated from the sensitivity scenarios of the change in the continuous model parameters.

A comparison of the scenarios according to the *PWRMSE* measure is given in Figure 67. The results closely follow the pattern of the *RRMSE* results. Even here the model was most sensitive to the groundwater layer storage and percolation parameters, and on both baseflow parameters (*Bs* and *Br*). Moderate sensitivity with *PWRMSE* between 10-20% was observed for the soil storage parameters and the groundwater storage coefficient.

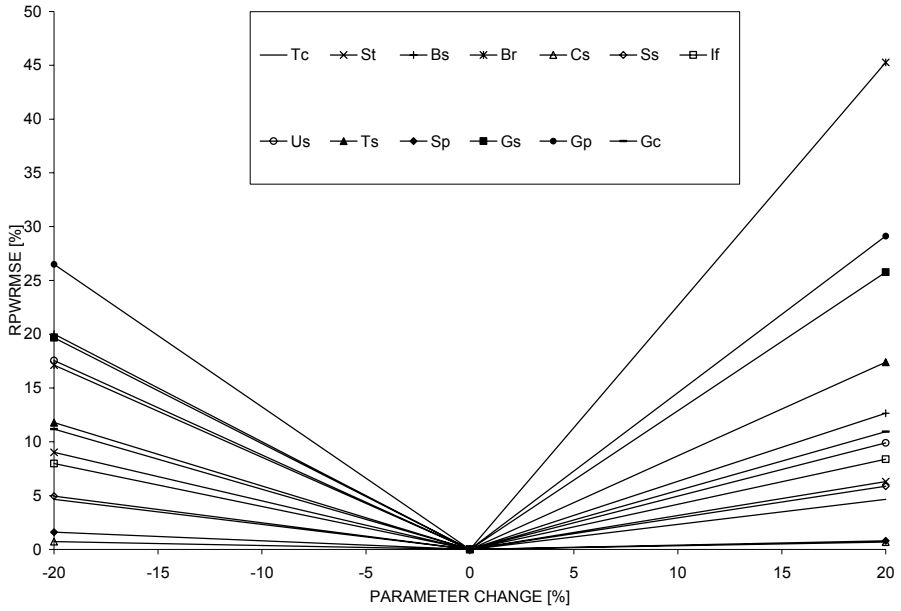

Figure 67. Relative *PWRMSE* of the model results generated from the sensitivity scenarios of the change in the continuous model parameters.

The continuous UTRb hydrologic model is targeted at simulating dry, low flow periods, autumn type of rainfall-driven high flow events, and spring snowmelt-induced flood hydrographs. With respect to flood magnitudes, the Clark's storage coefficient and the parameters describing physical properties of the soil (infiltration rate and soil layer storage) were again found to be the parameters that have the greatest impact on peak hydrographs. These results are consistent with the sensitivity results of the event model. In terms of the peak volume, the continuous model was found to be most sensitive to the SMA groundwater layer parameters. The SMA groundwater parameters in combination with the baseflow parameters are also most important for simulating low flows, and for the overall goodness-of-fit of the continuous model.

Fleming and Neary (2004) performed a similar sensitivity analysis of a continuous HEC-HMS model of the Dale Hollow basin in Kentucky and Tennessee. They concluded that the maximum infiltration rate, *If*, the maximum soil depth, *Us*, and the tension zone depth, *Ts*,

caused the most variation in simulated streamflow when adjusted. The difference between the sensitivity results from Fleming and Neary (2004) and the results obtained in this study can be attributed to the limitation of a local sensitivity analysis, which depends on the actual combination of model parameters. For example, if the percolation rate between the soil and the first groundwater layer is high, then the model will be less sensitive to the parameters describing water content in the soil. On the other hand, if the deep percolation rate between the two groundwater layers is low, then the parameters of the first groundwater layer are likely to be the highly sensitive parameters of the SMA model, because the water will tend to retain in this layer longer than in the other layers of the model.

IV. CONCLUSIONS

This report provides in-depth information on the event and continuous versions of the HEC-HMS hydrologic model of the Upper Thames River basin. The report describes the structure of the event and continuous models, procedures adopted for their calibration and verification, as well as their sensitivity to individual parameters. The enclosed appendixes provide the information necessary for using the model, including the values of all calibrated model parameters, names of project files, and the relevant input data (except streamflow, precipitation and temperature time series).

The structure of the event model comprises six model components describing main hydrologic processes in the river basin. Solid precipitation, evapotranspiration, and detailed soil moisture accounting are processes not important in the event hydrologic modeling, and were not included in the event model structure. The calibration procedure adopted in the event modeling involved a combination of both manual and automated calibrations. The event model was calibrated and verified on intensive summer storm events, and its use should be limited to the simulation of such events. The results from the calibration showed that more detailed accounting of the movement and storage of water through the system is necessary for simulation of autumn rainfall events, and therefore these events are modeled with the continuous version of the UTRb model.

The structure of the continuous model resembles the event model structure. In addition, snow accumulation and melt, evapotranspiration and detailed soil moisture accounting are extra processes simulated by this version of the UTRb model, because in continuous hydrologic modeling, detailed accounting of the movement and storage of water through all components of the river basin system is necessary. Due to the limitations of the HEC-HMS software, the

calibration procedure adopted in the continuous modeling involved only manual calibration. The use of the continuous model is aimed at the modeling of spring snowmelt-induced events, modeling of low flows, and late autumn rainfall events with more complex antecedent soil moisture patterns. Because of the identified discrepancy between the nonlinear rainfall-runoff response and the linear structure of the SMA model, a semiannual parametrization approach was applied to the continuous UTRb modeling.

The verification results of the event model showed that the model performs well in the simulation of peak flows. The recession parts of streamflow hydrographs preceding and succeeding the peak are underestimated by the model. This also leads to a slight underestimation of the total flood volume. However, the error in flood volume (excluding errors in recession hydrograph ordinates) should not exceed 5-10%. A correction factor can be derived for an accurate estimation of flood volumes based on the analysis of the modeled and observed hydrographs.

The verification results of the continuous model demonstrated that the snow component can adequately reproduce snow accumulation and melt in the UTRb. The performance of the continuous model in the simulation of dry periods of low flows is also good. The seasonal model shows no systematic bias in the winter season peaks and summer season peaks. The model performance improves with increasing basin area and spatial detail. The continuous model systematically underestimates total streamflow volumes by 10-15%. A correction factor should be therefore applied when the objective of the analysis is the estimation of streamflow volumes.

Both the event and continuous models were calibrated and verified on spatially and temporally interpolated precipitation. The spatial and temporal distribution of the interpolated precipitation may not always correspond well to the true precipitation distribution. Moreover, for

practical applications of the model, it is important to remember that the interpolated precipitation distribution is also reflected in the calibrated model parameters.

A local approach to sensitivity analysis was adopted for evaluating the event and continuous models. The results showed that with respect to flood magnitudes, the event model is most sensitive to the Clark's storage coefficient. In terms of peak volume, the event model is most sensitive to the initial and constant loss parameters, baseflow recession, and the Clark's storage coefficient. The Clark's storage coefficient and the parameters describing physical properties of the soil (infiltration rate and soil layer storage) were found to be the parameters that have the greatest impact on peak hydrographs generated by the continuous model. The SMA groundwater parameters in combination with the baseflow parameters are also most important for simulating low flows, and for the overall goodness-of-fit of the continuous model.

To conclude, the results presented in this report finalize the project Task 1 (Development of a hydrologic model). Subsequent specific applications of the event and continuous versions of the hydrologic model defined in the project objectives will be parts of the project Task 4 (Assessment of risk and vulnerability) and Task 5 (Case study).

V. REFERENCES

[1] Arnold, J.G., Muttiahb, R.S., Srinivasan, R. and P.M. Allen, 2000. Regional estimation of base flow and groundwater recharge in the Upper Mississippi river basin. *Journal of Hydrology*, 227, 21–40.

[2] Clark, C.O., 1945. Storage and the unit hydrograph: *Transactions: American Society of Civil Engineers*, 110, 1419-1488.

[3] Cunderlik, J.M., and S.P. Simonovic, 2003. Hydrologic model selection for the CFCAS project: Assessment of Water Resources Risk and Vulnerability to Changing Climatic Conditions. CFCAS Project Report I., 38 p.

[4] Cunderlik, J.M., and S.P. Simonovic, 2004. Selection of calibration and verification data for the HEC-HMS hydrologic model. CFCAS Project: Assessment of Water Resources Risk and Vulnerability to Changing Climatic Conditions. Project Report II., 30 p.

[5] Doorenbos, J., and W. 0. Pruitt., 1975. Guidelines for predicting crop water requirements. FAO irrigation and drainage paper 24.

[6] Eckhardt, K., and J.G. Arnold, 2001. Automatic calibration of a distributed catchment model. *Journal of Hydrology*, 251/1-2, 103-109.

[7] ICLR, 2004. Institute for Catastrophic Loss Reduction home page. Assessment of Water Resources Risk and Vulnerability to Changing Climatic Conditions project web page, http://www.engga.uwo.ca/research/iclr/fids/CFCAS_Project/CFCAS_main_page.htm.

[8] Fleming, M., and V. Neary, 2004. Continuous hydrologic modeling study with the Hydrologic Modeling System. *Journal of Hydrologic Engineering*, 9/3, 175-183.

[9] GeoSyntec Consultants, Inc., 2003. Hydromodification management plan draft interim report: Assessment of the lower Silver-Thompson Creek subwatershed. Prepared for Santa Clara Valley Urban Runoff Pollution Prevention Program, CA, USA, 91 p.

[10] Haan, C.T., 2002. *Statistical methods in hydrology*. Second Edition, Iowa State Press, 496 p.

[11] Henneman, H., 2003. Hydrologic modeling for ecosystem restoration, Lockport Prairie, Illinois. In: 30th Natural Areas Conference: Defining a Natural Areas Land Ethic, September 24-27, 2003, Madison, Wisconsin, 10 p.

[12] Hock, R., 2003. Temperature index melt modeling in mountain areas. *Journal of Hydrology*, 282, 104-115.

[13] Hydrology Standards, 1996. Sacramento City/County Drainage Manual.

[14] Leavesley, G.H., Lichty, R.W., Troutman, B.M., and L.G. Saindon, 1983. *Precipitation-runoff modeling system user's manual*. Water-Resources Investigations, 83-4238. US Dept. of the Interior, Geological Survey, Denver, CO.

[15] Madsen, H., 2000. Automatic calibration of a conceptual rainfall–runoff model using multiple objectives. *Journal of Hydrology*, 235/3-4, 276-288.

[16] Madsen, H., Wilson, G., and H.C. Ammentorp, 2002. Comparison of different automated strategies for calibration of rainfall-runoff models. *Journal of Hydrology*, 261/1-4, 48-59.

[17] McCuen, R.H., 2003. *Modeling hydrologic change. Statistical methods*. Lewis Publishers, 433 p.

[18] Nelson, E.J., Smemoe, C.M., and B. Zhao, 1999. A GIS approach to watershed modeling in Maricopa County, Arizona. Proceedings of the 1999 ASCE Conference, Boston, USA, 10 p.

[19] Sabol, G.V., 1988. Clark unit hydrograph and r-parameter estimation. *Journal of Hydraulic Engineering*, 114/1, 103-111.

[20] Soil Conservation Service, 1972. *National Engineering Handbook*. United States Department of Agriculture, United States Government, Washington, USA.

[21] Sorooshian, S., Gupta, V.K., and J.L. Fulton, 1983. Evaluation of maximum likelihood parameter estimation techniques for conceptual rainfall-runoff models - influence of calibration data variability and length on model credibility", *Water Resources Research*, 19/1, 251-259.

[22] Straub, T.D., Melching, C.S., and K.E. Kocher, 2000. Equations for estimating Clark unit-hydrograph parameters for small rural watersheds in Illinois. Water-Resources Investigations Report 00–4184, USGS, 30 p.

[23] USACE, 1994. *Flood-runoff analysis*. Engineering Manual. US Army Corps of Engineers, EM 1110-2-1417, 214 p.

[24] USACE, 2000a. *Geospatial Hydrologic Modeling Extension HEC-GeoHMS*. User's Manual. US Army Corps of Engineers, Hydrologic Engineering Center, 267 p.

[25] USACE, 2000b. *Hydrologic Modeling System HEC-HMS*. Technical Reference Manual. US Army Corps of Engineers, Hydrologic Engineering Center, 149 p.

[26] USACE, 2001. *Hydrologic Modeling System HEC-HMS*. User's Manual, Version 2.1. US Army Corps of Engineers, Hydrologic Engineering Center, 178 p.

[27] USACE, 2002. *Hydrologic Modeling System HEC-HMS*. Applications Guide. US Army Corps of Engineers, Hydrologic Engineering Center, 106 p.

[28] USACE, 2003a. *HEC Data Storage System Visual Utility Engine*. User's Manual. US Army Corps of Engineers, Hydrologic Engineering Center.

[29] USACE, 2003b. *HEC DSS Microsoft Excel Add-In*. User's Manual. US Army Corps of Engineers, Hydrologic Engineering Center, 17 p.

[30] UTRCA, 2003. The Upper Thamer River Conservation Authority Home Page, http://www.thamesriver.org/.

[31] Yapo, P.O., Gupta, H.V., and S. Sorooshian, 1996. Automatic calibration of conceptual rainfall-runoff models: sensitivity to calibration data. *Journal of Hydrology*, 181/1-4, 23-48.

[32] Yapo, P.O., Gupta, H.V., and S. Sorooshian, 1998. Multi-objective global optimization for hydrologic models. *Journal of Hydrology*, 204/1-4, 83-97.

[33] Yu, P-S., and T-C. Yang, 2000. Fuzzy multi-objective function for rainfall-runoff model calibration. *Journal of Hydrology*, 238/1-2, 1-14.

VI. ABBREVIATIONS

BME	Basin Modeling Environment
CFCAS	Canadian Foundation for Climatic and Atmospheric Sciences
DSSVue	Data Storage System Visual Utility Engine
E	Elevation
EC	Environment Canada
ET	Evapotranspiration
HEC	Hydrologic Engineering Center
HMS	Hydrologic Modeling System
I	Input
IDM	Inverse Distance Method
NM	Nelder and Mead (optimization search method)
O	Output
PEPF	Percent Error in Peak Flow
PEV	Percent Error in Volume
PWRMSE	Peak Weighted Root Mean Squared Error
RBIAS	Relative Bias
RRMSE	Root Mean Squared Error
SA	Absolute Sensitivity
SAR	Sum of Absolute Residuals
SCS	Soil Conservation Service
SD	Deviation Sensitivity
SMA	Soil Moisture Accounting
SMU	Soil Moisture Unit
SR	Relative Sensitivity
SSR	Sum of Squared Residuals
UG	Univariate Gradient (optimization search method)
USACE	United States Army Corps of Engineers
UTRb	Upper Thames River basin
VB	Visual Basic

APPENDIX I. LIST OF PROJECT FILES

CONT_SNOW_PET.met ..... HEC HMS meteorologic component of the continuous model

CONTINUOUS+DAMS.basin.. HEC HMS continuous basin model

EC dam qs.dss..... HEC DSSVue database of reservoir outflow data

EC.dss ..... HEC DSSVue database of EC daily precipitation data

EVENT.basin ..... HEC HMS event basin model

EVENT.control ..... HEC HMS control specification for the event model

Hydat.dss..... HEC DSSVue database of daily streamflow data

IDM-NEW.met ..... HEC HMS Meteorologic component of the event model

NEW PRECIP.dss ..... HEC DSSVue database of precipitation data adjusted by the snow model

Snow.cls ..... VB class module of the snow accumulation and melt model used in the continuous HEC-HMS model

SUMMER.control..... HEC HMS control specification for summer seasons of the continuous model

UTRCA.dss ..... HEC DSSVue database of hourly rainfall and streamflow data

UTRCA_full.dsc..... HEC HMS catalog of records in the project DSS file

UTRCA_full.dss..... HEC HMS project DSS file

UTRCA_full.gage ..... HEC HMS definition of precipitation and discharge gages

UTRCA_full.hms ..... HEC HMS project file

UTRCA_full.smu ..... HEC HMS definition of SMA units

WINTER.control..... HEC HMS control specification for winter seasons of the continuous model

APPENDIX II. SUMMARY OF MODEL PARAMETERS

Appendix IIa. Summary of event model parameters

Parameter	Symbol	Units	Component
Initial loss	*Li*	[mm]	Rainfall loss
Constant loss rate	*Lr*	[mm×hr^{-1}]	
Impervious subbasin area	*Ai*	[%]	
Subbasin area	*As*	[km^2]	
Time of concentration	*Tc*	[hr]	Direct runoff
Storage coefficient	*St*	[hr]	
Storage-outflow	*SO*	[1000×m^3-m^{3}s^{-1}]	River routing
Number of subreaches	*Ns*	[#]	
Reach initial condition	*Ri*	[units of O or O=I]	
Initial baseflow	*Bi*	[m^{3}s^{-1} or m^{3}s^{-1}km^{-2}]	Baseflow
Recession constant	*Rc*	[-]	
Threshold	*Td*	[m^{3}s^{-1} or ratio-to-peak]	
Elevation-storage-outflow	*ESO*	[m-1000×m^3-m^{3}s^{-1}]	Reservoir
Initial condition	*Di*	[units of I=O or E or S or O]	

Appendix IIb. Summary of continuous model parameters

Parameter	Symbol	Units	Component
Upper temperature threshold	*Tmax*	[°C]	Snow
Lower temperature threshold	*Tmin*	[°C]	
Critical temperature for snowmelt	*Tcrt*	[°C]	
Snowmelt rate	*Mr*	[mm/°C/day]	
Initial canopy storage	*Ci*	[%]	Precipitation loss
Canopy storage capacity	*Cs*	[mm]	
Initial surface storage	*Si*	[%]	
Surface storage capacity	*Ss*	[mm]	
Infiltration rate	*If*	[mm×hr^{-1}]	
Initial soil storage	*Is*	[%]	
Soil storage capacity	*Us*	[mm]	
Tension zone capacity	*Ts*	[mm]	
Soil percolation rate	*Sp*	[mm×hr^{-1}]	
Initial groundwater 1 storage	*G1i*	[%]	
Groundwater 1 storage capacity	*G1s*	[mm]	
Groundwater 1 percolation rate	*G1p*	[mm×hr^{-1}]	
Groundwater 1 storage coefficient	*G1c*	[hr]	
Initial groundwater 2 storage	*G2i*	[%]	
Groundwater 2 storage capacity	*G2s*	[mm]	
Groundwater 2 percolation rate	*G2p*	[mm×hr^{-1}]	
Groundwater 2 storage coefficient	*G2c*	[hr]	
Impervious subbasin area	*Ai*	[%]	
Subbasin area	*As*	[km^2]	
Time of concentration	*Tc*	[hr]	Direct runoff
Storage coefficient	*St*	[hr]	
Storage-outflow	*SO*	[1000×m^3-m^{3}s^{-1}]	River routing
Number of subreaches	*Si*	[#]	
Reach initial condition	*Ri*	[units of O or O=I]	
Baseflow 1 storage coefficient	*B1s*	[hr]	Baseflow
Baseflow 1 number of reservoirs	*B1r*	[#]	
Baseflow 2 storage coefficient	*B2s*	[hr]	
Baseflow 2 number of reservoirs	*B2r*	[#]	
Elevation-storage-outflow	*ESO*	[m-1000×m^3-m^{3}s^{-1}]	Reservoir
Initial condition	*Di*	[units of I=O or E or S or O]	

APPENDIX III. MODEL INPUT DATA

Appendix IIIa. Storage-outflow curves of the reach components included in the event and continuous models.

R111		R222		R333		R560		R640		R750		R900	
S	O	S	O	S	O	S	O	S	O	S	O	S	O
0.00	0.00	0.00	0.00	0.00	0.00	0.00	0.00	0.00	0.00	0.00	0.00	0.00	0.00
50.50	4.40	95.13	7.00	107.93	10.80	389.67	20.70	271.15	25.30	104.90	27.50	182.90	31.90
86.16	8.80	156.33	14.00	169.42	21.60	657.93	41.40	440.87	50.50	177.99	55.00	297.24	64.00
196.43	21.60	378.48	35.00	311.18	54.00	1421.86	104.00	924.18	126.00	377.73	138.00	603.72	159.00
329.36	34.00	690.30	70.00	513.11	108.00	2607.09	207.00	1663.83	253.00	668.41	270.00	1058.99	345.00
580.92	74.00	1162.93	107.00	655.22	154.00	3508.72	292.00	2256.23	356.00	876.97	380.00	1369.71	487.00
673.32	83.50	1378.07	125.00	733.83	179.00	3860.86	355.00	2499.10	426.00	1028.77	461.00	1578.41	566.00
740.40	90.00	1642.92	140.00	809.86	204.00	5109.41	445.00	3106.65	534.00	1280.78	578.00	1866.99	657.00
794.03	93.50	1800.79	156.00	876.07	223.00	5650.00	508.00	3440.88	610.00	1332.32	660.00	2093.57	716.00
1058.11	130.00	2213.88	200.00	906.99	239.00	5984.53	550.00	3621.61	660.00	1391.07	715.00	2184.92	785.00
1655.93	211.00	3732.20	307.20	1542.14	414.00	7505.39	768.00	4737.15	937.00	1649.61	1021.00	2782.47	1183.00
R930		R1010		R1870		R1890		R1910		R1930		R2030	
S	O	S	O	S	O	S	O	S	O	S	O	S	O
0.00	0.00	0.00	0.00	0.00	0.00	0.00	0.00	0.00	0.00	0.00	0.00	0.00	0.00
67.00	3.00	309.23	33.50	264.88	13.20	404.07	9.10	837.87	36.10	225.94	44.00	585.96	21.00
95.00	5.00	503.96	67.00	474.80	26.40	543.70	18.10	1279.23	72.20	363.43	88.00	913.82	41.00
115.00	7.00	985.75	168.00	1321.19	67.00	958.47	45.30	2592.06	181.00	681.95	220.00	1829.99	104.00
138.17	10.00	1726.00	335.00	1810.16	120.00	1558.60	90.00	4971.75	361.00	1264.37	445.00	3183.52	188.00
208.56	20.00	2222.59	450.00	3810.08	214.00	2047.74	133.00	6159.72	447.00	1728.50	591.00	5691.37	333.00
319.53	30.00	2558.16	530.00	4278.23	249.00	2327.52	159.00	7120.41	535.00	1967.24	669.00	6608.67	387.00
543.70	50.00	2945.41	630.00	4675.72	280.00	2642.25	190.00	7712.24	579.00	2205.70	731.00	7421.55	435.00
1132.43	100.00	3234.45	705.00	5832.38	320.00	2881.41	214.00	8615.57	624.00	2461.66	801.00	8496.58	500.00
3021.35	151.00	3522.67	784.00	6291.38	360.00	3097.13	236.00	9436.37	744.70	2611.69	815.00	9469.84	560.00
5241.65	180.00	4514.07	1057.00	8737.16	572.00	3846.54	314.00	14583.16	1121.50	4386.31	1367.70	14140.82	870.00
R2040		R2050		R2120		R2290		R2300		R2430		R2440	
S	O	S	O	S	O	S	O	S	O	S	O	S	O
0.00	0.00	0.00	0.00	0.00	0.00	0.00	0.00	0.00	0.00	0.00	0.00	0.00	0.00
440.04	33.00	265.55	24.00	736.63	33.00	230.88	35.50	522.14	37.00	175.00	24.00	691.75	59.30
658.15	65.00	421.70	48.00	1110.68	65.00	371.24	71.00	788.88	74.00	344.31	48.00	1024.01	118.60
1007.31	130.00	908.26	122.00	1721.57	130.00	716.78	178.00	1430.77	184.00	582.38	122.00	1820.28	296.50
3191.60	651.00	1637.43	224.00	6531.27	651.00	1233.15	355.00	2343.38	369.00	976.73	224.00	3114.94	593.00
4271.63	926.00	2468.77	391.00	10598.20	926.00	1606.14	477.00	2964.62	496.00	1361.44	391.00	4105.96	843.00
4961.46	1110.00	2946.06	455.00	14004.89	1110.00	1852.44	562.00	3366.77	584.00	1615.79	455.00	4766.86	1010.00
5716.29	1320.00	3412.74	516.00	17214.60	1320.00	2149.65	668.00	9099.35	690.00	1885.80	516.00	5373.90	1170.00
6300.11	1490.00	3915.06	580.00	19991.89	1490.00	2376.79	748.00	9331.21	776.00	2285.38	580.00	6136.58	1370.00
6857.22	1658.00	4339.66	661.00	22381.16	1658.00	2599.42	833.00	9567.45	864.00	2656.99	661.00	6776.65	1489.00
8951.47	2340.00	6021.55	1019.00	33771.60	2340.00	3319.45	1121.00	10373.00	1164.00	4934.06	1019.00	9264.95	2200.00

S - Storage [1000 m^3] O - Outflow [m^3s^{-1}]

Appendix IIIb. Elevation-storage-outflow relationships of the Fanshawe, Wildwood and Pittock reservoirs.

Fanshawe			Pittock			Wildwood		
E	S	O	E	S	O	E	S	O
0.0	12350	1.00	0.0	0	0.00	0.0	2430	0.79
0.2	12900	3.00	0.2	100	0.40	0.5	3050	0.82
0.2	12900	5.76	0.2	100	2.70	1.0	3730	0.86
0.4	13450	5.76	0.4	260	2.90	1.5	4470	0.89
0.4	13450	29.94	0.6	470	3.00	2.0	5310	0.92
0.6	14000	50.55	0.8	680	3.20	2.5	6280	0.95
0.8	14550	75.30	1.0	890	3.33	3.0	7350	0.98
1.0	15150	103.76	1.0	890	5.90	3.5	8520	1.01
1.2	15700	135.65	1.5	1500	7.30	4.0	9780	1.03
1.4	16250	141.80	2.0	2240	8.50	4.5	11120	1.06
1.6	16850	155.40	2.5	3070	9.50	5.0	12580	1.08
1.8	17400	167.60	3.0	4040	10.40	5.5	14180	1.10
2.0	18000	178.80	3.5	5110	11.30	6.0	15880	3.00
2.4	19300	199.00	4.0	6340	12.10	6.5	17730	3.00
2.8	20600	217.00	4.5	7700	14.30	6.6	18100	3.00
3.2	21950	234.00	4.5	7700	27.10	6.7	18470	4.33
3.6	23250	248.70	5.0	9250	35.00	6.8	18840	5.66
3.6	23250	321.00	5.0	9250	48.10	6.9	19250	7.37
4.0	24650	341.00	5.5	10950	59.00	7.0	19660	18.60
4.5	26600	365.00	6.0	12880	72.00	7.2	20470	23.55
5.0	28550	388.00	6.5	14930	86.00	7.4	21290	29.35
5.0	28550	475.00	6.5	14930	101.12	7.6	22110	35.87
5.5	30600	502.00	7.0	17160	117.00	7.8	22930	43.02
6.0	32700	530.00	7.0	17160	180.00	8.0	23800	60.66
6.5	34950	558.00	7.4	18940	196.00	8.2	24670	68.92
7.0	37200	586.00						
7.0	37200	694.00						
8.0	42050	763.00						
9.0	47250	836.00						
9.0	47250	1335.00						
9.9	52300	1453.00						

E - Elevation [m]
S - Storage [1000 m^3]
O - Outflow [m^3s^{-1}]

Appendix IIIc. Evapotranspiration zones of the continuous model.

ET [mm]	Zone 1	Zone 2	Zone 3	Pan coef
January	0.1	0.1	0.1	0.7
February	0.0	0.0	0.0	0.7
March	6.5	11.0	19.5	0.7
April	59.8	62.7	66.4	0.7
May	96.8	99.1	101.8	0.7
June	116.3	119.6	124.6	0.7
July	127.6	128.6	134.6	0.7
August	99.5	100.9	105.6	0.7
September	64.8	65.6	68.4	0.7
October	29.7	31.1	31.8	0.7
November	8.6	8.9	8.8	0.7
December	0.0	0.0	0.1	0.7

Zone 1: subbasins Nr 1
Zone 2: subbasins Nr 2-14, 18, 23
Zone 3: subbasins Nr 15-17, 19-22, 24-34

APPENDIX IV. CALIBRATED MODEL PARAMETERS.

Appendix IVa. Calibrated event model parameters.

Subbasin	As [km^2]	Ai [%]	Li* [mm]	Lr [mm/hr]	Tc [hr]	St [hr]	Bi* [m^{3}s^{-1}km^{-2}]	Rc [-]	Td [-]
1	175.982	0.000	30.000	1.000	8.000	10.000	0.005	0.400	0.700
2	129.523	0.000	30.000	1.000	10.000	12.000	0.005	0.400	0.700
3	47.745	0.000	12.000	1.100	12.000	6.000	0.006	0.400	0.400
4	151.189	0.000	15.000	1.000	12.000	10.000	0.005	0.400	0.500
5	76.820	0.000	13.000	1.100	7.000	6.000	0.006	0.400	0.400
6+7	144.000	2.000	5.000	1.000	5.000	10.000	0.005	0.400	0.100
8	88.355	0.000	12.000	1.000	11.000	7.000	0.006	0.400	0.400
9	78.476	0.000	13.000	1.100	7.000	6.000	0.006	0.400	0.400
10	141.118	0.000	12.000	1.100	13.000	9.000	0.006	0.500	0.400
11	28.942	0.000	12.000	1.200	9.000	5.000	0.006	0.300	0.400
12	35.466	0.000	16.000	1.300	10.000	8.000	0.007	0.300	0.400
13	153.721	0.000	16.000	1.000	13.000	14.000	0.007	0.300	0.400
14	84.539	0.000	17.000	1.500	14.000	10.000	0.007	0.300	0.400
15	94.198	0.000	25.000	2.000	15.000	20.000	0.007	0.300	0.400
16	75.363	5.000	25.000	2.000	16.000	16.000	0.010	0.500	0.300
17	202.478	0.000	60.000	2.300	24.000	20.000	0.010	0.500	0.100
18	148.318	0.000	15.000	1.000	10.000	9.000	0.010	0.400	0.800
19	96.840	0.000	15.000	1.100	15.000	9.000	0.010	0.300	0.800
20	97.910	0.000	2.000	1.000	2.000	3.000	0.005	0.500	0.100
21	170.704	0.000	5.000	1.300	24.000	12.000	0.020	0.600	0.500
22	42.859	0.000	5.000	1.300	24.000	9.000	0.020	0.600	0.500
23	291.080	0.000	18.000	3.500	7.000	17.000	0.010	0.500	0.200
24	35.861	0.000	5.000	1.400	25.000	8.000	0.010	0.500	0.200
25	165.973	0.000	5.000	2.000	25.000	15.000	0.003	0.700	0.700
26	120.935	0.000	5.000	1.300	20.000	10.000	0.020	0.600	0.500
27	104.945	0.000	18.000	3.500	15.000	16.000	0.010	0.500	0.100
28	61.195	0.000	5.000	1.400	20.000	8.000	0.020	0.600	0.500
29	22.556	40.000	18.000	2.200	4.000	6.000	0.010	0.500	0.300
30	30.002	30.000	18.000	2.300	7.000	10.000	0.010	0.500	0.300
31	32.409	0.000	16.000	2.200	6.000	6.000	0.010	0.500	0.300
32	88.845	0.000	14.000	4.000	20.000	14.000	0.000	0.600	0.400
33	50.486	0.000	16.000	2.400	8.000	7.000	0.010	0.500	0.300
34	168.719	2.000	16.000	3.000	12.000	8.000	0.001	0.300	0.050

* Initial conditions based on the July 2000 event

Appendix IVb. Calibrated continuous model parameters.

a) Snow, direct runoff and baseflow components.

Subbasin	Mr [mm/°C/day]	Tcrt [°C]	Tmin [°C]	Tmax [°C]	Tc [hr]	St [hr]	B1s [hr]	B1r [#]	B2s [hr]	B2r [#]
1+2	4	0	-4	-2	24	22	5	1	35	7
3	4	0	-4	-2	6	8	5	1	40	5
4	4	0	-4	-2	24	24	5	1	60	8
5	4	0	-4	-2	18	18	5	1	55	7
6+7	4	0	-4	-2	12	16	5	1	65	10
8	4	0	-4	-2	16	20	5	1	45	5
9	4	0	-4	-2	12	18	5	1	55	8
10	4	0	-4	-2	22	24	5	1	55	8
11	4	0	-4	-2	12	18	5	1	55	5
12	4	0	-4	-2	18	18	5	1	70	5
13	4	0	-4	-2	24	24	5	1	50	5
14	4	0	-4	-2	18	18	5	1	55	5
15	4	0	-4	-2	12	18	5	1	75	5
16	4	0	-4	-2	12	18	5	1	75	5
17	4	0	-4	-2	18	20	5	1	30	5
18	4	0	-4	-2	18	24	5	1	75	5
19	4	0	-4	-2	6	10	5	1	75	5
20	4	0	-4	-2	18	26	5	1	70	5
21	4	0	-4	-2	18	22	5	1	80	5
22	4	0	-4	-2	12	18	5	1	65	5
23	4	0	-4	-2	24	25	5	1	75	5
24	4	0	-4	-2	12	18	5	1	65	5
25	4	0	-4	-2	24	24	5	1	75	5
26	4	0	-4	-2	12	24	5	1	75	5
27	4	0	-4	-2	18	22	5	1	70	5
28	4	0	-4	-2	12	18	5	1	70	5
29	4	0	-4	-2	6	11	5	1	50	5
30	4	0	-4	-2	6	8	5	1	45	5
31	4	0	-4	-2	6	8	5	1	45	5
32	4	0	-4	-2	18	18	5	1	65	5
33	4	0	-4	-2	6	10	5	1	45	5
34	4	0	-4	-2	24	28	5	1	55	5

b) Precipitation loss component (SMA parameters).

Subbasin	Cs [mm]	Ss[1] [mm]	Ss[2] [mm]	If[1] [mm×hr^{-1}]	If2 [mm×hr^{-1}]	Us [mm]	Ts [mm]	Sp [mm×hr^{-1}]	G1s [mm]	G1p [mm×hr^{-1}]	G1c [hr]	G2s [mm]	G2p [mm×hr^{-1}]	G2c [hr]
1+2	2	22	11	4.8	0.35	60	15	3	45	1	150	40	1	290
3	2	34	17	4.9	0.36	57	21	3	40	2	180	40	1	260
4	2	23	12	4.8	0.35	70	15	3	50	2	175	50	1	230
5	2	23	12	4.8	0.35	70	15	3	50	2	175	50	1	230
6+7	2	23	12	4.8	0.35	70	15	3	50	2	175	50	1	230
8	2	34	17	4.9	0.36	57	21	3	40	2	180	40	1	260
9	2	38	19	4.9	0.36	72	22	3	45	2	170	50	1	250
10	2	38	19	4.9	0.36	72	22	3	45	2	170	50	1	250
11	2	38	19	4.9	0.36	72	22	3	45	2	170	50	1	250
12	2	32	16	5.0	0.37	55	17	3	40	2	150	45	1	280
13	2	34	17	4.9	0.36	57	21	3	40	2	180	40	1	260
14	2	32	16	5.0	0.37	55	17	3	40	2	150	45	1	280
15	2	32	16	5.0	0.37	55	17	3	40	2	150	45	1	280
16	2	26	13	5.0	0.37	58	18	3	58	2	145	55	1	290
17	2	30	15	2.5	0.18	50	20	3	40	2	225	40	1	275
18	2	34	17	4.9	0.36	70	30	3	50	2	80	40	1	275
19	2	37	19	4.9	0.36	80	40	2	60	2	140	40	1	300
20	2	37	19	4.9	0.36	80	40	2	60	2	140	40	1	300
21	2	37	19	4.9	0.36	80	40	2	60	2	140	40	1	300
22	2	37	19	4.9	0.36	80	40	2	60	2	140	40	1	300
23	2	23	12	4.8	0.35	80	50	3.5	70	2	130	50	1	290
24	2	23	12	4.8	0.35	80	50	3.5	70	2	130	50	1	290
25	2	37	19	4.9	0.36	80	40	2	60	2	140	40	1	300
26	2	37	19	5.0	0.37	60	40	3.5	70	2	130	50	1	300
27	2	37	19	5.0	0.37	60	40	3.5	70	2	130	50	1	300
28	2	37	19	5.0	0.37	60	40	3.5	70	2	130	50	1	300
29	2	26	13	5.0	0.37	58	18	3	58	2	145	55	1	290
30	2	26	13	5.0	0.37	58	18	3	58	2	145	55	1	290
31	2	30	15	2.5	0.18	50	20	3	40	2	225	40	1	275
32	2	30	15	2.5	0.18	50	20	3	40	2	225	40	1	275
33	2	30	15	2.5	0.18	50	20	3	40	2	225	40	1	275
34	2	31	16	4.9	0.36	55	10	3	60	2	140	45	1	290

[1]summer season, [2]winter season

APPENDIX V. SENSITIVITY ANALYSIS RESULTS.

Appendix Va. Event model sensitivity analysis.

	Parameter change [%]						
Li	-30	-20	-10	0	10	20	30
PEPF [%]	6.025	4.093	2.074	0.000	2.089	4.234	6.309
PEV [%]	6.401	4.359	2.227	0.000	2.322	4.702	6.929
CORR [-]	1.000	1.000	1.000	1.000	1.000	1.000	1.000
RBIAS [%]	-4.117	-2.865	-1.513	0.000	1.806	4.402	5.889
RRMSE [%]	7.071	5.245	3.050	0.000	5.473	19.768	21.188
RPWRMSE [%]	7.129	5.102	2.821	0.000	4.358	14.595	16.103
Lr	-30	-20	-10	0	10	20	30
PEPF [%]	10.161	7.011	3.633	0.000	3.763	7.784	11.911
PEV [%]	10.249	7.074	3.668	0.000	3.942	8.208	12.500
CORR [-]	1.000	1.000	1.000	1.000	1.000	1.000	1.000
RBIAS [%]	-6.134	-4.243	-2.205	0.000	2.346	4.889	7.574
RRMSE [%]	7.991	5.525	2.871	0.000	3.057	6.369	9.873
RPWRMSE [%]	9.243	6.385	3.314	0.000	3.552	7.400	11.344
Tc	-30	-20	-10	0	10	20	30
PEPF [%]	3.145	1.769	1.321	0.000	0.666	1.983	2.638
PEV [%]	0.316	0.165	0.122	0.000	0.084	0.198	0.261
CORR [-]	0.992	0.997	0.999	1.000	0.999	0.997	0.993
RBIAS [%]	0.302	0.211	0.008	0.000	-0.079	-0.008	0.022
RRMSE [%]	6.639	4.622	2.380	0.000	2.559	5.239	8.102
RPWRMSE [%]	8.786	5.988	3.039	0.000	3.162	6.385	9.696
Sc	-30	-20	-10	0	10	20	30
PEPF [%]	24.340	16.258	8.133	0.000	7.802	15.662	23.510
PEV [%]	7.871	4.910	2.302	0.000	2.033	3.890	5.562
CORR [-]	0.989	0.995	0.999	1.000	0.999	0.997	0.993
RBIAS [%]	0.240	0.457	0.361	0.000	-0.576	-1.248	-1.959
RRMSE [%]	7.840	5.399	2.776	0.000	2.944	5.924	8.995
RPWRMSE [%]	12.943	8.575	4.259	0.000	4.197	8.291	12.308
Bi	-30	-20	-10	0	10	20	30
PEPF [%]	0.015	0.010	0.005	0.000	0.005	0.010	0.015
PEV [%]	0.530	0.352	0.175	0.000	0.177	0.351	0.526
CORR [-]	1.000	1.000	1.000	1.000	1.000	1.000	1.000
RBIAS [%]	17.584	10.234	4.552	0.000	-3.713	-6.853	-9.463
RRMSE [%]	27.488	16.000	7.159	0.000	5.831	10.693	14.751
RPWRMSE [%]	19.714	11.498	5.153	0.000	4.215	7.743	10.704
Rc	-30	-20	-10	0	10	20	30
PEPF [%]	0.041	0.036	0.021	0.000	0.031	0.077	0.138
PEV [%]	8.136	5.577	2.866	0.000	3.032	6.225	9.571
CORR [-]	0.999	0.999	1.000	1.000	1.000	0.999	0.998
RBIAS [%]	115.050	56.650	22.058	0.000	-14.959	-25.527	-33.325
RRMSE [%]	159.518	75.745	28.726	0.000	18.726	31.508	40.648
RPWRMSE [%]	114.813	55.089	21.159	0.000	14.230	24.375	32.038
Td	-30	-20	-10	0	10	20	30
PEPF [%]	0.000	0.000	0.000	0.000	0.000	0.000	0.000
PEV [%]	2.671	1.771	0.876	0.000	0.866	1.720	2.558
CORR [-]	1.000	1.000	1.000	1.000	1.000	1.000	1.000
RBIAS [%]	5.992	3.705	1.719	0.000	-1.539	-2.916	-4.160
RRMSE [%]	9.447	5.814	2.687	0.000	2.382	4.486	6.366
RPWRMSE [%]	7.996	4.984	2.332	0.000	2.101	3.988	5.697

Appendix Vb. Continuous model sensitivity analysis.

	Parameter change [%]				Parameter change [%]		
Tc	-20	0	20	Us	-20	0	20
PEPF [%]	1.167	0.000	2.708	PEPF [%]	5.161	0.000	3.466
PEV [%]	0.001	0.000	0.001	PEV [%]	8.513	0.000	4.194
CORR [-]	0.997	1.000	0.997	CORR [-]	0.994	1.000	0.999
RBIAS [%]	0.247	0.000	-0.130	RBIAS [%]	0.962	0.000	0.378
RRMSE [%]	3.031	0.000	3.054	RRMSE [%]	18.093	0.000	9.663
RPWRMSE [%]	4.655	0.000	4.652	RPWRMSE [%]	17.557	0.000	9.907
St	-20	0	20	Ts	-20	0	20
PEPF [%]	8.853	0.000	9.204	PEPF [%]	4.213	0.000	4.222
PEV [%]	0.002	0.000	0.001	PEV [%]	4.071	0.000	5.671
CORR [-]	0.996	1.000	0.997	CORR [-]	0.998	1.000	0.997
RBIAS [%]	1.771	0.000	-1.077	RBIAS [%]	-0.928	0.000	2.746
RRMSE [%]	8.844	0.000	5.385	RRMSE [%]	11.630	0.000	19.884
RPWRMSE [%]	9.015	0.000	6.289	RPWRMSE [%]	11.780	0.000	17.402
Bs	-20	0	20	Sp	-20	0	20
PEPF [%]	0.079	0.000	0.069	PEPF [%]	0.000	0.000	0.000
PEV [%]	0.043	0.000	0.044	PEV [%]	0.023	0.000	0.001
CORR [-]	1.000	1.000	1.000	CORR [-]	1.000	1.000	1.000
RBIAS [%]	8.504	0.000	-2.708	RBIAS [%]	-0.064	0.000	0.022
RRMSE [%]	26.967	0.000	16.634	RRMSE [%]	1.128	0.000	0.542
RPWRMSE [%]	20.005	0.000	12.652	RPWRMSE [%]	1.592	0.000	0.789
Br	-20	0	20	Gs	-20	0	20
PEPF [%]	0.059	0.000	0.099	PEPF [%]	0.494	0.000	0.412
PEV [%]	0.052	0.000	0.919	PEV [%]	8.697	0.000	6.839
CORR [-]	1.000	1.000	0.999	CORR [-]	1.000	1.000	0.982
RBIAS [%]	6.739	0.000	7.643	RBIAS [%]	21.016	0.000	-11.364
RRMSE [%]	22.772	0.000	64.168	RRMSE [%]	24.569	0.000	28.689
RPWRMSE [%]	17.140	0.000	45.274	RPWRMSE [%]	19.664	0.000	25.768
Cs	-20	0	20	Gp	-20	0	20
PEPF [%]	0.000	0.000	0.000	PEPF [%]	0.548	0.000	0.445
PEV [%]	0.114	0.000	0.078	PEV [%]	8.433	0.000	7.416
CORR [-]	1.000	1.000	1.000	CORR [-]	0.981	1.000	0.983
RBIAS [%]	-0.054	0.000	0.070	RBIAS [%]	-13.186	0.000	17.480
RRMSE [%]	0.750	0.000	0.702	RRMSE [%]	29.307	0.000	33.466
RPWRMSE [%]	0.718	0.000	0.673	RPWRMSE [%]	26.500	0.000	29.124
Ss	-20	0	20	Gc	-20	0	20
PEPF [%]	0.538	0.000	0.544	PEPF [%]	0.655	0.000	0.494
PEV [%]	1.458	0.000	1.337	PEV [%]	8.091	0.000	7.105
CORR [-]	0.999	1.000	1.000	CORR [-]	0.999	1.000	0.999
RBIAS [%]	0.399	0.000	-0.105	RBIAS [%]	-11.476	0.000	11.584
RRMSE [%]	4.735	0.000	6.168	RRMSE [%]	12.119	0.000	12.254
RPWRMSE [%]	4.949	0.000	5.881	RPWRMSE [%]	11.185	0.000	10.944
If	-20	0	20				
PEPF [%]	2.607	0.000	2.488				
PEV [%]	3.596	0.000	3.137				
CORR [-]	0.999	1.000	0.999				
RBIAS [%]	0.119	0.000	0.410				
RRMSE [%]	8.113	0.000	8.303				
RPWRMSE [%]	7.983	0.000	8.381				

APPENDIX VI. COMPUTER PROGRAMS

The subroutine "Snow_Model" simulates snow accumulation and melt based on daily precipitation and temperature data. The output is a time series of adjusted daily precipitation used as an input into the HEC-HMS continuous model. The subroutine is written in Visual Basic 5.0, and saved in a VB class module "Snow.cls".

```
'---------------------------------------------------------------------
Option Explicit: Option Base 1
Sub Snow_Model(P!(), T!(), R!(), S!(), NP!())
'---------------------------------------------------------------------
'Written by JMC, March 18 2004
'---------------------------------------------------------------------
'Input:      P = Daily precipitation amount [mm]
'            T = Daily average temperature [degrees Celsius]
'Output:     R = Daily rainfall amount separated from precipitation [mm]
'            S = Accumulated snowfall [mm]
'           NP = New daily precipitation amount for HEC - adjusted
'                for snow accumulation and melt [mm]
'Parameters:MR = Melt rate [mm/degree/day]
'         Tcrt = Critical temperature for snowmelt [degrees Celsius]
'         Tmin = Lower temperature threshold [degrees Celsius]
'         Tmax = Upper temperature threshold [degrees Celsius]
'Auxiliary:  N = Record length [days]
'            M = Daily melt amount [mm]
'            i = Loop counter
'---------------------------------------------------------------------
Dim N&, i&, M!
Const MR = 4, Tcrt = 0, Tmin = -4, Tmax = -2
N = (UBound(P()) - LBound(P()) + 1) 'determining record length
For i = 1 To N
    'separating rainfall and snowfall precipitation
    If T(i) <= Tmin Then
        S(i) = P(i): R(i) = 0
    ElseIf Tmin < T(i) And T(i) < Tmax Then
        S(i) = P(i) * ((Tmax - T(i)) / (Tmax - Tmin)): R(i) = P(i) - S(i)
    ElseIf T(i) >= Tmax Then
        S(i) = 0: R(i) = P(i)
    End If
    'accumulating snowfall
    If i > 1 Then S(i) = S(i) + S(i - 1)
    'calculating snowmelt
    M = MR * (T(i) - Tcrt)
    'calculating adjusted precipitation
    If M > 0 Then
        If S(i) > 0 Then
            If S(i) > M Then
                S(i) = S(i) - M: NP(i) = R(i) + M
            Else
                NP(i) = R(i) + S(i): S(i) = 0
            End If
        Else
            NP(i) = R(i)
        End If
    Else
        NP(i) = R(i)
    End If
Next i
End Sub
'---------------------------------------------------------------------
```